September 2015

Nanomechanical and Nanotribological Characterization of Sub-Micron Polymeric Spheres

Himanshu Kumar Verma
University of South Florida, hverma@mail.usf.edu

Nanomechanical and Nanotribological Characterization of Sub-Micron Polymeric Spheres

by

Himanshu K. Verma

A dissertation submitted in partial fulfillment
of the requirements for the degree of
Doctor of Philosophy
Department of Physics
College of Arts and Sciences
University of South Florida

Major Professor: William Garrett Matthews, Ph.D.
Pritish Mukherjee, Ph.D.
Inna Ponomareva, Ph.D.
Jianjun Pan, Ph.D.

Date of Approval:
July 9, 2015

Keywords: Nanoindentation, Lateral Force Microscopy, Size, Elastic Modulus, Adhesion Force

Dedication

I dedicate this dissertation to my parents, my maternal uncle & aunt, my family and last but not the least, to my beloved wife. Without their love, support and encouragement, an endeavor like this would have never been possible. They are the foundation of who I am today and who I am yet to be.

Acknowledgments

I would like to extend my deepest gratitude and appreciation to Dr. William Garrett Matthews for preserving with me as my advisor throughout the time it took me to complete this research and dissertation. I am indebted to him for all the academic, moral and personal support during the entire course of this work.

I would like to express my thanks to my dissertation committee members Dr. Pritish Mukherjee, Dr. Inna Ponomareva, and Dr. Jianjun Pan for serving on my dissertation committee and for all the valuable advices that helped me, turned into a better researcher.

I am thankful to my colleagues Dr. Heather Harper, Erin Brownell, Michael Cross, Stephanie Holdener, Chad Becker, and Bart Graham for all the valuable information and help in the lab. I would also like to thank my office –mate Dr. Jagannath Devkota for all the suggestions and help.

I would like to thank Dr. Gerald Woods, Lab Director and Dr. Pritish Mukherjee, Department Chair, for trusting in me for my teaching skills and for the continued assistantship during this entire doctoral program. I must acknowledge Dr. Robert Hyde and Dr. Devajyoti Mukherjee for the help and training they provided me on the user facilities in the physics department. I would also like to thank physics office staff members Mary-Ann Prowant, Daisy Matos, and Candice Pietri for always welcoming me with a smiling face and helping me with all the technical prospect in this doctoral program.

This research was supported in part by the American Chemical Society (ACS) through Petroleum Research Fund (PRF) Grant Number 48982ND5. The financial support for industrial practicum at the Army Research Lab was provided through Frank Duckwall Fellowship 2014.

Table of Contents

List of Tables

List of Figures

Abstract

Friction between nanoscale objects has been a subject of great interest and intense research effort for the last two decades. However, the vast majority of the work done in this area has focused upon the sliding friction between two rigid, atomically smooth surfaces. Thus the parameter most explored has been the corrugation in the atomic potentials and how this affects the force required to slide one object across another. In truth, many nanoscale objects whose translation force is of practical interest are more spherical in nature. We hypothesize that the factors that determine the translation force will be related, not only to the interfacial adhesion, but also to the mechanical properties of the translating object and its underlying surface. The dependence on these quantities of the friction is not known. In this dissertation we have utilized Atomic Force Microscopy and Force Spectroscopy to study the tribological properties of submicron scale polymeric particles to explore how the friction between these submicron spherical objects translating over planar substrates is related to interfacial energy and the mechanical properties for these particles. A technique for modifying the mechanical properties was developed and used to provide a set of samples over which we had control of the elastic modulus without corresponding changes in the chemical bonds. The modified mechanical properties were tested against the Flory-Rehner theory. Lateral force microscopy was used to measure the force required to translate asymmetric, nanoscale particles of controlled size, surface chemistry and moduli. Silicon wafers were used as the substrate. The effects of work of adhesion, elastic modulus of polystyrene microspheres, and contact radius between particle and substrate have been studied for the different modes of particle translation under an external force.

1.0 Introduction

1.1 Motivation

The understanding of physical motions such as rolling, sliding, stick-slip, and spinning is of great importance, since the energy loss and wear between the contacting surfaces is determined by the mode of motion of these particles [1]. When a lateral force is applied onto a submicron size particle lying on a surface, what happens to its translational motion? Does it roll, does it slide, or both? How can the force required be predicted from the particle's properties? These questions have relevance in technological applications where submicron size particles are used as lubricants or as components in lubricating mixtures and in nano-electromechanical devices where they are used as building blocks [2]. Using Lateral Force Microscopy to provide the forces required to produce translational motion of micro/nano-sized particles across a planar substrate will help understand the tribological properties that inform their use in such applications (adhesion, friction, lubrication, and wear). Such knowledge will help, for example, in designing new lubricants, hard disk storage technology, new materials for post chemical mechanical polishing (CMP), and generally in the reliable, repeatable and controllable manipulation of micro/nano-size particles on substrates [3, 4].

In the transition from the macro to the nano world, novel phenomena result from the decreased dimensions of the object. The scaling leads to changes in geometrical and physical properties of the small object [5]. Friction and adhesion forces become of increased importance when small particles are considered for a variety of important phenomena. For example,

aggregation and dispersal of powders, colloidal dispersions, and the flow properties of granular materials [6]. Friction has been one of the fundamental research areas for centuries; however, the vast majority of the studies only have been done at the macroscopic scale. Research at the micro-scale has been more limited [7]. From the work that has been done, it is clear that friction at nanoscale differs markedly from the macro scale. Objects at the nanoscale are totally wear-less and adhesion (the force that holds two bodies in contact) dominates at lower loads while friction becomes an intrinsic property of the particle interface [3, 4]. The primary goal of this research is to develop a deep understanding of how the physical properties of a nanoscale spherical object affect the translational properties when a lateral force is applied to it. Using an Atomic Force Microscope (AFM), the adhesion and mechanical properties of different sized polystyrene microspheres will be measured. Again using AFM, the lateral force required for translation across rigid, flat substrates (polished silicon wafer) can then be characterized. Relationships between the properties of the microspheres and the lateral force will be tested. A few models exist in the literature, and their validity will be tested against our data.

1.2 Previous work

1.2.1 Macroscopic rolling and sliding friction

When an object is moving along a surface, or through a viscous liquid or gas, it experiences resisting forces known as friction. The mode of translation governs the energy loss, and wear impacting the interacting surfaces. The modern study of friction dates back to nearly 500 years ago when Leonardo da Vinci recorded the relative motion of a rectangular object sliding over a planar surface [8]. Unfortunately his work never was published. In the year 1699, French physicist Guillaume Amontons is credited for publishing the first account of friction laws for solid surfaces

in sliding contact. Amontons reported that friction forces are independent of area of contact. He concluded that a small block experiences same magnitude of friction as does a large block as long as their weights are same. However, Amonton's laws failed a variety of attempts to explain the fundamental, underlying basis of friction [9]. Among the most significant tribological studies can be attributed those of Heinrich Hertz almost 150 years ago. He studied two elastic bodies in contact under an external load; unfortunately, he ignored the attractive inter-particle forces [10]. When particles are in contact, they are inevitably deformed because of their finite elasticity. Johnson, Kendall, and Roberts (popularly known as the JKR model) explained the contact between two solid spheres [11]. A couple of years later, in 1975, Derjaguin, Muller, and Toporov (the well-known DMT model) published an alternative theory that also accounted for the non-contact forces in the vicinity of the contact area. After further studies, it was found that the JKR model is more appropriate for large, soft bodies with high surface energies, whereas the DMT model applies well to small, hard solid particles with low surface energy [12, 13]. Though largely successful, it has been shown that both models have limitations [14].

1.2.2 Nano-scale rolling and sliding friction

With the advent of the Atomic Force Microscope in 1980 by Binning, Quate, and Rohrer [15], the versatility and capability of imaging and manipulating all types of nanomaterials under different conditions, researchers began using AFM for tribological studies at the microscopic scale. Mate et al. in 1987 reported how the atomic structure of a graphite surface influences the frictional dynamics of an AFM tip sliding on its surface. They also reported the first ever stick-slip observation at the atomic scale on mica surfaces [16]. Presenting joint results from theoretical and experimental studies using an AFM, Landman et al. showed that contact formation between a hard tip (nickel) approaching a soft metallic substrate (gold) is associated with an instability which

involves an inelastic response of the atoms in the interfacial region of the gold substrate [17]. Heim et al. measured rolling friction forces for the first time at the micro-scale by combining atomic force microscopy and optical microscopy. They used silica microspheres of different sizes ranging between 0.5 to 2.5 μm. The measured rolling friction forces, analyzed using the DMT model, were 100 times smaller than the corresponding adhesion forces [6]. Comparing macro-tribology to micro/nano-tribology, Achanta et al. showed how capillary forces, surface topography, and phase composition of interacting materials becomes evident while dealing in micro/nano-tribology [18]. With the introduction of lateral force microscopy (LFM), it was now possible to study sensitive surface interactions at the micro/nano-scale under ultra-low force and small length scale. The tribological properties of islands of C_{60} deposited on NaCl (001) at the mesoscopic scale were studied by Luthi et al. An extremely small dissipation energy of 0.25 meV per molecule and cohesive energy of 1.5 eV were observed. A low shear strength ranging 0.05 to 0.1 MPa was found [19]. Falvo et al. reported controlled rolling of carbon nanotubes (CNTs) on a graphite surface using lateral force microscopy. They observed changes in nanotube topography directly related to stick slip behavior and in-plane rotation of these tubes while lateral force was applied. When the CNT was pushed on edge, sliding behavior was observed with a relatively smooth lateral force data. When they compared the stick peaks in the rolling data to the lateral force data while sliding, they found a higher force needed to sustain sliding. This result implies that the energy cost for rolling is higher than that needed for sliding, however, this result was dependent upon the intermeshing of the carbon lattice in the two surfaces(see their later study cited below) [20]. Buldum et al. modelled different types of motions of carbon nanotubes on a graphite substrate. They found unique energy minimized orientations for the CNTs depending on their surface structure. A combination of atomic scale spinning and sliding motions were observed. The

potential energy barrier for rolling nanotubes was much smaller than for sliding [7]. In another study by Falvo et al., it was found that the evidence of rolling motion of CNT was dependent upon commensurate contact on the hexagonal surface of the HOPG substrate. The transition from the incommensurate to commensurate state was accompanied by a corresponding transition from sliding motion to gear like rolling motion [21]. Tivet et al. reported the rolling, sliding and exfoliation behavior of fullerene like nanoparticles of WS_2 (and MoS_2). They found rolling behavior required the nanoparticles to be spherically shaped and mechanically stable, whereas sliding required particles at low friction, mechanically stable, low adhesion and chemical affinity to the underlying surfaces. Rolling was dominant under low shear rates and normal stress of 0.96±0.38 GPa, and sliding occurred around normal stress of 1.34 GPa [22]. Korayem et al. investigated the sensitivity of the critical parameters in AFM based nano-manipulation. Their model included adhesion and normal friction forces. They defined the critical force (the required pushing force for the particle on the substrate to overcome the sticking state to slide or roll) and the critical time (the moment when particle start sliding or rolling) and diagramed them against all spatial parameters possible (listed below) in the nano-manipulation process. They concluded that all of these parameters can affect the nano-manipulation process. Parameters increasing the critical force and time included particle radius, initial deformation of the cantilever, surface energy, sliding friction coefficients, and surface adhesion (while sliding). Cantilever length, and reduced modulus decreased the critical force and critical time. They found no effect from tip radius, probe/particle contact angle, rolling friction coefficients, and surface adhesion (while rolling). Simulation results indicated sliding occurs first and was more likely for small particles rather than rolling. Increasing the particle size it changed to rolling. Simultaneous sliding/rolling occurred if the applied force was higher than the critical force for sliding and rolling [5]. Using a ball-on-flat tribometer, Vilt et

al. presented the frictional performance of silica microspheres on a silicon substrate. This kind of tribometer is normally used for macro scale tribological studies, but they optimized a nano-tribometer for the nanotribological characterization purpose. The rolling behavior was highly dependent on the load and the sphere diameter. The surface energy of the lubrication scheme was altered by means of coating. The spheres used were 4, 2, and 0.5 μm in size. The lubrication scheme could not confirm the rolling behavior, but the coefficients of friction were measured for 4 and 2 μm size particles, which were found to be slightly higher for the 4 μm spheres. The 0.5 μm size spheres failed to record any data. These experiments demonstrated the size dependence of the coefficients of friction for these spheres [23]. ZnO nanowire were subjected to rolling and sliding behavior by Kim et al. They measured the friction forces during the manipulation of a single ZnO nanowire of mass 18.7 ng on a Si wafer using LFM. They found simultaneous occurrence of rolling and sliding, followed by sliding, which were attributed to the state of contact, hence the frictional force between the nanowire and the substrate. The average dynamic frictional force measured during rolling/sliding was 33.7 nN, while the average dynamic frictional force measured during sliding was 36.9 nN [24].

Both rolling and sliding have been observed at the micro/nano-scale. A number of impacting factors, such as lateral force, contact area, shape of the translating material, particle radius, cantilever length, and the applied load to name a few, were attributed to the translational motions. In this work, we consider friction, adhesion, particle size, and elastic modulus of the translating particle to predict the physical motion (rolling or sliding) of a translating particle under the lateral force. We also investigate the transition from rolling to sliding and the underlying factors responsible for this transition.

1.2.3 Nano-scale rolling and sliding models by Sitti et al. and Krijt et al.

Sitti et al. predicted the translation motion of a submicron sized latex particle on a silicon substrate under a lateral force based on their experimental lateral force versus position data. They predicted a short noisy peak to represent sliding, a peak of almost double the height of the sliding peaks characterized by a periodic feature for rolling, and a wide peak that is almost 10 times larger, as indicating rotational (spinning) motion [25]. In an another study Metin Sitti predicted the nanoscale translational motion of particles by conducting lateral force microscopy on a 500 nm gold coated latex particle deposited on a SiO_2 substrate. The cantilever deflection versus particle position data were recorded. The particle first showed rolling behavior, then started sliding. If a significant offset from the center of the sphere occurs it starts rotating. The cantilever deflection observed was much higher in the case of sliding than rolling. There was minimal difference in the cantilever deflection from rolling to rotating [26]. Basing their calculations on lateral force microscopy based pushing of micro/nano-size particles, Sumer et al. simulated a rolling resistance model. Using this friction model they studied the effect of work of adhesion, effect of Young's modulus, and contact radius (particle size) on the translational motions such as sliding, rolling and spinning. They modeled the sliding friction motion as single asperity contact which changes with the change in the real contact area such as,

$$F_{slide} = \tau A \qquad (1.1)$$

where τ is the interfacial shear strength and

$$A = \pi a^2 \qquad (1.2)$$

In equation 1.2, 'a' is the real contact radius. Results from surface force apparatus (SFA) experiments showed that shear strength is scale dependent. At some point τ must decrease as the

contact size increases from the nano to micro scale. This establishes the frictional stress as a function of contact area though there is no experimental evidence till date [27]. They proposed a model for a wide range of particle radii. From the results, they defined τ, which is a function of a, as,

$$\tau(a) = \begin{Bmatrix} G/43, & a < 20\ nm \\ G\ 10^N\ (a/b)^M, & 20\ nm < a < 40\ \mu m \\ G/1290, & a > 40\ \mu m \end{Bmatrix} \quad (1.3)$$

In equation 1.3, N is $28b$ and b = 0.5 nm, and $M = \tan^{-1}[(G/43 - G/1290) / (8*10^4 b - 28b)]$. Where $G = 2G_1G_2 / (G_1+G_2)$ is the effective shear modulus given in terms of shear moduli (G_1, G_2). For a particle and a substrate G is defined as $Gi = E_i / [2(1 + v_i)]$, in which E is the Young's modulus and v is the Poisson ratio. This sliding friction model clearly predicted the dependence of the translation force on the particle size of the microspheres.

They compared their friction model's findings with their experimental data. Polystyrene micro/nano-spheres of 0.05, 0.5, 5 and, 15 μm size were deposited on a glass substrate. The simulation data showed micron sized particles in most cases first started to roll, then slide at higher lateral forces. However, nanoparticles first started to slide and then start rolling. If the particles were pushed with an offset, they spin. Combining the simulation data with the experiment, the critical rolling distance found was directly proportional to the particle radius. The rolling friction force also was in direct relationship with the size of the particles. This differs from the shear strength, which also contributes to the sliding force and had an inverse relationship with the particle size [1].

In a most recent study published last year in April 2014, Krijt, Dominik and, Tielens derived an analytical theory for the rolling friction based upon the difference in surface energies

for the opening and closing of cracks. They considered an asymmetric contact in rolling with one side featuring an opening crack and other a closing crack. The contact radii will vary for these different parts of the contact region, and it no longer remains circular. Including this asymmetry, the total elastic force they predicted was,

$$F_E = \frac{2E^* a}{3R}\,(3\delta R - a^2 - 3\xi^2) \qquad (1.4)$$

where E^* is the combined elastic modulus, and 'a' is the average contact radius, R is radius of the sphere, δ is the distance of mutual approach, and ξ is the rolling displacement. The total torque was,

$$M = \xi\left[-F_E + \frac{4E^* a^3}{3R}\right] \qquad (1.5)$$

And in the case of zero load (F_E = 0),

$$M = 6\pi\gamma R\xi \qquad (1.6)$$

where γ is the combined surface energy. They compared their theory with the experimental results, which were in good agreement. They revealed that their new model is capable of explaining two important results, one was the variation of the rolling force with particle radius and the other was the finding that rolling displacement can be much larger than the interatomic distance as thought previously. From the equations it can be explained that elastic modulus and surface energy both significantly contribute to the rolling friction [28].

The parameters predicted to affect nanoscale friction in these two models [1] and [28] are particle size, elastic modulus, and interfacial surface energy. We will measure all of the affecting parameters and use these two models to predict the translational behaviors of our nano-scale spheres. The models will be tested against the experimental data. Our results also will help

establish the experimental evidence of the dependence of these parameters on the different modes of translation at the micro/nano-scale.

1.2.4 Nano-scale adhesion

Atomic force microscope has been widely used in various studies to predict the nature and magnitude of surface forces between two micro/nano-size asperities. In 1990, Burnham et al. studied the attractive and adhesion forces between an AFM tip and sample surfaces as function of sample surface energy. They found both forces are heavily dependent on sample surface energy, and adhesion is always greater [29]. Blackman et al. used AFM to study boundary lubrication. They studied Langmuir-Blodgett films of cadmium arachidate deposited on a silicon wafers. They found that upper layers were easily worn away with the AFM tip whereas the bottom layers close to the substrate were not easy to remove [30]. Surface force interaction was investigated by Schaefer et al. for polystyrene spheres on a p-type silicon substrate. The force to remove a particle and the degree of freedom were measured as a function of loading force. They also studied the effect of surface contamination and concluded that contamination on the surface of the substrate affects the adhesion force [31]. This study highlighted the importance over the control of the surface chemistry when performing such studies. Using an oscillating cantilever technique, Gady et al. analyzed the interaction force gradient between a micron-size polystyrene sphere and an atomically flat, highly oriented pyrolytic graphite (HOPG) substrate as a function of surface to surface separation distance z. They found for $z \geq 30$ nm, an electrostatic force from the charge trapped on the polystyrene sphere dominates, for $z \leq 30$ nm, a van der Walls interaction was observed [32]. The effect of tip radius on adhesive forces and coefficient of friction was studied by Bhushan et al. They reported that at low humidity the adhesive forces do not change with the tip radius however these increase with tip radius at high humidity. Coefficient of friction increases

at all humidifies with the increase in tip radius [33]. This study heighted the importance of capillary condensation and the need to control the environment under which these surface studies are performed.

In the proposed investigation, for the first time each of the quantities that affect the mode of translation at the micro/nano-scale, as predicted in the models described above i.e. in [1] and in [28], will be measured and correlated with the lateral force required. The models will be tested against the experimental data.

1.2.5 Nano-scale indentation

Micro/nano-spheres, which include beads, cells, and microcapsules, are used to produce functional products. Their mechanical properties are important for understanding their performance during manufacturing, processing, and applications. Nanoindentation techniques using an AFM have proven effective for characterizing their mechanical properties. Applying a mechanical load onto a single microsphere and measuring the corresponding deformation on the cantilever allows extraction of the elastic modulus of the microsphere [34, 35]. Heim et al. performed nano-scale radial indentation using an AFM on native collagen fibrils, which were extracted from the inner dermis tissue of the sea cucumber. They reported the reduced elastic modulus of these fibrils as 1 – 1 GPa [36]. Friction and indentation studies were reported by Cohen et al. They used a sharp Iridium tip on a gold surface at loads ranging to submicron newton, and the contact varied at each given spot. The friction was much higher during unloading than the identical value of normal load. At the low range of loading forces it exhibited an elastic behavior [37]. In a most recent study, comparing the nano-indentation and AFM methods to determine the mechanical properties of polymers, Griepentrog et al. used Poly methyl methacrylate (PMMA)

and Polycarbonate (PC) as their samples, and reported that using an AFM and performing force curves, Hertz theory can be used to extract Young's modulus of polymers precisely [38].

1.2.6 Nano-scale manipulation

To manipulate and assemble structures on the atomic scale, Atomic Force Microscope had now found its use in sample deformation and patterning. Leung et al. reported the interaction between AFM tip and polystyrene molecules in a film spread on a substrate. The tip produced a persistent deformation in the film, and some of the polymer molecules were pulled up by the tip. A periodic nanometer size pattern was induced on the film surface [39]. Kim et al. used an AFM cantilever to machine complex patterns in the thin layers of MoO_3 grown on the surface of MoS_2 [40]. An AFM tip also can be used as a vector positioner. Schaefer et al. showed the ability of an AFM tip to arrange Au clusters into a complex two dimensional (2D) pattern. These clusters were found to be stable at room temperature [41]. Various other studies were performed using AFM as a precise, controlled manipulator. Junno et al. demonstrated controlled manipulation of nanometer sized particles with the AFM, analogous to atomic scale precision as compared with STM. By controlled manipulation of 30 nm GaAs particles, they were able to form arbitrary nanostructures [42]. Falvo et al. showed a great deal of AFM use as a manipulator in terms of dissecting, rotating, and translating individual tobacco mosaic viruses with the help of an AFM tip. They found that the substrate-virus adhesion and the virus' elastic properties play important roles in the ability to manipulate them without inducing any damage. They proposed a mechanical model in which the shape of the virus affects the mechanical stability of the virus on to the substrate by changing the friction force between the sample and the virus [43]. A modified scanning force microscope capable of magnetically driven intermittent contact mode (MDIC) which had a direct manipulation interface that allowed for controlled nano-manipulation and an easily identifiable resonance peak

in liquid, Guthold et al. successfully manipulated adenovirus on a Si surface submerged in water [44]. A nano-robotic manipulation system was developed using an atomic force microscope probe as the pushing manipulator. Sitti et al. successfully positioned different sizes of latex particles ranging from 242 nm to 484 nm on a Si substrate. They performed simulations and experiments to determine the conditions and strategies for reliable manipulation and sought the affecting parameters [25].

1.3 Research significance and application

Overcoming the limitations of the Scanning Tunneling Microscope, AFM has become a powerful tool to understand micro/nano-scopic science because of its straightforward three dimensional measurements which can be extended to a wide variety of samples under different conditions [42, 45]. The use of atomic force microscopy/friction force microscopy (AFM/FFM) for nano-tribological studies has increased tremendously in the recent years to study surface properties at scales ranging from atomic, molecular, to micro-scales. These techniques are used to study friction, adhesion, scratching, wear, surface roughness, indentation, material transfer, and for nanofabrication or nano-machining purposes. Friction and wear are well studied at the macro-scale but are also very crucial in a fundamental understanding at the micro/nano-scale [7]. For a sliding interface such as magnetic storage which requires a near zero friction and wear, and, therefore, suitable lubricant coating, nano-tribological characterization becomes most significant [33]. The most popular word in the field of science research has become Nanotechnology. The aim in this field is the miniaturization of devices and machines down to atomic and molecular size (examples are micro/nano-size sensors, tera-byte capacity super compact memories, micro/nano-robots for materials and biological applications, DNA computers, quantum devices, micro/nano-scale intelligence system devices, actuators and communication tools). Success requires a precise

control over the position of atoms, molecules or nano scale objects. AFM or LFM is helping as a nano-manipulator to achieve this goal [25].

Nanoparticles are used as lubricants or building blocks in micro/nano-electromechanical system/devices (MEMS/NEMS) which require a clear understanding of these particles behavior during nano-manipulation [2]. Stiction, friction and wear have profound influence on the performance of these devices. Stiction and wear can lead to the failure of integrated accelerometers, which are used in the development of air bags in automobile engineering and digital micro-mirror devices. The ability to control stiction, friction and wear will significantly help the MEMS/NEMS industry [46]. The AFM cantilever has proven its ability in nano-manipulation of devices.

The nano-tribological characterization presented in this study likely will be used to understand and control the frictional behavior of micro/nano-size particles for prototypes particle based micro/nano devices and fabrication templates, particle based lubrication, aerosol, and particle removal applications [1, 41]. The study outcomes will help understand the different interaction forces such as electrostatic, van der Waals interactions etc. and how they affect the interfacial energy between a micro/nano-sphere and a flat surface [32]. One suitable application of the findings from this study would be in the cleaning of semiconductor wafers. Unwanted particulates on a semiconductor wafer can cause circuit defects which yields loss in the final product. Chemical mechanical polishing (CMP) is used to planarize the wafer surface, but it leaves residue on the wafer and, again, may cause circuit failure. Post CMP cleaning is expensive and causes critical environmental issues. Using AFM as nano-manipulator and understanding the particle adhesion of these particles on the wafer can help achieve defect free semiconductor wafer post fabrication by removing unwanted particles efficiently and economically [47].

1.4 References

[1] B. Sümer, M. Sitti, Rolling and spinning friction characterization of fine particles using lateral force microscopy based contact pushing, J Adhes Sci Technol, 22 (2008) 481-506.

[2] M. Evstigneev, K. Mougin, P. Reimann, Modeling of nanoparticle manipulation by AFM: Rolling vs. sliding regimes, Epl-Europhys Lett, 101 (2013).

[3] M. Sitti, Atomic force microscope probe based controlled pushing for nanotribological characterization, Ieee-Asme T Mech, 9 (2004) 343-349.

[4] B. Bhushan, Handbook of micro/nano tribology, CRC press, 1998.

[5] M.H. Korayem, M. Zakeri, Sensitivity analysis of nanoparticles pushing critical conditions in 2-D controlled nanomanipulation based on AFM, Int J Adv Manuf Tech, 41 (2009) 714-726.

[6] L.O. Heim, J. Blum, M. Preuss, H.J. Butt, Adhesion and friction forces between spherical micrometer-sized particles, Phys Rev Lett, 83 (1999) 3328-3331.

[7] A. Buldum, J.P. Lu, Atomic scale sliding and rolling of carbon nanotubes, Phys Rev Lett, 83 (1999) 5050-5053.

[8] H.P. Jost, Tribology—origin and future, Wear, 136 (1990) 1-17.

[9] J. Krim, Resource Letter: FMMLS-1: Friction at macroscopic and microscopic length scales, American Journal of Physics, 70 (2002) 890-897.

[10] H. Hertz, Ueber die Berührung fester elastischer Körper, Journal für die reine und angewandte Mathematik, 92 (1882) 156-171.

[11] K. Johnson, K. Kendall, A. Roberts, Surface energy and the contact of elastic solids, Proceedings of the royal society of London. A. mathematical and physical sciences, 324 (1971) 301-313.

[12] D. Tabor, Surface forces and surface interactions, Journal of Colloid and Interface Science, 58 (1977) 2-13.

[13] V.M. Muller, V.S. Yushchenko, B.V. Derjaguin, General theoretical consideration of the influence of surface forces on contact deformations and the reciprocal adhesion of elastic spherical particles, Journal of Colloid and Interface Science, 92 (1983) 92-101.

[14] D. Maugis, Adhesion of spheres: the JKR-DMT transition using a Dugdale model, Journal of Colloid and Interface Science, 150 (1992) 243-269.

[15] G. Binnig, C.F. Quate, C. Gerber, Atomic force microscope, Phys Rev Lett, 56 (1986) 930.

[16] C.M. Mate, G.M. Mcclelland, R. Erlandsson, S. Chiang, Atomic-Scale Friction of a Tungsten Tip on a Graphite Surface, Phys Rev Lett, 59 (1987) 1942-1945.

[17] U. Landman, W.D. Luedtke, N.A. Burnham, R.J. Colton, Atomistic Mechanisms and Dynamics of Adhesion, Nanoindentation, and Fracture, Science, 248 (1990) 454-461.

[18] S. Achanta, T. Liskiewicz, D. Drees, J.P. Celis, Friction mechanisms at the micro-scale, Tribol Int, 42 (2009) 1792-1799.

[19] R. Luthi, E. Meyer, H. Haefke, L. Howald, W. Gutmannsbauer, H.J. Guntherodt, Sled-Type Motion on the Nanometer-Scale - Determination of Dissipation and Cohesive Energies of C-60, Science, 266 (1994) 1979-1981.

[20] M.R. Falvo, R.M. Taylor, A. Helser, V. Chi, F.P. Brooks, S. Washburn, R. Superfine, Nanometre-scale rolling and sliding of carbon nanotubes, Nature, 397 (1999) 236-238.

[21] M.R. Falvo, J. Steele, R.M. Taylor, R. Superfine, Evidence of commensurate contact and rolling motion: AFM manipulation studies of carbon nanotubes on HOPG, Tribol Lett, 9 (2000) 73-76.

[22] O. Tevet, P. Von-Huth, R. Popovitz-Biro, R. Rosentsveig, H.D. Wagner, R. Tenne, Friction mechanism of individual multilayered nanoparticles, P Natl Acad Sci USA, 108 (2011) 19901-19906.

[23] S.G. Vilt, N. Martin, C. McCabe, G.K. Jennings, Frictional performance of silica microspheres, Tribol Int, 44 (2011) 180-186.

[24] H.J. Kim, K.H. Kang, D.E. Kim, Sliding and rolling frictional behavior of a single ZnO nanowire during manipulation with an AFM, Nanoscale, 5 (2013) 6081-6087.

[25] M. Sitti, H. Hashimoto, Controlled pushing of nanoparticles: Modeling and experiments, Ieee-Asme T Mech, 5 (2000) 199-211.

[26] M. Sitti, Nanotribological characterization system by AFM based controlled pushing, in: Nanotechnology, 2001. IEEE-NANO 2001. Proceedings of the 2001 1st IEEE Conference on, 2001, pp. 99-104.

[27] J.A. Hurtado, K.S. Kim, Scale effects in friction of single–asperity contacts. I. From concurrent slip to single–dislocation–assisted slip, Proceedings of the Royal Society of London. Series A: Mathematical, Physical and Engineering Sciences, 455 (1999) 3363-3384.

[28] S. Krijt, C. Dominik, A. Tielens, Rolling friction of adhesive microspheres, Journal of Physics D: Applied Physics, 47 (2014) 175302.

[29] N.A. Burnham, D.D. Dominguez, R.L. Mowery, R.J. Colton, Probing the Surface Forces of Monolayer Films with an Atomic-Force Microscope, Phys Rev Lett, 64 (1990) 1931-1934.

[30] G.S. Blackman, C.M. Mate, M.R. Philpott, Atomic Force Microscope Studies of Lubricant Films on Solid-Surfaces, Vacuum, 41 (1990) 1283-1286.

[31] D.M. Schaefer, M. Carpenter, R. Reifenberger, L.P. Demejo, D.S. Rimai, Surface Force Interactions between Micrometer-Size Polystyrene Spheres and Silicon Substrates Using Atomic-Force Techniques, J Adhes Sci Technol, 8 (1994) 197-210.

[32] B. Gady, D. Schleef, R. Reifenberger, D. Rimai, L.P. DeMejo, Identification of electrostatic and van der Waals interaction forces between a micrometer-size sphere and a flat substrate, Phys Rev B, 53 (1996) 8065-8070.

[33] B. Bhushan, S. Sundararajan, Micro/nanoscale friction and wear mechanisms of thin films using atomic force and friction force microscopy, Acta Mater, 46 (1998) 3793-3804.

[34] R. Mercadé-Prieto, Z. Zhang, Mechanical characterization of microspheres-capsules, cells and beads: a review, Journal of microencapsulation, 29 (2012) 277-285.

[35] J. Chen, Understanding the nanoindentation mechanisms of a microsphere for biomedical applications, Journal of Physics D: Applied Physics, 46 (2013) 495303.

[36] A.J. Heim, W.G. Matthews, T.J. Koob, Determination of the elastic modulus of native collagen fibrils via radial indentation, Appl Phys Lett, 89 (2006) 181902.

[37] S.R. Cohen, G. Neubauer, G.M. Mcclelland, Nanomechanics of a Au-Ir Contact Using a Bidirectional Atomic Force Microscope, J Vac Sci Technol A, 8 (1990) 3449-3454.

[38] M. Griepentrog, G. Krämer, B. Cappella, Comparison of nanoindentation and AFM methods for the determination of mechanical properties of polymers, Polymer Testing, 32 (2013) 455-460.

[39] O.M. Leung, M.C. Goh, Orientational Ordering of Polymers by Atomic Force Microscope Tip-Surface Interaction, Science, 255 (1992) 64-66.

[40] Y. Kim, C.M. Lieber, Machining Oxide Thin-Films with an Atomic Force Microscope - Pattern and Object Formation on the Nanometer Scale, Science, 257 (1992) 375-377.

[41] D.M. Schaefer, R. Reifenberger, A. Patil, R.P. Andres, Fabrication of 2-Dimensional Arrays of Nanometer-Size Clusters with the Atomic-Force Microscope, Appl Phys Lett, 66 (1995) 1012-1014.

[42] T. Junno, K. Deppert, L. Montelius, L. Samuelson, Controlled Manipulation of Nanoparticles with an Atomic-Force Microscope, Appl Phys Lett, 66 (1995) 3627-3629.

[43] M.R. Falvo, S. Washburn, R. Superfine, M. Finch, F.P. Brooks, V. Chi, R.M. Taylor, Manipulation of individual viruses: Friction and mechanical properties, Biophys J, 72 (1997) 1396-1403.

[44] M. Guthold, G. Matthews, A. Negishi, R. Taylor, D. Erie, F. Brooks, R. Superfine, Quantitative manipulation of DNA and viruses with the nanomanipulator scanning force microscope, Surface and interface analysis, 27 (1999) 437-443.

[45] K.A. Ramirez-Aguilar, K.L. Rowlen, Tip characterization from AFM images of nanometric spherical particles, Langmuir, 14 (1998) 2562-2566.

[46] H.W. Liu, B. Bhushan, Nanotribological characterization of molecularly thick lubricant films for applications to MEMS/NEMS by AFM, Ultramicroscopy, 97 (2003) 321-340.

[47] W. Shin, J. An, J. Kim, H. Jeong, Determination of Adhesion Force of Particles on Substrate Surface using Atomic Force Microscopy, in: Planarization/CMP Technology (ICPT 2012), International Conference on, VDE, 2012, pp. 1-6.

2.0 Experimental methods and techniques

2.1 Atomic force microscopy

Since its invention in 1980 by Gerd Binnig and Heinrich Rohrer, which earned them a Nobel Prize in Physics in 1986, the Atomic Force Microscope has become a popular tool for investigating surface and mechanical properties of biological and semiconductor materials. It can create 3-D micrographs with resolution down to the nano-scale or even sub-angstrom level. The cantilever is the key imaging element of an AFM. This cantilever is typically etched from single crystal silicon or cast from silicon nitride. A sharp tip extends from one end of this cantilever, and the sharpness of this tip in large part determines the lateral resolution of the images it produces. The probe tip is brought into close proximity with the sample, either in contact or oscillated to make intermittent contact. The base of the cantilever, affixed through a larger piece of material from which it is comprised, is mounted physically to a piezoelectric crystal, the so-called z-piezo. Voltage applied across the electrodes of the piezo results in motion in in the microscopic range, providing positional control on the sub-Angstrom level. The tip then is raster scanned over a region of the sample surface. The lateral motion for the scan is produced either by torsion of the z-piezo to which the cantilever is attached or by using additional piezos (the x-piezo for the fast scan direction and the y-piezo for the slow scan direction) to translate the sample underneath the tip. Deflections of the cantilevered beam are monitored by tracking the spot of a laser reflected from the side of the cantilever opposite that of the tip. This tracking is accomplished through the use of a four quadrant photodiode array – vertical deflections are registered as the difference in the sum

signal of the top two quadrants and that of the bottom two quadrants. Likewise, torsion of the cantilever is measured by the difference between the sum of the left two quadrants and the sum of the right two quadrants [1].

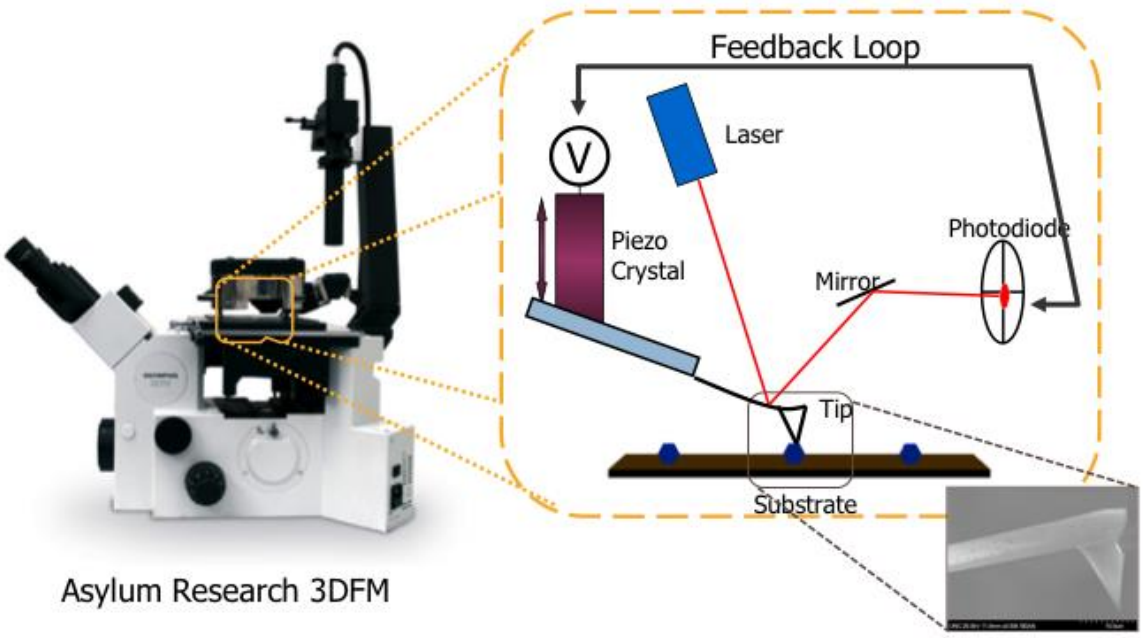

Figure 2.1: Schematic of an Atomic Force Microscopy.

The instrument commonly is operated in one of two different modes, contact mode (or DC mode) or intermittent contact mode (or AC mode). In contact mode, as the tip is scanned over the surface, interactions of the tip with the topographic features cause the cantilever to deflect either upward for raised features or downward for cavities. A feedback loop is established to minimize such deflections by varying the voltage on the z-piezo in response to vertical motion of the laser spot of the diode, moving the base of the cantilever to compensate for changes in the surface topography and maintaining a constant deflection of the cantilever. By doing so, a nearly constant force between the tip and the sample is maintained while the required voltage applied to the z-piezo provides a record of the surface contour. Calibration of the voltage response of the z-piezo

allows for a spatial reconstruction of the surface. This contact mode of imaging is the simplest method that provides a constant tip-sample contact force; however, it also results in relatively large shearing forces between the tip and the sample. AC mode was developed, in part, to improve upon this weakness. In AC mode, the cantilever is driven on resonance by either a small sinusoidal signal applied to the z-piezo or to a dithering piezo inserted in mechanical connection with the cantilever. The resulting oscillatory motion of the tip-end of the cantilever is monitored by the photodiode. The feedback loop, instead of maintaining a constant deflection, is now used to maintain a constant amplitude for the oscillating tip. Otherwise, the operation of the instrument is quite similar to contact mode. The tip is raster scanned, interactions of the tip with the sample either damp or increase the oscillation amplitude as the surface rises toward or falls away from the tip, the feedback loop minimizes these fluctuations in amplitude by varying the voltage applied to the z-piezo and, thereby, the position of the base of the cantilever, and the surface topography is reproduced based upon this applied voltage.

While the instrument has a rather simple method by which it operates, it has significant power. The resolution of AFM in the vertical direction is comparable to that of the best electron microscopes, but the AFM has the advantage that its mechanical method of collecting images requires neither vacuum nor stains. Materials may be imaged under a variety of solvents. In particular, biological samples may be imaged under aqueous buffers that are much closer to their native environments. And, these samples can be prepared by simple adsorption from solution onto planar substrates without the use of a heavy metal dye or coating. Likewise, polymeric samples can be imaged under varying solvent conditions, again with rather simple sample preparation.

Beyond the topographical image of a sample, the AFM also can extract a variety of other important physical properties from a sample, including mapping of magnetic domains, adhesion,

elasticity, and friction. Because the deflection of the cantilevered beam is monitored as the tip interacts with the surface, including both in the normal direction as well as in torsion, this instrument can be used to characterize the interaction strength between the tip and the substrate both vertically and horizontally. Careful calibration of the mechanical properties of the cantilever allows for the quantification of these measurements [2]. The work presented in this document focuses primarily on extracting the elastic modulus and adhesion forces of nanoscale samples using forces applied by the tip in the vertical direction. Details of this process will be given below. Future experiments are proposed in which the torsion of the cantilever will be used to measure the friction between similar samples and the underlying substrate. The measured friction forces will be interpreted using the results of the elasticity and adhesion experiments.

2.2 Scanning probe force microscopy

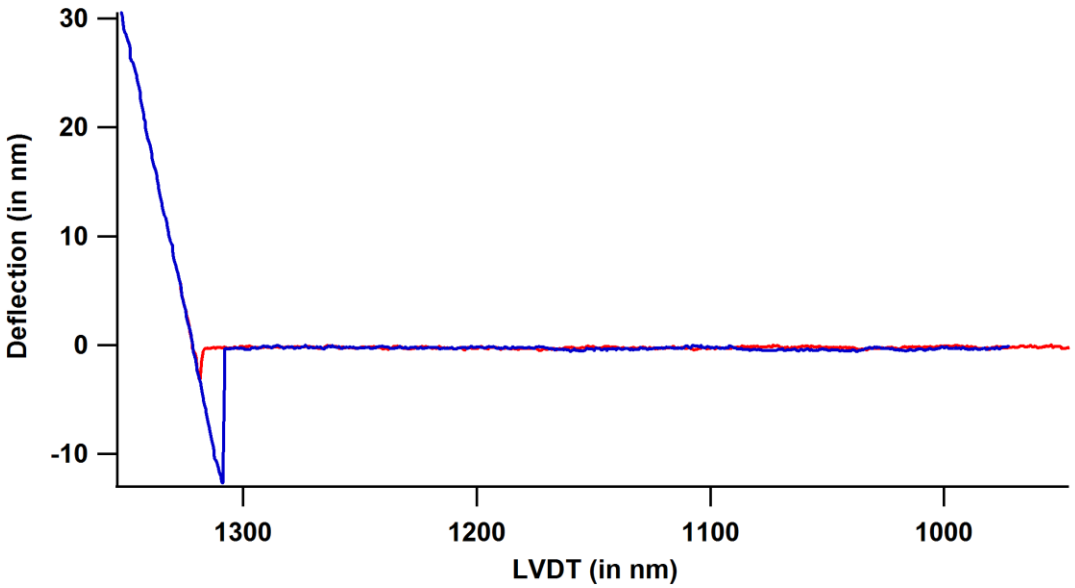

Figure 2.2: Plot of the Deflection versus Linear Variable Differential Transformer (LVDT) in a typical force curve. LVDT is the distance the z-piezo moves and tracks the position of the base of the cantilever. The Deflection is the distance the tip end of the cantilever has been displaced from its rest position. Positive deflection is away from the sample, negative is toward the sample. The approach curve is shown in red, the withdrawal in blue.

Scanning probe microscopy (SPM), a name given to a class of nanoscale materials characterization tools based upon AFM, has become a popular method with which to explore the surface properties at the nanoscale. In particular, for our applications it is the best tool for directly measuring nanomechanical properties and nanoscale friction [2].

Nanoindentation is the most common technique used for the extraction of the elastic modulus of samples with sizes below 1 μm. While other tools exist, AFM and SPM have come to dominate this field. A typical indentation experiment using AFM (called a force curve) is performed by using the z-piezo to first approach and then withdraw the base of the cantilever over some linear distance on the order of a micron (see figure 2.2). During the approach process

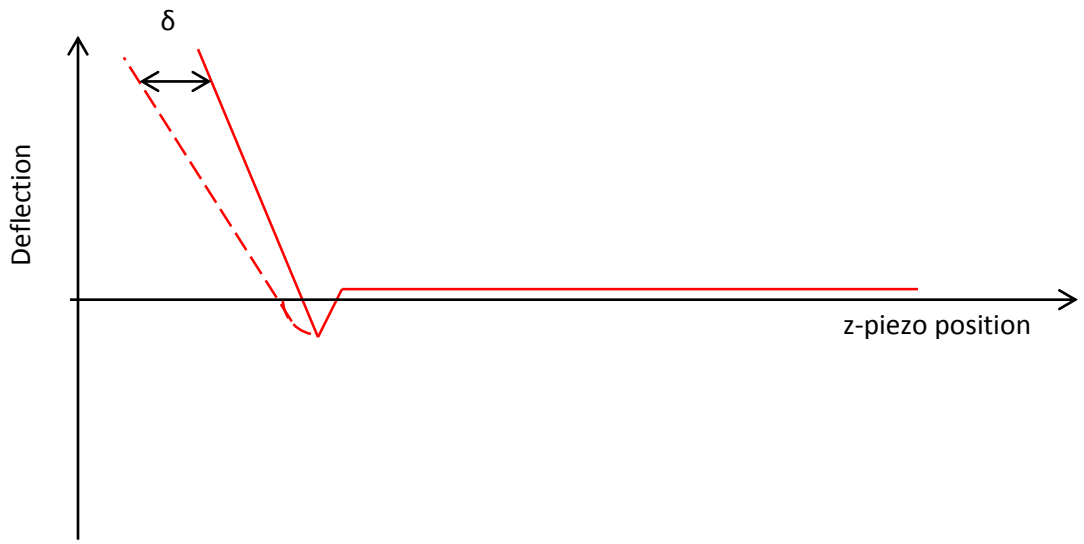

Figure 2.3: Schematic of the approach curve for a hard sample (solid line) and a soft sample (dashed line). The indentation δ of the soft sample is the horizontal difference in the deflection.

(shown in red in the figure 2.2), the sharp tip of the cantilever first nears the sample, then makes contact, followed by being pressed into the sample by a force applied through the cantilever. The system is quasi-static in nature, so the sample pushes back with an equal force. The cantilever bends in a direction normal to the surface, and, through knowledge of the mechanical properties of the cantilevered beam plus its deflection, the force required to indent the sample can be

determined. The extent of the indentation for the paired applied force is found by performing an initial force curve on an 'infinitely hard' (much more rigid than the sample) surface. The difference between the deflection of the cantilever on the hard surface and the softer sample provides the indentation (see figures 2.3 and 2.4). The second half of the force curve reverses the process with the cantilever withdrawing to its original starting position. During the withdrawal,

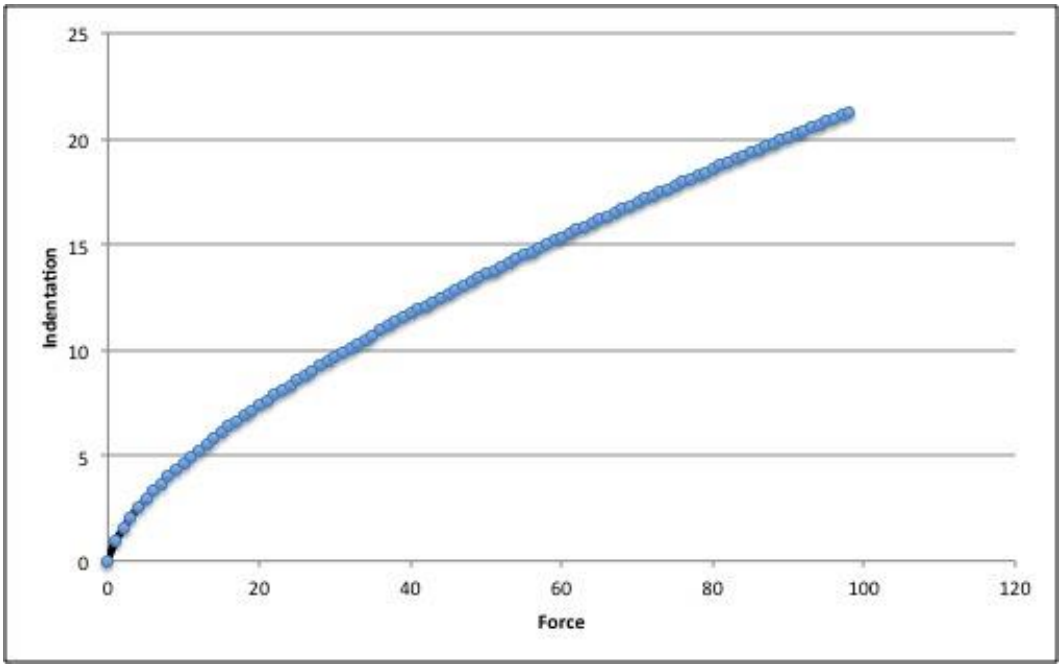

Figure 2.4: Schematic of a plot of Indentation versus Force. The axes have arbitrary scale.

the deflection of the cantilever decreases, reflecting the decreasing force applied by the tip on the sample. Eventually a zero applied force is reached, after which the cantilever bends toward the sample – the cantilever is pulling on the tip which is adhered to the surface. This deflection toward the sample continues to increase until the cantilever is pulling with a force large enough to overcome the adhesion between the tip and the sample. The tip snaps free from the surface, and the cantilever returns to its rest position as it continues to the stopping distance above the sample [2].

2.3 Elastic modulus and Hertz model

In the work to be presented, we indent polystyrene microspheres with the help of an AFM tip. Under certain conditions, both the silicon tip and the microsphere can be considered elastic in nature. When elastic bodies are pressed against each other, they deform each other's surfaces. Heinrich Hertz was the first quantitatively measure and describe the interaction between two smooth surfaces in 1895. In this work, the Hertz model will be used to analyze the data recorded [3-5]. This choice is appropriate for systems with a weak surface interaction, which we expect for our samples under solution.

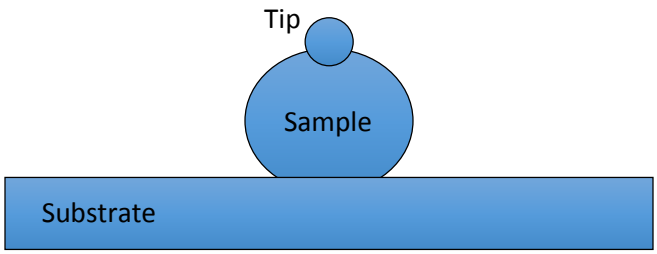

Figure 2.5: Schematic of the spherical sample being deformed by the tip and the supporting substrate.

From the Hertz model, when two elastic spheres are pressed one against the other, the indentation δ as a function of the applied force F is given by

$$\delta = \left[\frac{9}{16}(k_1 + k_2)^2 \frac{R_1+R_2}{R_1 R_2}\right]^{\frac{1}{3}} F^{\frac{2}{3}} \qquad (2.1), \text{ with}$$

$$k_1 \equiv \frac{1-\nu_1}{E_1} \qquad (2.2), \text{ and}$$

$$k_2 \equiv \frac{1-\nu_2}{E_2} \qquad (2.3).$$

where R_1 and R_2 are the radii of the spheres, E_1 and E_2 are their elastic moduli, and ν_1 and ν_2 are their Poisson ratios. In our system we will be using a silicon AFM tip (which is essentially spherical) to indent polymeric spheres, and in the equations above subscript 1 will be assigned to

the sample and 2 to the tip. The elastic modulus of silicon is much, much larger than that expected for the polymer sphere; therefore $k_1 >> k_2$ and k_2 can be neglected. So, for the tip indenting the sample a slightly simplified equation can be used:

$$\delta = \left[\frac{9}{16}k_1^2\frac{R_1+R_2}{R_1R_2}\right]^{\frac{1}{3}}F^{\frac{2}{3}} \qquad (2.4)$$

In our experiments, the sample spheres are supported by a planar silicon substrate. If we again consider the Hertz equation given above with the sample's characteristics labeled 1 and the substrate's 2, $k_1 >> k_2$ as before. However, since the radius of the flat substrate approaches infinity.

$$\frac{R_1+R_2}{R_1R_2} \rightarrow \frac{1}{R_1}$$

The resulting equation for indenting the spherical sample with the planar substrate then is given by,

$$\delta = \left[\frac{9}{16}\frac{k_1^2}{R_1}\right]^{\frac{1}{3}}F^{\frac{2}{3}} \qquad (2.5)$$

The total indentation is the sum of these two indentations, which simplifies to

$$\delta = \left[\frac{9}{16}k_1^2\frac{R_1+R_2}{R_1R_2}\right]^{\frac{1}{3}}F^{\frac{2}{3}} + \left[\frac{9}{16}\frac{k_1^2}{R_1}\right]^{\frac{1}{3}}F^{\frac{2}{3}} = \left(\frac{9}{16}k_1^2\right)^{\frac{1}{3}}\left[\left(\frac{R_1+R_2}{R_1R_2}\right)^{\frac{1}{3}} + \left(\frac{1}{R_1}\right)^{\frac{1}{3}}\right]F^{\frac{2}{3}} \qquad (2.6)$$

The 2/3 dependence of the indentation on the force was used to generate the schematic data shown in figure 2.4 above and can be seen in the negative curvature in this plot.

2.3.1 Adhesion measurements from force curves

Adhesion measurement of the force of adhesion between AFM tips and substrates is another common application of SPM. Simply, the adhesive force is found from the largest downward deflection of the cantilever during the withdrawal portion of the force curve [6, 7]. In figure 2.2, this would be the point (1320 nm, -13 nm) along the blue trace. After calibration of the spring constant of the cantilever, multiplication of this spring constant with the largest downward deflection gives the force of adhesion. More detail of such experiments will be given below.

2.4 Lateral force microscopy

The force required to translate a nanoscale object across a surface is measured by the torsion of the cantilever during the process. Commonly the torsion spring constant is found through beam mechanics from the normal spring constant:

$$k_{tor} = 1.33 \frac{G}{E} \left(\frac{L}{l_{tip}} \right)^2 k_n \qquad (2.7)$$

where G and E are the shear and elastic moduli of silicon (the material from which the cantilever is etched, L is the length of the cantilever, l_{tip} is the length of the tip, and k_{tor} and k_n are the torsion and normal spring constants, respectively. The length of the cantilever is supplied by the manufacturer and typically has a very small tolerance. The length of the tip, though also specified by the manufacturer, often has larger variation and will be measured in the Scanning Electron Microscope (SEM). Once calibrated, the force creating the torsion of the cantilever is found by multiplying the lateral deflection with the torsion spring constant.

In a typical friction measurement, the tip starts from a stationary position in contact with the substrate. The cantilever is moved laterally toward the object of interest through some

predetermined distance. The path is chosen such that the direction of motion is perpendicular to the long axis of the cantilever, thereby producing maximal torsional deflections of this beam and a maximal signal for measurement. Because the tip has adhered to the substrate, as the motion begins the cantilever moves before the end of the tip. The cantilever twists increasingly until the force generated on the tip is large enough to overcome the adhesion, and the tip starts sliding. When the tip makes initial contact with the object under investigation, it either becomes stationary or slows its motion. The cantilever continues to move laterally, increasing its torsion and the lateral force applied by the tip to the object. Once the lateral force is large enough to displace the object, the object begins to translate with the tip. The force required for this translation includes the friction force between the tip and the substrate, between the sample object and the substrate, and (potentially, if there is rolling) between the tip and the sample object. Measurements of the friction between the object and the substrate thus require knowledge of the friction between the tip and the substrate, to be subtracted out as a background, and the mode of translation – rolling or sliding. If the object is rolling, then the tip surface and that of the substrate must be accounted for. The easiest way to do this is to make both surfaces match. For this reason we will be using silicon cantilevers/tips as well as silicon substrates. The same silane chemistry will be done on each to simplify this analysis.

Knowledge of the mode of translation is a unique aspect of this work. In previous work investigating the translation of icosahedral virus capsids (adenovirus) [8] it was observed that Fourier transforms of the lateral force data trace (see figure 2.6) highlighted periodic features

within the trace, and these features could be ascribed spatially to dislodging facets of the icosahedron as the tip rolled the virus. When spherical control objects were translated in a similar manner, the periodic features disappeared. Thus the Fourier analysis of the lateral data trace offers

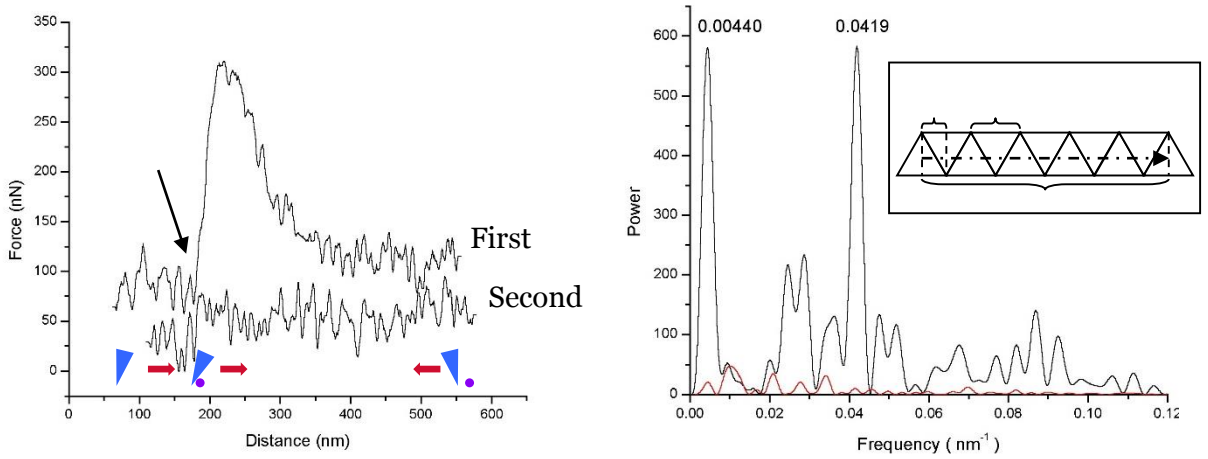

Figure 2.6: Left: Sample force traces (plot of lateral force versus distance moved by the AFM tip) for the first and second time a capsid is translated. The arrow indicates the increase in the lateral force that occurs as the tip contacts the virus (shown schematically along the Distance axis. **Right:** Fourier spectra of second trace shown on the left and a trace taken while translating a 100 nm polystyrene microsphere (curve lying near the horizontal axis). The labeled peaks correspond to the distance between facets and the capsid circumference, illustrated schematically in the inset. Further enhance data not shown in [24].

a powerful means to discover the modes of translocation between rolling and sliding. In the present study, Fourier analysis will be used to investigate the translocation mode of polystyrene microspheres. However, because our samples are spherical, an asymmetry must be introduced.

This will be achieved by performing a normal force curve to the microspheres, applying a force that exceeds the plastic limit. An indentation should be left in the surface of the sphere, giving us the asymmetry needed to produce periodic features for detection by Fourier analysis. If such features are not apparent, it is likely that the sample is sliding.

2.5 Cantilever spring constant measurement

The nanoindentation and lateral force measurements will be performed using the tip of an AFM, as described above. Calibration of the spring constant of the AFM cantilevers will be carried out using the standard thermal method. In the thermal method, the AFM cantilever is approximated as a simple harmonic oscillator with one degree of freedom for small deflections. The equipartition theorem assigns an average of (1/2)*k_B*T, to each degree of freedom in this system, where k_B is Boltzmann's constant, and T is temperature. Simply, the thermally driven resonance spectrum of the cantilever is recorded and fit to an equation.

$$\frac{1}{2} k_B T = \frac{1}{2} k x^2 \qquad (2.8)$$

where k is the cantilever's spring constant and x^2 is the root mean square (RMS) displacement of the cantilever due to thermal excitation. This RMS displacement is the measured cantilever deflection signal, converted from a voltage into a displacement by first calibrating the cantilever's sensitivity or InvOLS (Inverse Optical Lever Sensitivity). It is calculated by integrating under the square of the thermal plot (amplitude spectral density) of the cantilever. From this equation, the spring constant is extracted [9]. The technique is established well enough that it is now implemented through the manufacturer's software.

The Hertz equations used require knowledge of the radii of the microsphere and the tip. The radius of the microspheres can be determined directly as half of the height of the sphere when imaged by AFM. The radius of the tip can be extracted from the 'tip artifact' caused by the combination of the tip shape with that of the imaged sample. If x is half the measured width of the microsphere and R_1 and R_2 the radii of the sphere and tip, respectively, then

$$x = 2\sqrt{R_1 R_2} \qquad (2.9)$$

x is easily measured from the image collected of the sphere, and the radius of the microsphere is half of the measured height.

2.6 Plasma cleaning

To achieve optimum results during every step of this project, it is necessary to have a clean, contamination free substrate. Cleaning the substrate only with organic solvents leaves the substrate

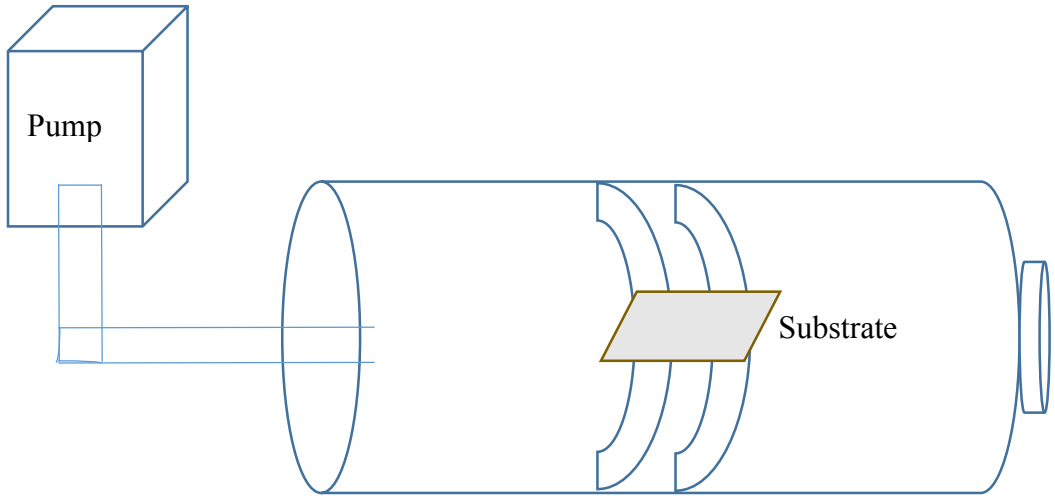

Figure 2.7: A schematic of the Plasma Cleaner.

with difficult to remove organic contaminants. Such contamination can limit the ability to perform accurate force microscopy analysis in this project. Plasma cleaning of the specimen has proven to be a highly effective method in microscopic analysis [10].

A schematic is shown in figure 2.7. Plasma is created using different gaseous species inside the thick walled glass chamber using high frequency voltage (in the range kHz to MHz). In this process various gases react with different materials. Gases such as oxygen, argon, as well as mixtures of air and hydrogen/nitrogen are used. These gas atoms are excited to higher energy states and ionized. When atoms or molecules relax to their ground state they release characteristic

photons. Oxygen plasma removes hydrocarbon contamination by converting it to carbon monoxide (CO), carbon dioxide (CO_2), and water vapor (H_2O), which are evacuated by the vacuum system. The color of the plasma plume depends on the gas used to generate plasma. We have utilized PDC – 32G plasma cleaner manufactured by Harrick Plasma. The background used in this system is air and the color of the plasma is purple. We bleed in small amounts of air, which changes the plasma color to rose. The color indicates the increased oxygen in the chamber.

2.7 Ultrasonic cleaning

Contamination present on a specimen can be complex in nature where the use of ultrasonic cleaning takes place. The importance and application of ultrasonic cleaning have been growing recently to achieve the maximum results towards precision cleaning [11]. Ultrasonic cleaning is one of the most efficient non-abrasive methods of cleaning which does not use the chemical dissolution of the substrate. This method is capable of removing more complex contaminants without damaging the surface of the substrate [12].

Ultrasonic cleaning uses cavitation and momentum transfer by the propagation of high intensity acoustic waves. In this process, ultrasound (ranging 20 – 400 kHz) is combined with an appropriate solvent to accomplish the complex cleaning. High frequency sound waves are used to agitate a liquid which produces very high forces on the contaminants adhered to the substrate. The specimen to be cleaned is placed in the chamber containing the cleaning solvent. Ultrasound is generated by piezoelectric transducers, which produces compressive ultrasonic waves. These waves tear the liquid apart by creating partial vacuum bubbles also known as cavitation. These bubbles collapse with very high energy, removing the dirt and contaminants from the specimen surface. Frequency can be increased to achieve precision cleaning of more intricate specimen. We

have used FS20H ultrasonic cleaner manufactured by Fisher Scientific. We have utilized two steps of cleaning (acetone and ethanol) followed by one step of rinsing in DI water. Each step undergoes a relatively long length (~ 15 minutes) cleaning to accomplish a crystal clean substrate.

2.8 References

[1] G. Binnig, C.F. Quate, C. Gerber, Atomic force microscope, Phys Rev Lett, 56 (1986) 930.

[2] H.-J. Butt, B. Cappella, M. Kappl, Force measurements with the atomic force microscope: Technique, interpretation and applications, Surface science reports, 59 (2005) 1-152.

[3] K. Johnson, K. Kendall, A. Roberts, Surface energy and the contact of elastic solids, Proceedings of the royal society of London. A. mathematical and physical sciences, 324 (1971) 301-313.

[4] H. Hertz, Ueber die Berührung fester elastischer Körper, Journal für die reine und angewandte Mathematik, 92 (1882) 156-171.

[5] L.D. Landau, E.M. Lifshitz, Course of Theoretical Physics Vol 7: Theory and Elasticity, Pergamon Press, 1959.

[6] D.C. Lin, E.K. Dimitriadis, F. Horkay, Robust strategies for automated AFM force curve analysis—I. Non-adhesive indentation of soft, inhomogeneous materials, Journal of biomechanical engineering, 129 (2007) 430-440.

[7] F. Rico, P. Roca-Cusachs, N. Gavara, R. Farré, M. Rotger, D. Navajas, Probing mechanical properties of living cells by atomic force microscopy with blunted pyramidal cantilever tips, Physical Review E, 72 (2005) 021914.

[8] M. Guthold, G. Matthews, A. Negishi, R. Taylor, D. Erie, F. Brooks, R. Superfine, Quantitative manipulation of DNA and viruses with the nanomanipulator scanning force microscope, Surface and interface analysis, 27 (1999) 437-443.

[9] J.L. Hutter, J. Bechhoefer, Calibration of atomic-force microscope tips, Review of Scientific Instruments, 64 (1993) 1868-1873.

[10] T. Isabell, P. Fischione, Applications of plasma cleaning for electron microscopy of semiconducting materials, in: MRS Proceedings, Cambridge Univ Press, 1998, pp. 31.

[11] F.J. Fuchs, Ultrasonic cleaning: Fundamental theory and application, (1995).

[12] A. Pereira, Ultrasonic cleaning: overview and state of the art, in, ATCP Physical Engineering, (2010) 1-14.

3.0 Materials

The experiments are designed to characterize the dependence of rolling and sliding friction upon such physical properties as size, elastic modulus, and adhesion. Thus we need samples that allow for these properties to be varied. For this reason polystyrene microspheres of different diameters and polished Si as surface substrate, were chosen.

3.1 Polystyrene microspheres

Polystyrene microspheres are available in a broad range of sizes extending down to a radius of 50 nm. Their elastic modulus can be varied through the use of solvents: polystyrene is soluble in ethanol but not water, and ethanol is miscible in water. By varying the dilution of ethanol in water the degree of swelling of the polymeric spheres can be tuned, and this swelling will modify the modulus. Control over the adhesion can be achieved through surface chemistry. The surface chemistry of the microspheres can be varied, either as purchased with amino- or carboxy-terminated groups on the surface or through further in-lab modification using coupling chemistry with these surface groups.

3.2 Polystyrene introduction

Polystyrene (abbreviation ‘PS’) also known as ‘Thermocole’ belongs to the group of thermoplastics which also includes polyethylene, polypropylene, and pol-vinyl chloride. Polymerization of styrene monomers results in Polystyrene. Figure 3.1, below shows the chemical structure of styrene monomer. PS is a long chain hydrocarbon where alternating carbon atoms are

attached to an aromatic benzene ring. During polymerization the C-C pi bond from the benzene group is broken to form a new C-C sigma bond and attaches another styrene monomer to the chain.

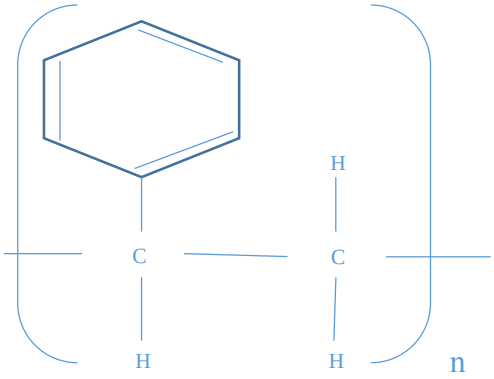

Figure 3.1: Showing chemical structure of Poly-styrene.

This newly formed sigma bond is much stronger than the pi bond, making it difficult to depolymerize the polystyrene. The chemical formula for polystyrene is $(C_8H_8)_n$. Short range van der Waals attraction between the polymer chains defines the materials properties. In general PS molecules contain thousands of atoms and the total attractive force between the molecules is large. Polystyrene melts at 240 ^oC, though decomposes at much lower temperature. In general polystyrene is clear, hard, brittle, and transparent [1].

3.3 Polystyrene application

Polystyrene comes in various forms and shapes and it is found almost everywhere in our daily life usage. Polystyrene products are heat resistant. They provide practical toughness, lightness, and strength to a wide range of uses such as electronic, appliances, packaging and medical products. The special property of polystyrene makes it very popular for various industrial applications. It is one of the most highly consumed materials worldwide which makes it a quantitatively important chemicals. In daily life it finds its use in protective packaging, containers, bottles, trays, lids etc. Foamed polystyrene is used in chemical packaging [2].

3.4 Polystyrene degradation

Polystyrene is chemically inert to acids and bases, though it can dissolve easily into chlorinated solvents and various other aromatic hydrocarbon solvents. Upon burning polystyrene breaks into CO_2 and water vapor. One of the biggest disadvantages is its non-biodegradability. Discarded PS does not degrade for hundreds of years, and it also is resistant to photolysis, creating a huge environmental concern [3].

3.5 Silicon substrate

The silicon substrate surface can be modified simply using silane chemistry. Thus this combination of polystyrene microspheres on silicon wafer allows for the control over the surface chemistry and adhesion needed for the investigation.

3.6 References

[1] J.R. Wünsch, Polystyrene: Synthesis, production and applications, iSmithers Rapra Publishing, 2000.

[2] J.E. Mark, Polymer data handbook, Oxford University Press, 2009.

[3] M.P. Stevens, Polymer chemistry, oxford university press New York, 1990.

4.0 Elastic modulus of polystyrene microspheres of different sizes

4.1 Introduction

Investigation of mechanical properties has become one of the most fundamental studies in mechanical characterization. The mechanical testing provides important information about materials structure. The local mechanical properties of polymers at the nano/micro-sphere level is of fundamental importance for their use in the scientific and technological applications. This information is useful both at the bulk and nanostructured scales. Furthermore, recent technological advancements require mechanical characterization of nanosized or nanostructured materials, this has become important since the knowledge of mechanical properties gained by conventional methods on the macro scale is not always valid at the nano/micro-scale. A semi crystalline polymer may be treated as homogenous at the bulk for the mechanical properties, but at the nano/micro-scale it potentially can have both crystalline and amorphous mechanical properties [1, 2].

Nano/micro-spheres, which includes beads, cells, and microscapsules, have become an area of extensive research. The characterization of these nano/micro-spheres has a wide range of applications. It is important to characterize nano/micro-spheres for their mechanical properties before any manipulation. In bio-technology the knowledge of mechanical properties of cells is required. Some examples include; why some cancer cells are less stiff than the regular cells, to understand the effect of drug in cell stiffness, the mechanical effects of the non-uniform geometry of viral capsid, etc. There are several novel techniques used to characterize the mechanical properties of nano/micro-spheres [3]. Nanoindentation is used to measure various mechanical

properties such as hardness, elastic modulus, viscoelastic properties, fracture toughness, and interface toughness. Nanoindentation can also help with some other information such as creep, induced phase transformation etc. In general, a sharp probe is used for tough materials like ceramic, metallic, and hard tissues. For soft materials like polymers, soft tissues and biological cells, a spherical indenter is used. Such nanoindentation analysis can be performed either by using an AFM or a nanoindenter [4-6].

Since its invention the Atomic Force Microscope (AFM) has emerged as a powerful tool to study surface properties of nano/micro-spheres. The capability to control the applied normal force in the range of nanonewtons to piconewtons by changing the tip curvature and cantilever stiffness, gives it an advantage over a nanoindenter. Thus, we can expect AFM nanoindentation to provide an effective method to measure the elastic modulus of nano/micro-spheres [7-10].

The basic technique used for the mechanical properties of nano/micro-spheres is the class of force spectroscopy known as force curve analysis. The AFM probe is extended to the surface at a fixed point while the force and vertical deflection of the cantilever are recorded. The force versus cantilever deflection is plotted and contains the information about the short and long term interactions representing the basic estimation of the elastic modulus. The Hertz model most often is used to describe the elastic deformation of two perfectly homogenous smooth bodies touching under a given load. The sample and the cantilever can be modeled as two springs in series as tip-sample stiffness and cantilever spring constant respectively. Hertz model assumes the sample as an isotropic and linear elastic solid. The formulation shown previously also assumes that the probe is not deformable and there are no further interactions between the probe and the samples [2, 6, 7].

4.2 Elastic modulus

In this work we have used an Atomic Force Microscope (model MFP-3D, Asylum Research; Santa Barbara, CA), which is capable of producing images with resolution well below one nanometer, and is well designed for use in Force Spectroscopy measurements. The noise floor of this instrument in our lab is limited to ~3 Å by the quality of the air table (TMC, Peabody, MA) used for mechanical isolation from the environment. Silicon probes (AFM tips) were used and are commercially available (Mikromasch; Moscow, Russia). The typical resonant frequencies for these probes range between 150 – 190 kHz, and the spring constant is nominally ~ 45N/m. Polished silicon wafers have been used as substrates for the deposition of polystyrene microspheres (Polysciences, Warrington, PA).

4.3 Sample preparation

Sample preparation began with the rigorous cleaning of the Si substrates. Initially, the silicon wafers were cleaved into 1 cm x 1 cm squares using a diamond scribe, followed by plasma cleaning. Afterwards the silicon substrates were subjected to solvent cleaning in an ultrasonic bath for 15 minutes each. Solvent cleaning was performed first by acetone, followed by ethanol. To get rid of any hydrocarbon residue from the substrates, they were further cleaned in DI water in the ultrasonic bath, and the substrate was dried by nitrogen. A final plasma cleaning, followed by a DI water rinse and nitrogen drying, was performed. This multi-stage cleaning process removed any contaminants from the surfaces, whether silicon chips from the cleaving process or organic deposits from air or other solvents. Such contaminants had been observed to appear very similar to the polystyrene microspheres of interest when imaged by the AFM [11].

Commercially available polystyrene microspheres of sizes 50nm, 100nm, 200nm, and 500nm were used in this work. These samples were diluted, 1 part in 1000 by volume, in DI water (Barnstead E-Pure, Thermo-Fisher; Waltham, MA) to reduce the density of the microspheres on the substrate as desired. The diluted sample was then drop-cast on the Si substrate: 5 µl of diluted microspheres was deposited onto the substrate, followed by a 5 minute incubation, rinsed quickly thereafter with DI water, and dried under a nitrogen stream. The sample was then mounted in the AFM.

4.4 Atomic force microscopy

The imaging was performed in air using intermittent contact (aka AC) mode. 5 µm x 5 µm scan sizes were used, along with a 500 pixel x 500 line resolution. This gave a 10 nm x 10 nm pixel size. For force spectroscopy, particles of the expected height were software selected for measurement. The cantilever approach and withdrawal speed was set to 1 µm/s, and a force limit of 0.1 V, corresponding to ~0.4 nN, was prescribed. Force curves were performed both on separate microspheres and repeated on individual microspheres to assess variation in the data. The cantilever spring constants were calibrated using the thermal method, and the deflection versus z-piezo position data was converted to indentation versus force [12, 13]. The Hertz model described previously was fit to this data, and the elastic modulus extracted.

4.5 Results and discussion

After force calibration, topographical images of different sizes of microspheres were obtained to confirm the density of microspheres over a given scan area (see figure 4.1). These images are gray scale – the tallest areas have the lightest shading. A tip artifact is apparent in 4.1b and 4.1d, resulting in non-circular cross-sections of the spherical particles.

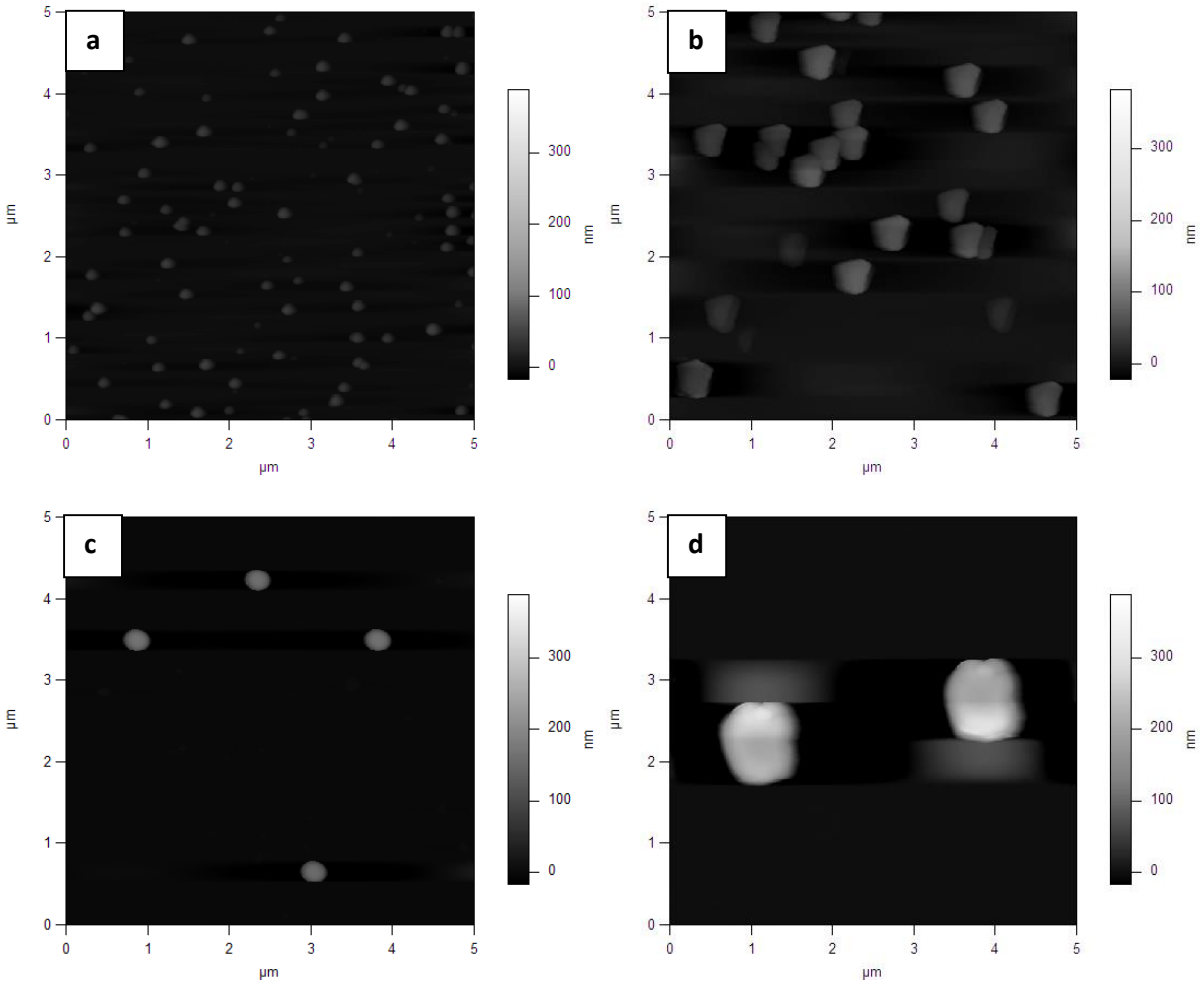

Figure 4.1: Atomic Force Microscope Images of Polystyrene microspheres of a) 50 nm, b) 100 nm, c) 200 nm, and d) 500 nm deposited on Si substrate.

The elastic modulus, E, was determined on a number of polystyrene microspheres by performing force spectroscopy in single and continuous modes. Microsphere sizes were chosen to be 50 nm, 100 nm, 200 nm, and 500 nm. A typical force curve and the resulting indentation versus force plot are shown in figure 2.2 above and figure 4.2 below, respectively. Table 4.1 summarizes the Elastic moduli as measured for these microspheres.

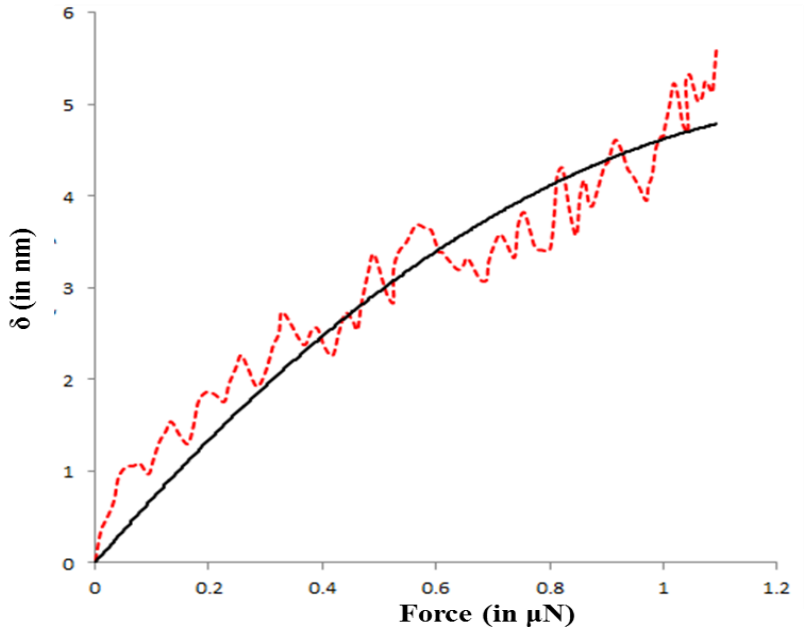

Figure 4.2: Indentation (δ) versus Force (F) graph (Fitted with Hertz model).

Table 4.1: The measured elastic modulus E of different sizes of microspheres in single and continuous mode and data comparison from the Student's t Test.

	Elastic Moduli (GPa)			
Size (nm)	Different PS Beads $\bar{\chi} \pm \sigma$ (N)	Same Bead $\bar{\chi} \pm \sigma$ (N)	Combined $\bar{\chi} \pm \sigma$ (N)	Student's t Test (Unpaired) P Value
50	1.94±0.63 (10)	2.27±0.49 (13)	2.13±0.57 (23)	0.1665
100	2.39±0.61 (9)	2.43±0.67 (9)	2.41±0.62 (18)	0.8884
200	2.21±0.75 (13)	2.27±0.49 (10)	2.24±0.64 (23)	0.8377
500	2.47±0.87 (10)	2.53±0.66 (11)	2.5±0.75 (21)	0.8730

Within table 4.1 are columns for measurements performed on multiple separate microspheres (Different PS Beads) and for repeated measures on the same microsphere (Same Bead). The elastic modulus of bulk polystyrene has been reported to be in the range of 2 – 5 GPa [11]. The E value obtained in the present study for the polystyrene microspheres in all cases is comparable to this bulk value. To assess the variability of the measured value for the elastic

modulus, a comparison between the results obtained for repeated measures on a single microsphere of a certain size and the results from measurements taken on multiple microspheres of that size was made. From the Student's t-test for unpaired data it was clear that the two data sets were indistinguishable. Because the data were indistinguishable, they were aggregated and listed in third column (combined) of table 4.1. These results demonstrate that, for this polymeric material, the bulk mechanical properties persist down to length scales on the 10's of nanometer. The larger variation in the moduli of the 50 nm microspheres potentially indicates that we are near the limit where the bulk values break down.

4.6 Conclusion

We report the elastic modulus E of commercially available polystyrene microspheres in the range of 1.94 – 2.53 GPa, which is comparable to the reported modulus of bulk polystyrene [11]. The work was carried out using an Atomic Force Microscopy, performing force spectroscopy on four different sizes of polystyrene microspheres deposited on a Si substrate. The obtained data from force spectroscopy was analyzed using Hertz model. The elastic moduli obtained were compared using Student's unpaired t tests. The probability P obtained among all sets of data, confirms that E values obtained are the same, regardless of whether taken from repeated measures on a single microsphere or aggregated measures from multiple microspheres. These results demonstrate both accuracy and precision for the technique. We conclude that the bulk mechanical properties of the material extend down to objects with dimensions of ~ 50 nm.

4.7 References

[1] M. Griepentrog, G. Krämer, B. Cappella, Comparison of nanoindentation and AFM methods for the determination of mechanical properties of polymers, Polymer Testing, 32 (2013) 455-460.

[2] D. Passeri, A. Bettucci, A. Biagioni, M. Rossi, A. Alippi, E. Tamburri, M. Lucci, I. Davoli, S. Berezina, Indentation modulus and hardness of viscoelastic thin films by atomic force microscopy: A case study, Ultramicroscopy, 109 (2009) 1417-1427.

[3] R. Mercadé-Prieto, Z. Zhang, Mechanical characterization of microspheres-capsules, cells and beads: a review, Journal of microencapsulation, 29 (2012) 277-285.

[4] J. Chen, Understanding the nanoindentation mechanisms of a microsphere for biomedical applications, Journal of Physics D: Applied Physics, 46 (2013) 495303.

[5] A.-Y. Jee, M. Lee, Comparative analysis on the nanoindentation of polymers using atomic force microscopy, Polymer Testing, 29 (2010) 95-99.

[6] T. Neumann, Determining the elastic modulus of biological samples using atomic force microscopy, JPK Instruments Application Report, (2008).

[7] T.G. Kuznetsova, M.N. Starodubtseva, N.I. Yegorenkov, S.A. Chizhik, R.I. Zhdanov, Atomic force microscopy probing of cell elasticity, Micron, 38 (2007) 824-833.

[8] T.-H. Fang, W.-J. Chang, S.-L. Tsai, Nanomechanical characterization of polymer using atomic force microscopy and nanoindentation, Microelectronics journal, 36 (2005) 55-59.

[9] K. Miyake, N. Satomi, S. Sasaki, Elastic modulus of polystyrene film from near surface to bulk measured by nanoindentation using atomic force microscopy, Appl Phys Lett, 89 (2006) 031925.

[10] K.D. Costa, M.M. Ho, C.T. Hung, Multi-scale measurement of mechanical properties of soft samples with atomic force microscopy, in: Summer Bioengineering Conference, 2003.

[11] S. Chizhik, Z. Huang, V. Gorbunov, N. Myshkin, V. Tsukruk, Micromechanical properties of elastic polymeric materials as probed by scanning force microscopy, Langmuir, 14 (1998) 2606-2609.

[12] B. Cappella, D. Silbernagl, Nanomechanical properties of polymer thin films measured by force–distance curves, Thin Solid Films, 516 (2008) 1952-1960.

[13] J.L. Hutter, J. Bechhoefer, Calibration of atomic-force microscope tips, Review of Scientific Instruments, 64 (1993) 1868-1873.

5.0 Tuning the mechanics of polymeric microspheres

5.1 Introduction

Mechanical properties have been demonstrated to play an important role in surface adhesion, friction and the translational properties of materials at the micro/nano-scale [1-4]. Thus understanding the mechanical properties of the polymeric materials at the micro/nano-scale has drawn great interest and inspired the tuning of these mechanical properties by various means [5]. While surface chemistry and topography of micro/nano-surfaces have been widely investigated and are considered equally important, new findings regarding the mechanical properties and how this can be tuned, has opened new possibilities. In particular, in the field of polymeric materials control over the mechanical properties expands the use of polymers for science, engineering, and biomedical applications [6].

Polymeric materials with different functional groups are widely available for numerous applications such as, osmotic pressure sensors, anti-corrosion coatings, free standing membranes, controlling wetting properties, and interactions with biological systems. Most relevant for the presented work, polymeric microspheres are found in the pharmaceutical, surface coating, food, and chemical industries. At the nanoscale these microspheres have mechanical properties that differ from those in bulk. A clear understanding of mechanical properties of these individual microspheres and developing techniques for the tuning of these mechanical properties over a broad range will further aid their applications within the above mentioned daily uses [7, 8].

Tuning the mechanics can be achieved from the outset of manufacturing of the material, using such approaches as changing the molecular weight of the polymer constituent of the microspheres, varying the cross-linking within microspheres, or using an appropriate additive. Other synthetic approaches relying on the use of random copolymers of controlled ratio of charged and uncharged monomers have also been used to tune the mechanics over many orders of magnitude [8].

Alternatively, the mechanics of the microspheres can be modified after their formation through varying the suspending solvent. It has been shown that the mechanical properties of the microcapsules depend on the encapsulated fluid and the shell thickness, and also on the pH and salt concentration when the capsules were kept in an aqueous medium. It was found that polyelectrolyte microcapsules are more rigid when filled with a polyelectrolyte solution rather than with pure water [9, 10]. Lubrasky et al., used UV irradiation in absence of oxygen, UV ozone combined, and UV irradiation (ozone only) to modify the near surface mechanical properties of polystyrene films [11]. There also have been efforts to tune mechanics of hydrated collagen fibrils. Grant et al., reported a decrease by three orders of magnitude of elastic modulus while under aqueous fluid when compared with those measured under the ambient conditions [12]. However, Yang et al., found very little change in shear modulus when a cross-linking molecule was applied to collagen fibrils [13].

We report tuning of the mechanics of polystyrene microspheres by varying the solvent, using DI water, ethanol, and varying water/ethanol mixtures. Polymeric materials suspended in water have many practical applications, such as immunoassays and drug delivery systems. A greater understanding of the interactions between polymers and such ethanol or a water-ethanol mixtures will find applications in the manufacturing of membranes, drug delivery systems, and

pervaporation [14, 15]. In this work we have developed a technique that precisely tunes the mechanics of polystyrene microspheres using DI water, ethanol, and mixture of DI water-ethanol as solvents. Water is a very weak solvent for polystyrene, and ethanol is only somewhat better. By using water and water/ethanol mixtures as a bathing solution, the polystyrene microspheres swell without dissolution. Such swelling dilutes the polymer molecules within the microspheres, spreading out the distances between entanglement points. This behavior will have the effect of reducing the elastic modulus as the microspheres swell. Here we discuss the measurement of the mechanics of PS microspheres under DI water, ethanol and their mixtures, following the microspheres' mechanics as they reach their absorption equilibrium volumes.

5.2 Flory-Rehner theory

The immiscibility of polystyrene in water and the complex nature of the water/ethanol mixture warrant further investigation of the swelling behavior of these microspheres [15]. Polymer swelling is an important technical topic which has applications in wide variety of technologies such as hydrogels, membrane science, biochemical protective clothing, and controlled release of drugs [16]. There is a long history of the theoretical understanding of swelling, and numerous molecular models have been developed to predict the elasticity and polymer swelling. The majority of these models were developed considering an ideal polymer network. A number of experimental works have been performed to test and evaluate these models, yet the validity and applicability of these models have not been established. Additionally, for non-ideal polymer networks, little is known about how the structure of a network influences the elasticity and swelling behavior [17].

By far, the most influential theoretical investigation of elasticity and polymer swelling was developed by Flory and Rehner in 1943. Since then, their theory has been applied to various cases

to explain the sorption equilibrium of cross-linked polymers exposed to a single solute. The three major interaction parameters found are cross-link density, temperature, and concentration. There have been considerable efforts made toward understanding the swelling in electrolytes and hydrogen bonding solvents [16]. S. V. Panyukov further developed the original idea of Flory-Rehner theory and presented equilibrium swelling of networks in a good solvent as a function of preparation conditions [18].

Flory-Rehner explained how the swelling equilibrium is dictated by a balance between the osmotic part of the free energy acting to swell the network and the elastic part of the free energy restricting the swelling [19, 20]. Experimentally, the swelling of the microspheres is tracked as ϑ, the volume fraction given by ratio of the condensed volume to the swollen volume, and the modulus is measured as this volume fraction varies. According to the Flory-Rehner theory, the modulus of elasticity of the gel is given by,

$$E = \left(\frac{R\,T\,\rho\,\upsilon^{\frac{1}{3}}}{M_c}\right)\left(1 + \frac{2}{\alpha^3}\right) \qquad (5.1)$$

where R is the gas constant, T is absolute room temperature, ρ is the density of the polymer, ϑ is the volume fraction, M_c is the molecular weight of the polymer chain, and α is the ratio of the elongated swollen polymer to its length in the unstressed condition. For the unswollen polymer, elasticity would be given by,

$$E = \left(\frac{R\,T\,\rho}{M_c}\right)\left(1 + \frac{2}{\alpha^3}\right) \qquad (5.2)$$

Clearly equation 5.1 differs by $\upsilon^{1/3}$ when compared with equation 5.2. This suggests that the modulus of the elasticity of the gel should decrease with the inverse cube root of the swollen volume, $E \sim 1 / \upsilon^{1/3}$. As part of our investigation, we attempted to validate this aspect of the Flory-

Rehner theory: does the elasticity indeed scale with polymer swelling within our polystyrene microspheres system in DI water and ethanol?

5.3 Experimental procedure

To determine how the solution surrounding the microspheres determines their mechanics, the experiments presented herein were performed on the same size range of polystyrene microspheres as had been used in our previous studies. We now performed the experiments under a varying but controlled fluid environment. We used ethanol and DI water as our primary solvents. Polystyrene microspheres were submerged in pure (95.27%) ethanol and 100% DI water during the force spectroscopy measurements. These two extremes provide the range over which we can expect to vary our sample modulus. The experiments were extended to include varying dilutions of ethanol in water for the solution in which the force spectroscopy experiments were performed.

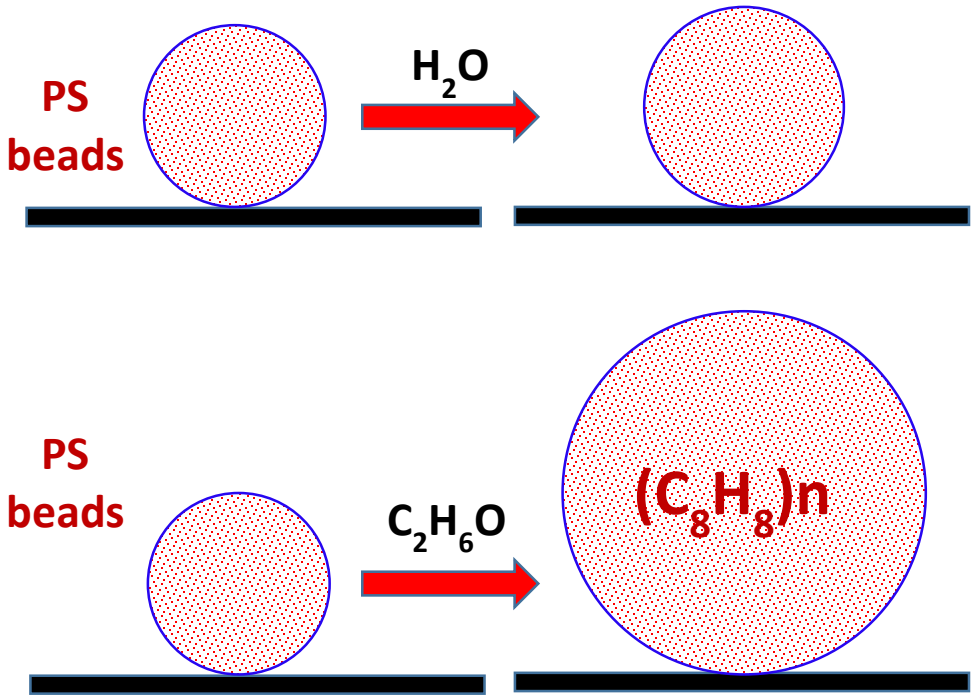

Figure 5.1: Schematic of PS beads treated with solvent to modify the modulus.

5.3.1 Sample preparation

We used 1 cm x 1 cm silicon substrates, which were cleaned through a multi-phase process as described previously. Polystyrene microspheres of the varying sizes (50, 100, 200, and 500 nm) were chosen for this investigation. The polystyrene microspheres were drop cast from diluted solution as before. After deposition, the substrate was momentarily (less than one second) placed on a hot plate measured to be 100^{o}C. This process slightly melted the microspheres at the substrate surface, increasing their adhesion and guaranteeing the presence of polystyrene microspheres on the Si substrate. Because the sample was submerged in solvents (DI water and ethanol), the adhesion between the microspheres and the substrate was weak, making imaging with the mechanical process employed by AFM difficult. By increasing the adhesion, this step improved confidence in imaging without chemical modification of the microspheres. A Petri dish was used to contain the fluid, allowing larger quantities of bathing solution and reducing the effects of evaporation during the experiments. Putty was used to mount our submerged sample in the liquid-containing Petri-dish. Typically, double-sided sticky tape is used to mount samples for use in the microscope; however, this tape likely would solubilize with time in our experiments and contaminate the sample surface. The putty was tested to show that it does not degrade under the solvents, and the surfaces remained clean in its presence. This Petri-dish was then mounted on a glass slide using a double-sided tape.

5.3.2 Atomic force microscopy

The Asylum AFM and Mikromasch AFM tips again were used; the spring constant of the cantilevers nominally was 14 N/m. Using the thermal method, the spring constant was calibrated to be 16.25 N/m. AC mode imaging was used under solution to locate the microspheres for measurement, and force curves were performed as described in Chapter 4. We again used 50 nm,

100 nm, 200 nm, and 500 nm size polystyrene microspheres. Initially, samples with microspheres of each size were submerged in 100% DI water. A 5 µm x 5 µm topographical image was obtained to locate clearly separated microspheres on the substrate. Single force curves were performed on five randomly chosen microspheres. Then continuous mode force spectroscopy was performed on a different microsphere to get repeated measures. This process was repeated for all sizes of microspheres. The solvent was then changed to pure ethanol, and the same force spectroscopy procedure was performed on these microspheres under the new conditions.

5.4 Results

Prior to performing the elastic modulus versus swelling experiments, a swelling profiling was done on these polystyrene microspheres to determine the length of time required for swelling to reach completion. PS beads of all sizes were submerged in ethanol for a given length of time. Images illustrating the swelling of the microspheres are shown in figure 5.2. Swollen volumes

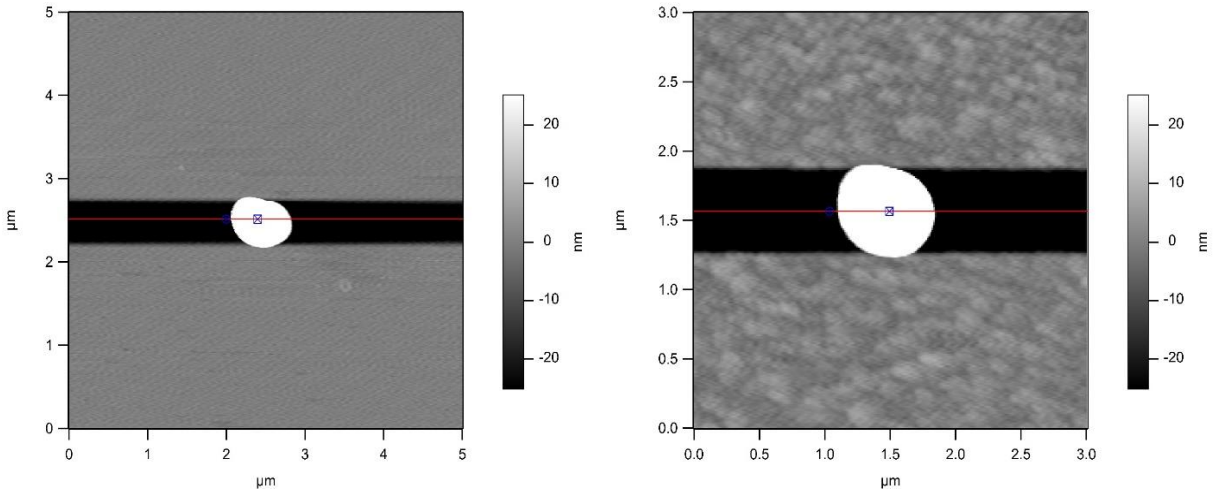

Figure 5.2: On the left showing AFM image of 500 nm PS beads swollen in ethanol for 6 hours, on the right shows swollen in ethanol for 12 hours.

(determined by measuring the diameter using line profiling) were measured, followed by force spectroscopy to extract the modulus. Table 5.1 below summarizes the swollen volume data for different swelling times. The volume data were then expressed as volume fraction (ϑ =

Volume/Maximally swollen volume) to produce a set that ranges from a volume fraction of ~0 initially to 1 when fully solvated. This analysis highlights the similarity in the absorption curves as can be seen in the plot of figure 3.

Table 5.1: Showing the swollen diameters of polystyrene microspheres in pure ethanol at different length of time used for the plot in figure 5.3.

Swelling Hours	PS beads 50 nm	PS beads 100 nm	PS beads 200 nm	PS beads 500 nm
0	35 nm	69 nm	170 nm	373 nm
2	48.5 nm	106 nm	240 nm	423 nm
6	53.1 nm	142 nm	312 nm	555 nm
12	58.6 nm	168 nm	350 nm	650 nm
18	62.6 nm	172 nm	352 nm	685 nm
24	65.1 nm	175 nm	365 nm	747 nm

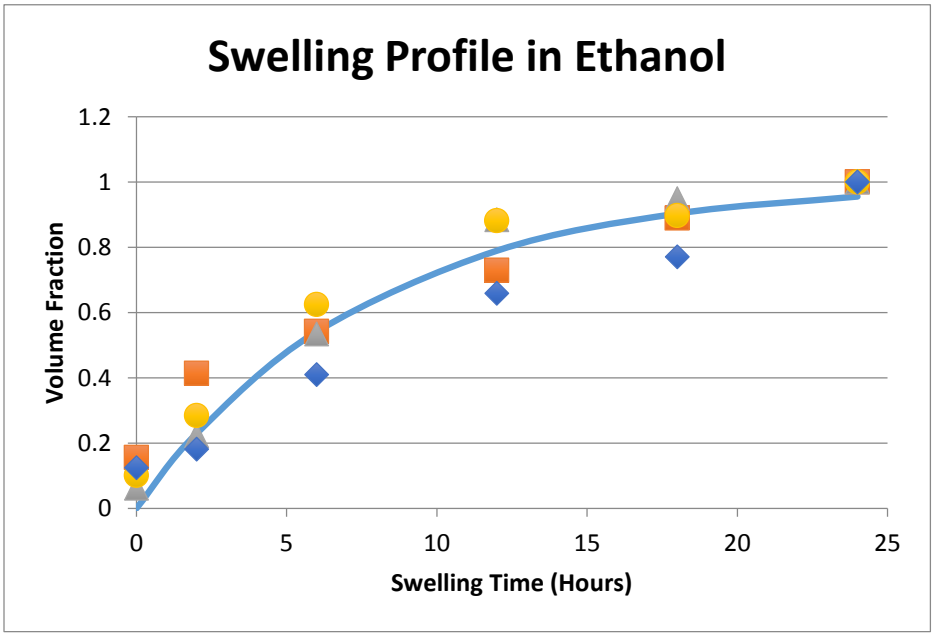

Figure 5.3: Plot of the swelling fraction (υ) for all sizes of microspheres versus swelling time. The solid line is an exponential fit to the data. (50nm = squares, 100nm = triangles, 200nm = circles, 500nm = diamonds)

Below, table 5.2 lists the elastic moduli of these microspheres (soaked in 100% DI water for 2 hours, and pure ethanol for 24 hours) as extracted by the method described in Chapter 4. As expected, the elastic modulus of the polystyrene microspheres decreased significantly under ethanol. Though polystyrene has low miscibility in water, it was found that the modulus still

decreased by a factor of ~3 when compared with our previously measured modulus in air. Under ethanol, however, the change is ~3 orders of magnitude. As is clear from figure 5.3, the ethanol absorbed microspheres swelled as expected. As shown in table 5.2, they also became significantly softer. Their elastic moduli range from ~ 2 - 3.55 GPa, which is a decrease by 3 orders of magnitude as previously mentioned.

Table 5.2: Showing the elastic modulus E of different sizes of microspheres in single and continuous mode under 100% DI water and pure ethanol.

Elastic Modulus (in Pa) → Size (nm) ↓	100% DI Water (single) $\bar{\chi} \pm \sigma$ (N)	100% DI Water (continuous) $\bar{\chi} \pm \sigma$ (N)	Pure Ethanol (single) $\bar{\chi} \pm \sigma$ (N)	Pure Ethanol (continuous) $\bar{\chi} \pm \sigma$ (N)
50	$(8.07\pm1.13)\times10^8$ (8)	$(8.14\pm0.44)\times10^8$ (8)	$(2.49\pm0.20)\times10^6$ (5)	$(3.11\pm0.94)\times10^6$ (2)
100	$(7.39\pm1.09)\times10^8$ (9)	$(8.40\pm0.76)\times10^8$ (7)	$(2.63\pm0.19)\times10^6$ (5)	$(2.90\pm0.16)\times10^6$ (2)
200	$(8.37\pm0.94)\times10^8$ (9)	$(8.42\pm0.46)\times10^8$ (8)	$(3.14\pm0.13)\times10^6$ (5)	$(3.16\pm0.15)\times10^6$ (2)
500	$(7.46\pm1.18)\times10^8$ (9)	$(7.88\pm0.33)\times10^8$ (8)	$(3.55\pm0.32)*\times10^6$ (5)	$(3.47\pm0.39)*\times10^6$ (2)

Elastic moduli were measured also as a function of time during the swelling process. Table 5.3 shows the elastic moduli of the swollen PS beads as they absorbed an increasing number of solvent molecules. These data were further expressed as a ratio of the volume of the polymer (the unswollen volume) to the total volume of the polymer and the sorbate, the volume fraction, υ. Table 5.4 shows the logarithmic values of volume fraction vs logarithmic values of elastic moduli E. Data from this table were plotted both superimposed in figure 5.4 and separately in figure 5.5. A least squares linear fit was applied to the data for all points prior to when swelling reached saturation.

Table 5.3: Showing the modified moduli of polystyrene microspheres in pure ethanol at different length of time.

Swelling Hours	PS beads 100 nm	PS beads 200 nm	PS beads 500 nm
0	$2.41x10^9$ Pa	$2.24x10^9$ Pa	$2.5x10^9$ Pa
2	$9.97x10^8$ Pa	$8.57\ x10^8$ Pa	$1.38x10^9$ Pa
6	$5.33x10^8$ Pa	$4.95\ x10^8$ Pa	$5.77x10^8$ Pa
12	$8.59x10^7$ Pa	$9.19\ x10^7$ Pa	$2.87x10^8$ Pa
18	$5.23x10^6$ Pa	$8.23\ x10^7$ Pa	$8.88x10^7$ Pa
24	$2.63x10^6$ Pa	$3.14\ x10^6$ Pa	$3.55x10^6$ Pa

Table 5.4: Showing the volume and elastic moduli of 100 nm, 200 nm and 500 nm beads.

100 nm Log (φ)	Log (E)	200 nm Log (φ)	Log (E)	500 nm Log (φ)	Log (E)
0	9.38	0	9.35	0	9.40
-0.56	8.99	-0.45	8.93	-0.16	9.14
-0.94	8.72	-0.79	8.69	-0.52	8.76
-1.16	7.94	-0.94	7.96	-0.73	8.46
-1.19	6.72	-0.95	7.91	-0.80	7.95
-1.21	6.42	-0.99	6.50	-0.90	6.55

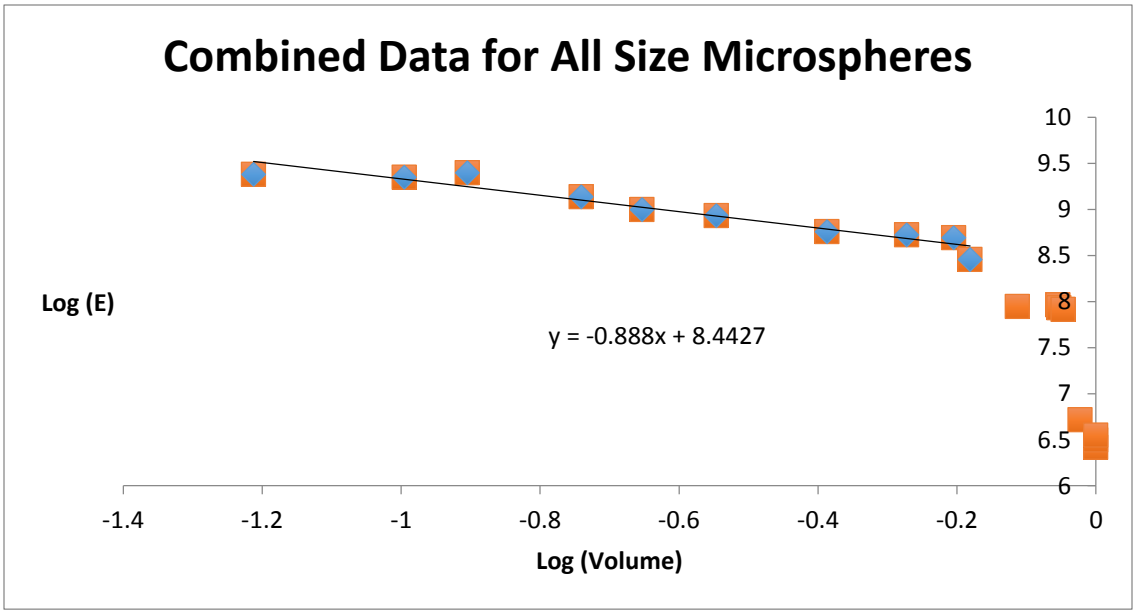

Figure 5.4: Log-log plot of the elastic modulus versus the volume for the combined data sets for all sizes of microspheres. The solid line is a linear least squares fit to the data, excluding the final time points at which the swelling had saturated.

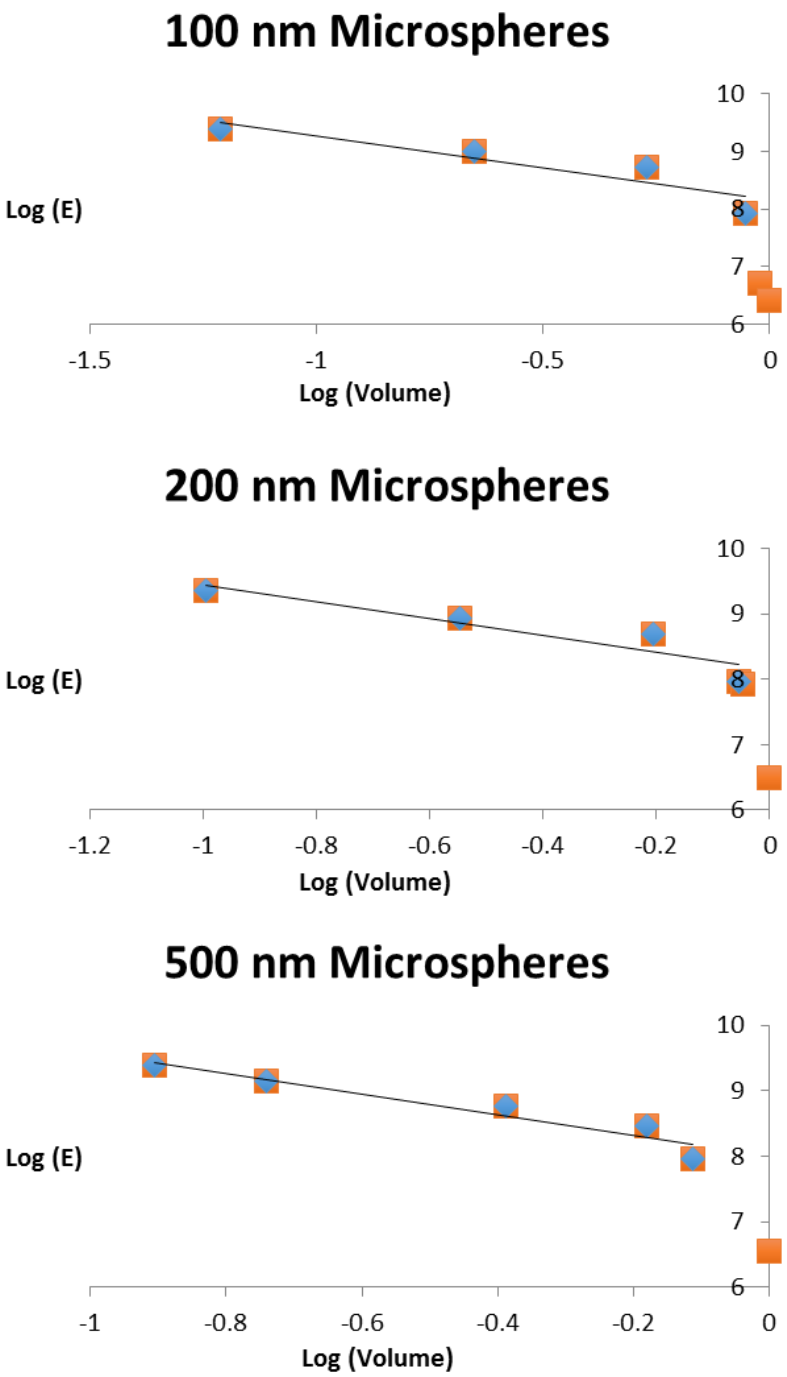

Figure 5.5: Log-log plot of the elastic modulus versus the volume for the individual sizes of microspheres. The solid line is a linear least squares fit to the data, excluding the final time points at which the swelling had saturated.

5.5 Discussion

The effects of partial solvation of the polymer contained in polystyrene microspheres was investigated for particle sizes well below 1 μm. How well bulk models describe material behaviors is not known on this length scale. In particular, the iconic Flory-Rehner model for swelling and elasticity previously had not been tested for such small volumes of polymers.

These experiments began with a study to determine the time required for the microspheres to become 'saturated' with solvent molecules. We used the increased volume that results from the absorption of solvent as our measure, allowing the absorption process to continue until an equilibrium volume was reached for microspheres submerged in near 100% ethanol. Because ethanol is not a good solvent for polystyrene, we were confident that the microspheres would not completely dissolve at the room temperature of our experiments.

Figure 5.2 above shows AFM images of swollen polystyrene microspheres after 2 (left) and 6 (right) hours in ethanol. The original diameter of this particular microsphere originally was 373 nm before absorption had begun. After 2 hours the diameter of the PS microsphere changed from 373 nm to 423, and at 6 hours it was measured 555 nm. Table 5.1 above summarizes the swelling data as a function of time. A gradual increase in the diameters was observed for the swelling polystyrene microspheres. This absorption process was not linear, but rather exponential, which is evident from figure 5.3, the graph of volume fraction versus solvation time. All sizes of beads show the same pattern of swelling, and the rate constant calculated using equation 5.3, was 0.13.

$$Vol = 1 - e^{-k\,(Time)} \qquad (5.3)$$

Table 5.3 above shows the elastic moduli of these polystyrene microspheres at their respective swollen volumes in ethanol, collected during the swelling process. Absorption of solvent and the resulting swelling increased the distance between the cross-link sites within the gel. This increased distance made the gel 'appear' to be less highly cross-linked, and the elastic modulus decreased as a result. Figure 5.4 shows a superimposed log-log plot of elastic modulus versus volume for each of the size microspheres investigated: 100 nm, 200 nm, and 500 nm nominal diameters. Figure 5.5 above shows the individual log-log plots for the elastic modulus versus the volume for each of the size microspheres. The plots were done on a log-log scale to highlight the power law being followed: the slope of these curves is the γ in

$$E \propto v^{\gamma} \qquad (5.4)$$

Such an analysis was performed in order to compare our results with equation 5.2, the Flory-Rehner equation predicting the behavior of a polymer as a function of the swollen volume. The plots are linear after the removal of points associated with an approximately constant maximally swollen volume. The slope obtained for the combination of all data (100 nm, 200 nm, and 500 nm diameter polystyrene microspheres) was 0.89, which possibly should have been -1. At the very least, this power law was clearly in violation of the prediction made by Flory-Rehner for an ideal polymer network as a function of the swelling volume. Flory-Rehner predicted a slope of (-1/3) for such an ideal polymer network. Our results implied that the elastic modulus had a much stronger dependence upon the volume. The effect of the increased distance between cross-links would seem to have been enhanced over that predicted.

Hedden et al., reported a slope of -1.83, for Poly-diethylsiloxane (PDES) treated in toluene, from the graph plotted for shear modulus and volume fraction [21]. Patel et al., obtained a slope

of -1.78 and -3.08 for poly-dimethylsiloxane (PDMS) treated in toluene. They used Flory-Rehner theory and further calculated volumes for affine network and phantom network [17]. The higher magnitude of the slope in our results reflects the poor quality of ethanol as a solvent for the polystyrene microspheres. The prediction made by Flory-Rehner considered a perfect polymer network. The presence of greater amount of pendant material in imperfect networks makes them ineffective in the trapping of entanglements. Flory-Rehner neglected this imperfection in their prediction. A further modification of Flory-Rehner theory will be needed to explain the elasticity and swelling of such imperfect networks.

5.6 Conclusion

The elastic modulus of these polystyrene microspheres was determined to be ~ 0.8 GPa under 100% DI water for both single and continues mode for all sizes of microspheres. The bulk macroscopic elastic modulus of polystyrene microspheres as reported in the previous section was ~ 2 – 5 GPa in air. This slight decrease in modulus was likely caused by the absorption of some small amount of water into these microspheres. There was a significant decrease in elastic modulus for these polystyrene microspheres when submerged in pure ethanol. The elastic modulus in pure ethanol ranged from ~ 2.49 – 3.55 MPa. A pattern in the modulus values depending on the size of these microspheres in pure ethanol was also observed, if the ethanol has not fully absorbed into the microspheres. Microspheres that had swollen in ethanol had smaller moduli. Because the time submerged approximately was constant across the differently sized microspheres at each time point, the distance into the microsphere that the solvent had permeated should have had the same dependence. Thus smaller microspheres saturate faster than the larger. DI water and pure ethanol were used successfully to modify the moduli of these microspheres. Flory-Rehner theory was tested with the elasticity and swollen volume of these polystyrene microspheres. The higher slope

magnitude obtained did not match the prediction made by Flory-Rehner. These larger slope magnitudes likely were caused by imperfections in the swollen network. Further modification in the Flory-Rehner theory is needed to precisely predict the elasticity and swelling behavior of polystyrene microspheres in ethanol. Future experiments are needed in which the dilution of ethanol in water is varied with the goal of producing microspheres with varying but controllable moduli.

5.7 References

[1] M. Sitti, H. Hashimoto, Controlled pushing of nanoparticles: Modeling and experiments, Ieee-Asme T Mech, 5 (2000) 199-211.

[2] S. Krijt, C. Dominik, A. Tielens, Rolling friction of adhesive microspheres, Journal of Physics D: Applied Physics, 47 (2014) 175302.

[3] R. Fuchs, T. Weinhart, J. Meyer, H. Zhuang, T. Staedler, X. Jiang, S. Luding, Rolling, sliding and torsion of micron-sized silica particles: experimental, numerical and theoretical analysis, Granular Matter, 16 (2014) 281-297.

[4] M. Zakeri, J. Faraji, Modeling of the rough spherical nanoparticles manipulation on a substrate based on the AFM nanorobot, Applied Physics A, 117 (2014) 1947-1962.

[5] L. Xia, M. Zhang, Nanoparticles to tune mechanical properties of adhesive and polymeric matrix: An inspiration from nature, in: Nanotechnology (IEEE-NANO), 2011 11th IEEE Conference on, IEEE, 2011, pp. 1592-1597.

[6] A. Schneider, G. Francius, R. Obeid, P. Schwinté, J. Hemmerlé, B. Frisch, P. Schaaf, J.-C. Voegel, B. Senger, C. Picart, Polyelectrolyte multilayers with a tunable Young's modulus: influence of film stiffness on cell adhesion, Langmuir, 22 (2006) 1193-1200.

[7] S. Tan, R.L. Sherman, W.T. Ford, Nanoscale compression of polymer microspheres by atomic force microscopy, Langmuir, 20 (2004) 7015-7020.

[8] K. Trenkenschuh, J. Erath, V. Kuznetsov, J. Gensel, F. Boulmedais, P. Schaaf, G. Papastavrou, A. Fery, Tuning of the Elastic Modulus of Polyelectrolyte Multilayer Films built up from Polyanions Mixture, Macromolecules, 44 (2011) 8954-8961.

[9] V.V. Lulevich, O.I. Vinogradova, Effect of pH and salt on the stiffness of polyelectrolyte multilayer microcapsules, Langmuir, 20 (2004) 2874-2878.

[10] J. Heuvingh, M. Zappa, A. Fery, Salt softening of polyelectrolyte multilayer capsules, Langmuir, 21 (2005) 3165-3171.

[11] G. Lubarsky, M. Davidson, R. Bradley, Elastic modulus, oxidation depth and adhesion force of surface modified polystyrene studied by AFM and XPS, Surface science, 558 (2004) 135-144.

[12] C.A. Grant, D.J. Brockwell, S.E. Radford, N.H. Thomson, Effects of hydration on the mechanical response of individual collagen fibrils, Appl Phys Lett, 92 (2008) 233902.

[13] L. Yang, K.O. Van der Werf, C.F. Fitié, M.L. Bennink, P.J. Dijkstra, J. Feijen, Mechanical properties of native and cross-linked type I collagen fibrils, Biophys J, 94 (2008) 2204-2211.

[14] K. Otake, S.E. Webber, P. Munk, K.P. Johnston, Swelling of polystyrene latex particles in water by high-pressure carbon dioxide, Langmuir, 13 (1997) 3047-3051.

[15] W.-Y. Chuang, T.-H. Young, D.-M. Wang, R.-L. Luo, Y.-M. Sun, Swelling behavior of hydrophobic polymers in water/ethanol mixtures, Polymer, 41 (2000) 8339-8347.

[16] O. Okeowo, J.R. Dorgan, Multicomponent swelling of polymer networks, Macromolecules, 39 (2006) 8193-8202.

[17] S.K. Patel, S. Malone, C. Cohen, J.R. Gillmor, R.H. Colby, Elastic modulus and equilibrium swelling of poly (dimethylsiloxane) networks, Macromolecules, 25 (1992) 5241-5251.

[18] S.P. Obukhov, M. Rubinstein, R.H. Colby, Network modulus and superelasticity, Macromolecules, 27 (1994) 3191-3198.

[19] P.J. Flory, J. Rehner Jr, Statistical Mechanics of Cross-Linked Polymer Networks I. Rubberlike Elasticity, The Journal of Chemical Physics, 11 (1943) 512-520.

[20] P.J. Flory, J. Rehner Jr, Statistical mechanics of cross-linked polymer networks II. Swelling, The Journal of Chemical Physics, 11 (1943) 521-526.

[21] R.C. Hedden, H. Saxena, C. Cohen, Mechanical properties and swelling behavior of end-linked poly (diethylsiloxane) networks, Macromolecules, 33 (2000) 8676-8684.

6.0 Adhesion and surface energy of polystyrene microspheres

6.1 Introduction

For macroscopic objects the interaction among objects largely depends on the force of gravity and/or inertia, however when the dimension of these objects are reduced, intermolecular forces become more significance. The surface area to volume ratio increases at the micro-nano scale, and interfacial surface forces become dominant over inertial forces. The properties related to adhesion, friction, and wear become critical in the mechanical performance of small scale mechanical systems. In particular, adhesion forces and the deformation caused by the contacting objects define the interaction. Thus the adhesion force and the surface energy between two solid surfaces are of great interest in various scientific and industrial applications. A clear understanding of and dependence upon these forces on different variables, are very important when the size of the interacting particles is reduced to micro-nano scale. Examples range from developing micro/nano-electromechanical systems (MEMS/NEMS) to understanding the aggregation and dispersal of powders and colloidal dispersion, and the flow properties of granular materials [1-4].

In order to understand the interaction between the small particles, it is important to understand the vertical and tangential forces acting between the two particles. When these particles come into contact they are deformed, with this deformation being defined by their finite elasticity. Several contact models have been developed and applied to the study of the mechanics of interacting pairs of spherical particles and spherical particles with flat substrates. In general, the contact between two spherical particles or a solid sphere with a flat surface is most commonly

described by either the model developed by Johnson, Kendall, and Roberts (JKR model) or that of Derjaguin, Muller, and Toporov (DMT model). Both of these models are based upon a Hertzian analysis, which considered two elastic bodies in contact under an external load. The JKR model assumes the effective steady state pressure in the contact circle as the superposition of the elastic Hertzian pressure and with the attractive surface forces that act only over the contact area. The pull off force then is given by,

$$F_{JKR} = \frac{3}{2}\pi R W_{12} \qquad (6.1)$$

In equation 6.1, W_{12} is the effective solid work of adhesion. R is the reduced radius of curvature of the two surfaces and is given by,

$$R = \frac{R_1 R_2}{(R_1 + R_2)} \qquad (6.2)$$

Alternatively, the DMT model also accounts for the non-contact forces in the vicinity of the contact area. Within this framework, the pull off force is given by,

$$F_{DMT} = 2\pi R W_{12} \qquad (6.3)$$

In this equation, again R and W_{12} are defined as in equation 6.1 above. Generically, the work of adhesion is given by the Dupre equation:

$$W_{12} = \gamma_1 + \gamma_2 - \gamma_{12} \qquad (6.4)$$

where γ_1 and γ_2 are the surface free energies of the contacting materials (polystyrene and silicon in our case) and γ_{12} is the interfacial energy between the two materials. However, the work of adhesion is often approximated as

$$W_{12} = 2\sqrt{\gamma_1 \gamma_2}. \qquad (6.5)$$

This approximation allows us to calculate the surface energy of our polystyrene microspheres from the measured force of adhesion using either the JKR or DMT model, given the surface energy of the silicon substrate.

Both models predict the separation force between the particles to be independent of their elastic material properties; however, this force would be expected to be a linear function of the particle size and the work of adhesion W_{12}. For this reason, experimental measurements of adhesion are often reported as a ratio of the force to the radius. Both the models have both strengths and limitations. The JKR approach is more applicable to the large, soft bodies, with high surface energy, whereas DMT approach works well with small, hard solid particles with low surface energy [5, 6].

There are several experimental approaches to study adhesion forces and interfacial surface energy, among which Atomic Force Microscopy (AFM) and the Surface Force Apparatus (SFA) are most popular. An atomic force microscope is commonly used for the investigation of these forces at the micro/nano scale and, especially, on individual particles. It is most convenient to use an AFM to determine the adhesion force with high spatial resolution. Moreover, AFM is less subject to contamination when compared with other apparatus to measure adhesion forces at the micro/nano-scale. In AFM, the adhesion measurement is made through the analysis of force displacement curves, performed by measuring the deflection of a cantilever as the tip approaches and retracts from the sample surface. The cantilever both controls the vertical separation between the samples of interest and measures the forces exerted during the process [2, 7].

There are many factors such as surface roughness, applied load, contact time, humidity, and temperature, all of which can influence adhesion force. Many of these are well studied and

reported in the literature. In this study we choose polystyrene microspheres of differing surface functionalizations. The different funtionalizations are as-received polystyrene microspheres, amine terminal group, and carboxylate terminal group, which provide different adhesion forces and interfacial surface energies between the microspheres and the planar silicon substrate against which they will be pressed.

The use of such microspheres with AFM is one variation within a class of experiments that has become known as the colloidal probe technique. The colloidal probe technique is a well-established and powerful method for the investigation of surface forces; however, it is recognized as being difficult to attach a single micro/nano sized particle on the AFM force sensor. We have established a unique method by which we are able to reliably attach these microspheres on the AFM force sensor. This technique has shown a very high success rate, with yields approaching 100%.

We have used our in-house prepared colloidal probes in force spectroscopy experiments. To account for variations in adhesion resulting from atmospheric surface contamination and capillary forces, these experiments were performed under deionized and polished water. To reduce the effects of the loading force, the applied loads were optimized to avoid plastic deformation and held constant between samples. Finally, because contact time is known to influence the measured adhesive force, the contact time was kept approximately constant. This time was also kept as a minimum to better model the situations expected during the future rolling experiments [2, 7-9]. All measurements were performed at room temperature, ~25°C.

6.2 Adhesion force measurement

We investigated the adhesion force between the surfaces of polystyrene microspheres and polished silicon surfaces. Polystyrene microspheres with different surface chemistries (regular, amine, and carboxylate), and, thus, the expected surface charge and surface energy, were utilized. From these experiments, the interfacial surface energy between the polystyrene microspheres and the silicon substrate was measured. The results provide data for testing the various friction models. Moreover, the results are of interest to the pharmaceutical industry and others reliant on an understanding of granular flow. The adhesion force was measured under solvent conditions for the polystyrene microspheres and the Si substrate. The solvent used in this measurement was pure deionized and polished water.

A schematic force curve is shown in figure 6.1, below [10]. When the force curve or particle indentation experiment is performed using an AFM, it starts with the tip (polystyrene microsphere attached) and sample (planar substrate in our measurements) separated, which also is known as the 'non-touching' regime. The tip then approaches the sample, which can be followed in the figure below as the horizontal line moving from right to left. When the tip – sample separation is small enough so that the attractive interaction is greater than the stiffness of the cantilever, the transition from non-touching regime to touching regime occurs. The tip now jumps into contact with the sample. Moving the cantilever base further into the sample reverses the deflection of the cantilever, applying force to the sample at the tip-sample contact region. By measuring this deflection and calibrating the spring constant of the cantilever, the applied force can be determined. After the maximum desired force has been reached, the direction of motion of the cantilever base is reversed. When retraction is done, moving left to right in the force curve figure, adhesion causes the cantilever to remain at the sample surface. Eventually the curve

approaches its lowest point along the force axis, at which point the cantilever force overcomes the adhesive force. In the figure this adhesion is highlighted. Now the tip loses contact with the sample, snaps back to the rest position, and is further withdrawn from the surface. This completes the force – distance curve approach and retraction cycle. The force required to pull the tip free from the sample is known as the adhesion force or pull-off force. This pull off force is calculated using Hooke's law:

$$F = k\,\Delta x \qquad (6.6)$$

where k is the spring constant and Δx is the maximum deflection of the cantilever during tip-sample adhesion. The precise measurement of the force depends upon the precise calibration of k, the spring constant of the cantilever, and the accuracy of the measured deflection of the cantilever during the pull off. The optical lever system employed in AFMs is capable of measuring the deflection of the cantilever with precision at the sub-angstrom level.

The Hertz model applied in the analysis of the elastic modulus predicts zero adhesion, a non-physical result [11]. Johnson, Kendall, & Roberts and Derjaguin developed theories to correct for this error [12]. The Derjaguin approximation predicts that the pull off force between a sphere and a flat surface would be, $F = 2\pi R W_{12}$, where R is the radius of tip, W_{12} is the work of adhesion. However, we elected to use the JKR model for our analysis. This model excludes sample interactions outside of the contact region, which was expected to be more suitable for our measurements performed submerged in a polar solvent. The JKR theory then suggests that the pull off force would be,

$$F = \frac{3}{2}\,\pi\,R\,W_{12} \qquad (6.7),$$

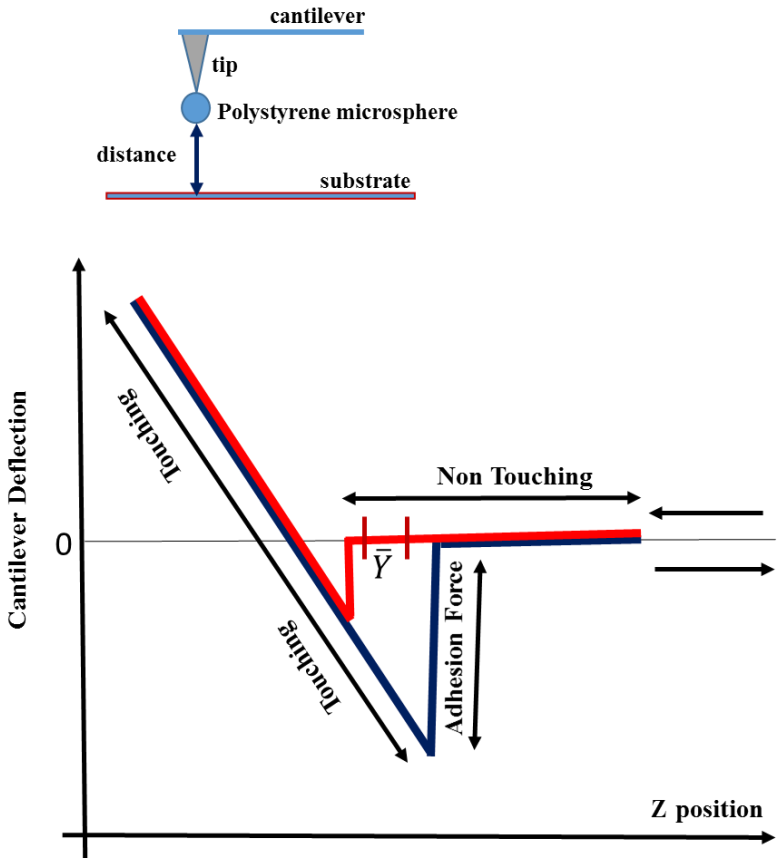

Figure 6.1: Schematic of AFM measurement of surface forces.

$$F = Deflection * k \qquad (6.8), \text{ and}$$

$$\Delta Deflection = D - \bar{Y} \qquad (6.9)$$

where D is the maximum negative (toward substrate) deflection of the cantilever and $\bar{Y}$ is the rest position of the cantilever just before the snap-in. $\bar{Y}$ is used instead of 0 to account for potential drift in the sensor away from the 0 position and is found by averaging the last 10 deflection points just before the snap-in. Combining equations 6.6, 6.7, 6.8, and 6.9, we get

$$W_{12} = \frac{2(D-\bar{Y})*k}{3\,\pi\,R} \qquad (6.10)$$

This is the equation used to calculate work of adhesion.

6.3 Experimental procedure

6.3.1 Sample preparation

Sample preparation was similar to that described in chapter 4. It began with the rigorous cleaning of the Si substrates. The silicon wafers were cleaved into 1 cm x 1 cm squares using a diamond scribe, followed by plasma cleaning. Afterwards the silicon substrates were subjected to solvent cleaning in an ultrasonic bath for 15 minutes each. Solvent cleaning was performed first by acetone, followed by ethanol. To get rid of any hydrocarbon residue from the substrates, they were further cleaned in DI water in the ultrasonic bath, and the substrate was dried by nitrogen. This cleaning process was repeated. This multi-stage cleaning process removed any contaminants from the surfaces, whether silicon chips from the cleaving process or organic deposits from air or other solvents.

In this study we have used 200 nm sizes of commercially available polystyrene microspheres of different surface functionalization. The polystyrene microspheres chosen for these experiments are functionalized differently (regular, amine, and carboxylate). Commercially available polystyrene microspheres typically are supplied with some small amount of detergent such as sodium dodecyl sulfate, which would contaminate the surfaces of interest. For this reason, the microspheres were rinsed triply in DI water. Briefly, as supplied suspended microsphere solution was centrifuged at 10000 RPM for 5 minutes in a Fisher Scientific microfuge. The supernatant was removed, and the pellet was resuspended in 100 µl of DI water. This process was repeated three times, and the final suspension was diluted 1000 fold in DI water. One disadvantage of rinsing was that the microspheres were difficult to resuspend as individual spheres – they clumped. To get rid of this clumping, the sample tube was ultrasonicated for 30 minutes. The

ultrasonic cleaner breaks these clumped microspheres into singlets, which was required for the attachment of a single bead onto the AFM tip. Differently functionalized polystyrene microspheres then were drop cast from the diluted solution onto 1 cm x 1 cm Si substrates as before.

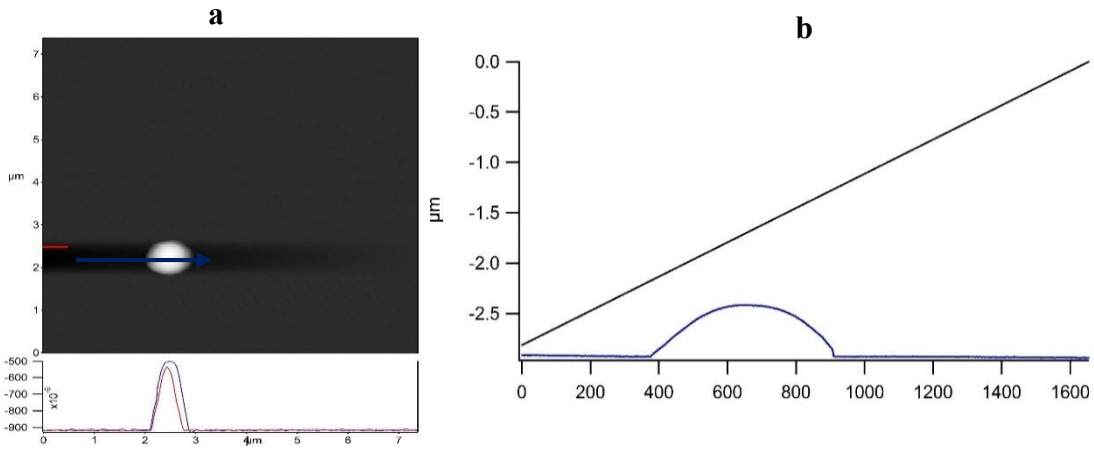

Figure 6.2: (a) Shows the horizontal litho panel. (b) Shows the adjustable height selection on the litho bead.

6.3.2 Atomic force microscopy

Spring constants (*k*) for each cantilever used were calibrated using the thermal method before the attachment of the microsphere. These cantilevers were found to have *k* values of 43.72 N/m, 43.44 N/m, and 44.68 N/m for regular polystyrene microspheres, amine microspheres, and carboxylate microspheres, respectively. It is important to perform the cantilever calibration prior to the attachment of the particles because the added mass would alter the assumptions that inform the calibration process.

Attaching the microspheres on the AFM tip was performed using the Litho function of the MFP -3D AFM software. The process is as follows: A typical intermittent contact mode (AC mode) scan is performed to locate a single microsphere. The AFM then is changed from AC to

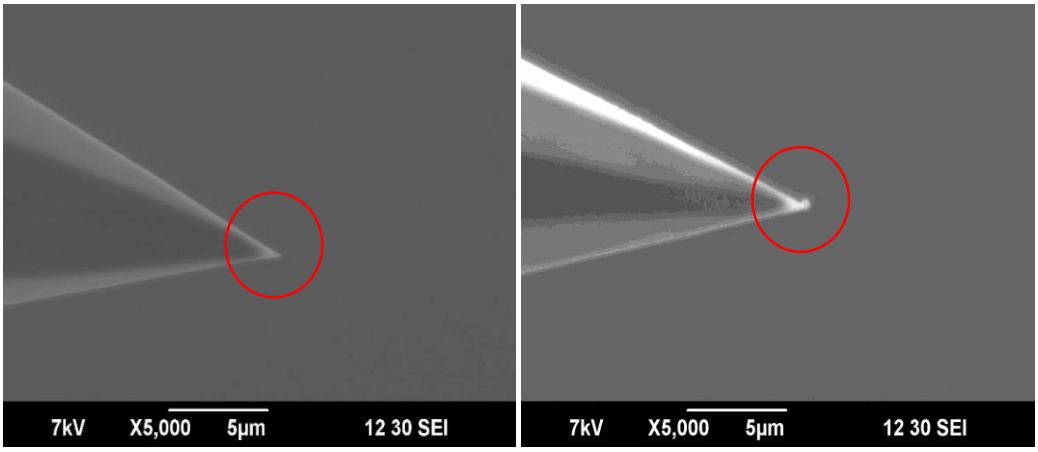

Figure 6.3: Showing a clean tip on the left and attached 500 nm Polystyrene bead on the right.

contact mode. Using the software, a path for the tip relative to the surface is defined. This path is drawn such that the tip crosses over the location of the microsphere. The manufacturer supplied software also allows for the adjustment of the z position (the height relative to the planar substrate) of the tip. The path of the tip is defined in this dimension as well, gradually ramping the height so that the tip just makes contact with the microsphere. This procedure is illustrated in figure 6.2. The ramping of the tip height illustrated in this figure would be optimized so that the tip just makes contact with the microsphere at the point where its lateral position crosses that of the microsphere.

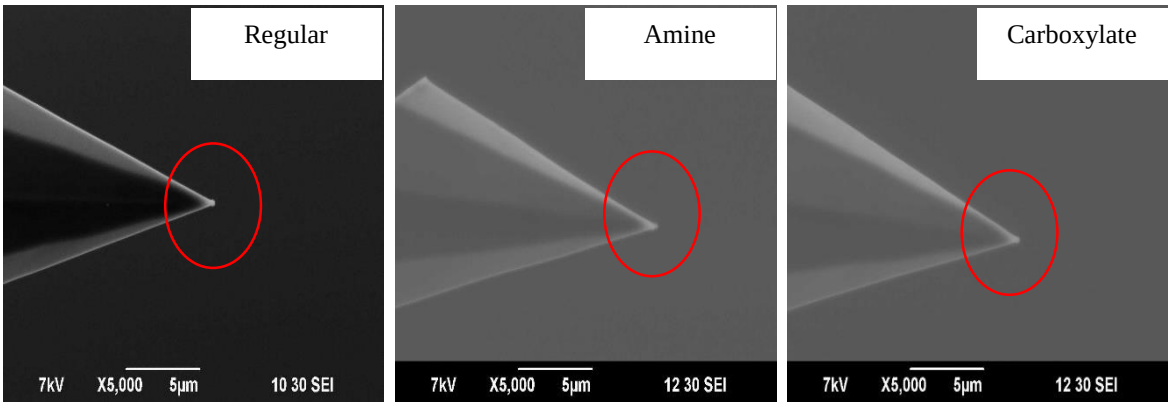

Figure 6.4: Showing SEM images of attached 200 nm Polystyrene beads attached on AFM tips.

This whole process was developed to attach the microspheres successfully on the AFM tip. The mounting of the bead on the AFM tip was further verified under the Scanning Electron Microscope (SEM) before each adhesion experiment.

A Petri dish mounted to a glass microscope slide was used as a sample chamber. The Petri dish was used to contain the fluid under which the experiments were to be performed, thereby allowing larger quantities of bathing solution and reducing the effects of evaporation during the experiments. Putty was used to mount our submerged sample in the liquid-containing Petri-dish. Typically, double-sided sticky tape is used to mount samples for use in the microscope; however, this tape likely would solubilize with time in our experiments and contaminate the sample surface. The putty was tested to show that it does not degrade under the relevant solvents, and the surfaces remain clean in its presence. This petri-dish was then mounted on a glass slide using a double-sided tape. This cantilever then was mounted onto the AFM and a regular force curve was performed against a clean Si substrate. During the force curve, the approach and retraction of the tip, the minimum vertical deflection of the cantilever represents the maximum adhesion of the microsphere to the substrate. The blue line of the force trace in figure 6.1 is the retraction part of the force curve. When this trace dips below zero that represents a force attracting the sphere to the substrate surface. The most negative value in this trace represents the adhesion data of interest and was extracted for use with equation 6.10 above, providing the interfacial surface energy. Such experiments were performed for different surface functionalizations of the polystyrene microspheres. The chosen functional groups also allow for future experiments in which cross-linking of other molecules to the microsphere surface is of importance.

6.4 Results and discussion

The adhesion force between the tip mounted polystyrene microspheres of different surface functinalizations and the silicon substrate was measured under DI water. From this data, the surface energy was extracted.

Table 6.1: The measured adhesion force scaled by radius for 200 nm diameter polystyrene microspheres of differing surface functionalization as measured under DI water.

	Adhesion force/microsphere radius (F/R; N/m)		
	F/100 nm (As received)	**F/100 nm (Amine)**	**F/100 nm (Carboxylate)**
Adhesion of individual microspheres	0.447	0.213	0.877
	0.452	0.235	0.882
	0.461	0.243	0.890
	0.435	0.226	0.842
	0.459	0.222	0.877
Repeated measurements on individual microspheres	0.449		0.868
	0.469		0.882
	0.491		0.886
Average F_{ad}/R (repeated)	0.451	0.228	0.874
Average F/R (combined)	**0.458**	**0.228**	**0.875**
Standard Deviation (all)	0.017	0.012	0.015

Table 6.1 above summarizes the data for the adhesion force scaled by the microsphere radius for 200 nm diameter polystyrene microspheres. The work of adhesion was calculated from the JKR model, equation 6.1, for these microspheres, yielding in descending order 0.0929 ± 0.0016 J/m^2 for the carboxylate microspheres, 0.0486 ± 0.0018 J/m^2 for the 'as received' microspheres, and 0.0242 ± 0.0012 J/m^2 for the amine microspheres. While the adhesive force is expected to depend upon the size of the microspheres, the work of adhesion would be expected to be approximately constant for a given surface functionalization.

From these work of adhesion values, the surface energy of the polystyrene microspheres can be calculated. The Dupre equation, equation 6.4 above, assumes the experiment is performed in vacuum, and the surface energies would be those for the materials in vacuum. Because our experiments were performed under water, a modification is required. Using the approximation for the W_{12} given in equation 6.5, along with the surface energy of water, γ_w = 0.073 J/m^2, and the surface energy of the <100> face of silicon in vacuum, γ_{si} = 2.13 J/m^2, from reference [13], we get that the surface energy under water for our silicon substrate would be given by, $\sqrt{\gamma_{si}\gamma_w}$. Likewise, the surface energy under water for the polystyrene microspheres would be given by $\sqrt{\gamma_{ms}\gamma_w}$. Combined we have,

$$W_{12} = 2\sqrt{\gamma_{si}\gamma_w}\sqrt{\gamma_{ms}\gamma_w} = 2\sqrt{\gamma_{si}\gamma_{ms}\gamma_w^2} \qquad (6.11)$$ and,

$$\gamma_{ms} = \frac{W_{12}^2}{4\gamma_{Si}\gamma_w^2}, \qquad (6.12)$$

which gives the surface energy of the polystyrene microspheres from our measured work of adhesion. Using this analysis, we get that the surface energy for the carboxylate functionalized microspheres was 0.190 J/m^2, for the 'as received' polystyrene microspheres was 0.052 J/m^2, and for the amine functionalized microspheres was 0.013 J/m^2. This result compares well with the commonly cited surface energy of bulk polystyrene: 0.04 – 0.05 J/m^2.

The choice of these three surface functionalizations provides us with a range that spans a factor of ~4 in work of adhesion, but only ~0.7 in surface energy. Because the silicon substrate is amenable to further chemical functionalization through silane chemistry, we hope to be able to expand this range further in the future.

Other studies have been performed investigating the adhesion of polystyrene microspheres, though not as a function of the surface functionalization. Additionally, these previous investigations were performed using significantly larger diameter spheres. Schaefer et al. [14] found that the F_{ad}/R was 0.5 N/m for 5 – 7 μm diameter microspheres in silicon under ambient conditions. That their value was slightly higher than ours but is in surprisingly good agreement when capillary forces are considered – such forces disappear when submerged in water, as was the case in our experiments. Biggs and Spinks in 2012 [15] reported the F/R for polystyrene microspheres on a mica substrate as measured under nitrogen. They found that this ratio was 0.7 N/m for this high energy surface substrate (higher than our silicon), though the values agree within a factor of 2. Their data was collected as a function of loading rate and dwell time, showing no dependence on the rate but an increased adhesion with time. Given that we limited our time in contact with the substrate, our data should best compare with their shortest dwell time.

6.5 Conclusion

The adhesion forces between the tip and the polystyrene microspheres of different surface chemistries were measured. From this data the work of adhesion and surface energy of differently functionalized polystyrene microspheres was extracted. The range in work of adhesion and surface energy was not as large as had been hoped, but could likely be expanded through surface chemistry applied to the silicon substrate. The carboxylate (COOH) functionalized microspheres had the largest interfacial surface energy whereas the amine functionalized microspheres had the lowest interfacial energy. The 'as received' microspheres (not functionalized with any group) have an interfacial surface energy somewhere between these two functionalized groups, and the data were in agreement with previously reported findings. For the -COOH functionalized microspheres, the work of adhesion was approximately four times that of amine functionalized beads. For the amine

functionalized beads, work of adhesion was half that of the 'as received' (not functionalized with any group) microspheres. Combined with the different sizes of polystyrene microspheres and their measured elastic moduli under different solvent conditions as described in chapter 4 and 5, we now have a set of data to apply to the models for the translational motion experiments using lateral force microscopy on polystyrene microspheres of different sizes, moduli, and surface chemistry.

6.6 References

[1] L.-O. Heim, J. Blum, M. Preuss, H.-J. Butt, Adhesion and friction forces between spherical micrometer-sized particles, Phys Rev Lett, 83 (1999) 3328.

[2] T. Lai, R. Chen, P. Huang, Temperature dependence of microscale adhesion force between solid surfaces using an AFM, J Adhes Sci Technol, 29 (2015) 133-148.

[3] B. Bhushan, C. Dandavate, Thin-film friction and adhesion studies using atomic force microscopy, Journal of Applied Physics, 87 (2000) 1201-1210.

[4] D. Grierson, E. Flater, R. Carpick, Accounting for the JKR–DMT transition in adhesion and friction measurements with atomic force microscopy, J Adhes Sci Technol, 19 (2005) 291-311.

[5] M. Zakeri, J. Faraji, Modeling of the rough spherical nanoparticles manipulation on a substrate based on the AFM nanorobot, Applied Physics A, 117 (2014) 1947-1962.

[6] K. Johnson, Adhesion and friction between a smooth elastic spherical asperity and a plane surface, in: Proceedings of the Royal Society of London A: Mathematical, Physical and Engineering Sciences, The Royal Society, 1997, pp. 163-179.

[7] B.J.R. Thio, J.C. Meredith, Measurement of polyamide and polystyrene adhesion with coated-tip atomic force microscopy, Journal of colloid and interface science, 314 (2007) 52-62.

[8] J. Drelich, Adhesion forces measured between particles and substrates with nano-roughness, Minerals and Metallurgical Processing, 23 (2006) 226-232.

[9] D. Guo, J. Li, L. Chang, J. Luo, Measurement of the friction between single polystyrene nanospheres and silicon surface using atomic force microscopy, Langmuir, 29 (2013) 6920-6925.

[10] J. Drelich, G.W. Tormoen, E.R. Beach, Determination of solid surface tension from particle–substrate pull-off forces measured with the atomic force microscope, Journal of Colloid and Interface Science, 280 (2004) 484-497.

[11] H. Hertz, Ueber die Berührung fester elastischer Körper, Journal für die reine und angewandte Mathematik, 92 (1882) 156-171.

[12] K. Johnson, J. Greenwood, An adhesion map for the contact of elastic spheres, Journal of colloid and interface science, 192 (1997) 326-333.

[13] R. Jaccodine, Surface energy of germanium and silicon, Journal of The Electrochemical Society, 110 (1963) 524-527.

[14] D.M. Schaefer, M. Carpenter, R. Reifenberger, L.P. Demejo, D.S. Rimai, Surface Force Interactions between Micrometer-Size Polystyrene Spheres and Silicon Substrates Using Atomic-Force Techniques, J Adhes Sci Technol, 8 (1994) 197-210.

[15] S. Biggs, G. Spinks, Atomic force microscopy investigation of the adhesion between a single polymer sphere and a flat surface, J Adhes Sci Technol, 12 (1998) 461-478.

7.0 Measurement of translational motion of polystyrene microspheres

7.1 Introduction

Particle technology and contact mechanics at the nano-scale find a multitude of applications in widely ranging fields, including the semiconductor, food, cosmetic, and pharmacological industries. Interestingly, properties of and interactions between nano-scale particulates are also of interest to those investigating the extremely macroscopic behaviors that result from these attributes, such as the coagulation of aerosols in the earth's atmosphere and the aggregation of particles in space that lead to planetary formation. In another application, understanding the relative motion of contacting objects will lead to better control over macroscopic lubrication and adhesion. The ability to manipulate the strength of interactions and control the relative motion of nano-scale objects are critical for micro/nano-scale electromechanical devices. Once in contact, the characteristics of the individual particles and the features of the contacting surfaces dominate the nature of the translational motion between the contacting particles [1, 2]. The rolling or sliding of an object under a lateral, shearing, load will largely define the energy loss mechanisms and mechanical wear. Rolling and sliding behaviors are largely determined by adhesion between the abutting surfaces and the deformation the results from their contact. It has been proposed, for example, that rolling can largely be described by the deformation component alone [3-5]. However, this conjecture seems unlikely, given that the deformation is, at least in part, determined by the adhesive forces between the two adjacent surfaces.

Macroscopically, we are all familiar with the idea that rolling tends to dominate over sliding for spherical objects subjected to forces parallel to its smooth, planar supporting surface. However, the same behavior is not a given as the size is reduced to the micro/nano scale; indeed, it has been hypothesized that sliding will dominate for objects with length scales below a certain threshold. So, what does happen if a sub-micron sized spherical particle is subjected to shearing forces? Such a situation occurs when these particles are trapped between two planar surfaces experiencing lateral tangential motion or when such a particle is caught in a shearing flow at a planar surface, such as a viral capsid on the wall of a blood vessel. Will the particles tend to roll or slide? Rolling of the particles potentially has substantial benefits. Introducing rolling objects between contacting planar surfaces undergoing shear will reduce the friction significantly: the rolling particulates reduce the shearing forces exerted on the planar surfaces, resulting greatly reduced wear. In the biomedical application mentioned, the rolling virus capsid continually varies the region contacting the endothelial surface, greatly increasing the likelihood of making the ligand-receptor bond required to trigger entry past the cell membrane. These are just a couple of examples highlighting the importance of maintaining the preference for rolling over sliding, even as the linear dimension diminishes. An enormous effort has been expended in increasing our understanding of the sliding motion at the micro/nano-scale, and substantial progress has resulted. However, a comparable insight is still lacking for rolling motion. In particular, the difficulty inherent in controlled mechanical manipulation of nano-scale objects has hampered experimental progress in this area [6, 7].

Atomic Force Microscope (AFM) has become the tool of choice for investigating translational motion at the sub-micron scale. In addition to its strength for imaging and topographical analysis, especially in non-vacuum environments, an AFM's real power becomes

apparent when it is used as a nano-manipulator. The tip of an AFM has capability to precisely control and assemble the nano-scale objects and structure, and it has been so used for applications such as assembling high capacity memories, micro/nano-size robots, DNA computers, and quantum devices [8-10]. By controlling the motion of a sharp tip above a sample surface with sub-nanometer precision, several approaches to the fabrication of structures have been achieved [11, 12]. For example, Guthold et al. modified a scanning probe microscope to quantitatively manipulate DNA and viruses in liquid environments [13, 14].

The experiments detailed in chapters 4, 5, and 6 regarding the control over the elastic modulus and interfacial surface energy of a range of sizes of polystyrene microspheres (all under 1 μm) equips us with the information needed to understand the underlying determinants of the translational mode of objects on the nano-scale. We now have attempted to use the lateral force microscopy (LFM) implementation of AFM to probe the translational mode of these polystyrene microspheres.

7.2 Lateral force microscopy (LFM)

7.2.1 Introduction

Atomic force microscopy (AFM) measurements were carried out to explore the mechanical properties of the sample either by moving the AFM probe in a direction that was either normal to or parallel to the planar substrate surface of our the sample. Previously, we performed measurements in the normal direction to extract topographical information, work of adhesion between the polymeric microspheres and the silicon substrate, and the elastic modulus or of the polymeric microspheres under various solvents. This work was described in the earlier chapters of this dissertation. Herein we detail our attempts to experimentally characterize the more complex

nature of motion in the lateral direction. These experiments seek to extract tribological information regarding the polystyrene microspheres and the silicon substrate.

The experimental collection of nano-scale tribological data is plagued by difficulties that arise from the method by which such experiments are often performed. Three major factors are: first, most lateral force microscopy measurements are performed under ambient conditions. Such experiments potentially suffer from surface adsorbates from the environment, plus changes in the relative humidity, which have a significant impact on the measured contact forces. To help avoid these issues, one might perform the experiments under vacuum. Unfortunately, this approach was not available to us either from an instrumentation perspective or from a technical design perspective – we need a bathing solvent in order to vary the elastic moduli of our samples. However, the bathing solvent has the added benefit of controlling the environment under which our experiments were performed, removing or reducing such issues as surface contaminants adsorbing from the atmosphere and capillary condensation resulting from humidity. Secondly, during the lateral scan the tip shape and contact area between the sample and tip, potentially change, making it difficult to reproduce the data even with the same AFM tip. We partially address this concern through the use of polished silicon wafer as our substrate – the highly planar surface (roughness below our noise floor of ~0.3nm) reduces the inconsistent contact between the tip and the substrate that results from less smooth surfaces. Thirdly, the incorrect analysis and calibration may affect the reproducibility of the experimental data even if the same instrument has been used. We carefully calibrate each tip's normal spring constant, which is related to the torsional spring constant through the material and geometric properties of the cantilever beam (see below). The largest variances would be expected in the thickness of the beam and the length of the protruding tip. The thickness of the beam is accounted for during the normal spring constant calibration

described earlier, and the length of the tip is characterized by SEM micrographs. Through such careful tracking of the force sensor in the lateral force microscopy experiments, the accuracy of the data is heightened. Moreover, because the interacting forces can be difficult to calculate [15], we have fully characterized the mechanical properties and surface energies for the samples to be used in our experiments. Through these efforts, we seek to reduce the difficulties that have been an issue in previous studies [16].

7.2.2 LFM methods and techniques

The force required to translate a nano-scale object across a surface is measured by the torsion of the cantilever during the process. The torsional spring constant was found through beam mechanics from the normal spring constant:

$$k_{tor} = 1.33 \frac{G}{E} \left(\frac{L}{l_{tip}} \right)^2 k_n \qquad (7.1)$$

where G and E are the shear and elastic moduli of silicon (the material from which the cantilever is etched, L is the length of the cantilever, l_{tip} is the length of the tip, and k_{tor} and k_n are the torsion and normal spring constants, respectively. The length of the cantilever is supplied by the manufacturer and typically has a very small tolerance. The length of the tip, though also specified by the manufacturer, often has larger variation and will be measured in the Scanning Electron Microscope (SEM). Once calibrated, the force creating the torsion of the cantilever is found by multiplying the lateral deflection by the torsion spring constant.

In a typical friction measurement, the tip starts from a stationary position in contact with the substrate. The cantilever is moved laterally toward the object of interest through some predetermined distance.

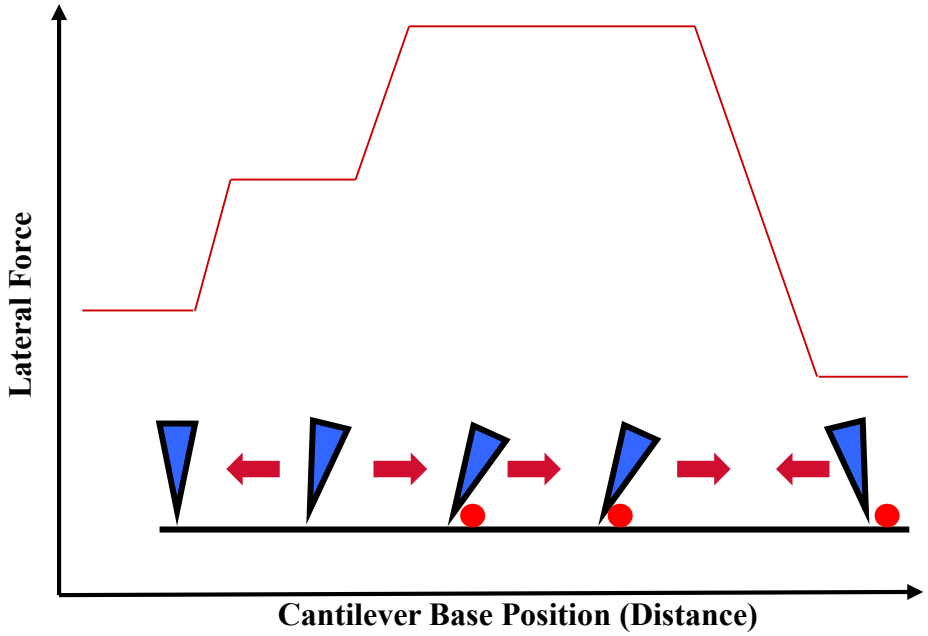

Figure 7.1: Showing the schematic of contact forces in lateral force microscopy.

The path is chosen such that the direction of motion is perpendicular to the long axis of the cantilever, thereby producing maximal torsional deflections of this beam and a maximal signal for measurement. Because the tip has adhered to the substrate, as the motion begins the cantilever moves before the end of the tip. The cantilever twists increasingly until the force generated on the tip is large enough to overcome the adhesion, and the tip starts sliding. When the tip makes initial contact with the object under investigation, it either becomes stationary or slows its motion. The cantilever continues to move laterally, increasing its torsion and the lateral force applied by the tip to the object. Once the lateral force is large enough to displace the object, the object begins to translate with the tip. The force required for this translation includes the friction force between the tip and the substrate, between the sample object and the substrate, and (potentially, if there is rolling) between the tip and the sample object. Measurements of the friction between the object and the substrate thus require knowledge of the friction between the tip and the substrate, to be subtracted out as a background, and the mode of translation – rolling or sliding. If the object is

rolling, then the tip surface and that of the substrate must be accounted for. The easiest way to do this is to make both surfaces match. For this reason we have used silicon cantilevers/tips as well as silicon substrates.

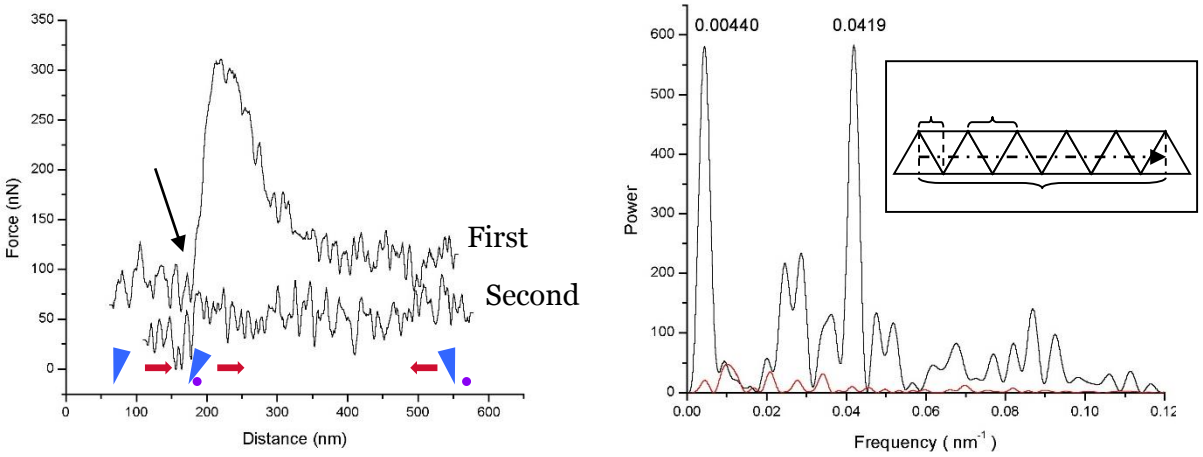

Figure 7.2: Left: Sample force traces (plot of lateral force versus distance moved by the AFM tip) for the first and second time a capsid is translated. The arrow indicates the increase in the lateral force that occurs as the tip contacts the virus (shown schematically along the Distance axis. **Right:** Fourier spectra of second trace shown on the left and a trace taken while translating a 100 nm polystyrene microsphere (curve lying near the horizontal axis). The labeled peaks correspond to the distance between facets and the capsid circumference, illustrated schematically in the inset. Further enhance data from reference 14.

Knowledge of the mode of translation is a unique aspect of this work. In previous work investigating the translation of icosahedral virus capsids (adenovirus), it was observed that Fourier transforms of the lateral force data trace (see Figure 7.2 above) highlighted periodic features within the trace, and these features could be ascribed spatially to dislodging facets of the icosahedron as the tip rolled the virus [14]. When spherical control objects were translated in a similar manner, the periodic features disappeared. Thus the Fourier analysis of the lateral force data trace offers a powerful means to discover the modes of translocation between rolling and sliding. In the present study, Fourier analysis was used to investigate the translocation mode of polystyrene microspheres. However, because our samples are spherical, an asymmetry must be introduced.

Attempts were made to create the asymmetry by performing normal force curves on the microspheres, applying as large a force as we could generate without breaking the tip in an effort to exceed the plastic limit. An indentation would have been left in the surface of the sphere, providing us the asymmetry needed to produce periodic features for detection by Fourier analysis. If such features are not apparent, it is likely that the sample is sliding.

7.3 Experimental procedure

Polystyrene microspheres of two surface energies (surface functionalized with either amine or carboxylate groups) and two different sizes (200 and 500 nm) were deposited on a cleaned Si substrate following the same method explained above in chapters 4 and 5. The amine and carboxylate functionalized microspheres were selected to probe the extremes in surface energies we can access in the absence of further surface chemical modifications. A topographical image was collected and saved by performing a typical intermittent contact scan of the sample. This image was used to locate the particles precisely. The AFM was changed to contact mode, and a force curve with a very high force limit was performed on a selected microsphere. This force curve was intended to leave a plastic deformation, a permanent indentation, on the surface of the microsphere, providing the asymmetry required for the discrimination between rolling and sliding translation when lateral forces were applied (see section 2.4). The AFM operating software then was optimized for lateral force microscopy. The AFM probe tip was brought into repulsive contact with the substrate with a defined deflection of the beam being used for feedback. A path was software defined, directing the tip to pass through the location of the microsphere. Once activated, the sample was moved laterally toward the tip at a constant velocity along the trace. The piezo controlling the horizontal position of the sample was used to first move the tip into contact with a microsphere, then past this position. During this process, an initial lateral force was applied to

slide the tip across the surface. After contact with the microsphere, the lateral force increased until the sphere broke free from the substrate and began translating across the surface. During this process, the lateral force was recorded as torsional deflection of the cantilever. Both, bending and twisting are recorded by means of movement of the reflected the laser beam from the back side of the cantilever. Only one sensor, a four-quadrant position sensitive photodiode, is required to measure the deflection and torsion of the cantilever. Normal bending is measured by subtracting the lower two quadrants of the diode from the upper two quadrants, i.e. (A+B) – (C+D), whereas subtracting the right pair of diode quadrants from the left pair gives the torsional measurement (A+C) – (B+D). This measurement was performed on both amine and carboxylate functionalized microspheres, both in air and liquid (DI water only) using different AFM probes varying in spring constants. AFM probes of spring constants 4.5 N/m, 14 N/m, and 45 N/m were selected. This provided a range in stiffness for the beam from softer to stiffer. The temporarily saved lateral force data were finally exported for analysis.

The lateral force data was then analyzed to determine the mode of translation. A Fourier transform of the lateral force data was used to distinguish between the modes of translation for these polystyrene microspheres. Periodic features in the Fourier spectrum served as a signature for the microsphere rolling while translating; the absence of periodic features served to indicate sliding. Comparison of the force required for translation predicted by the models, using the data from sections 4.5, 5.4, and 6.4 with data from this section, will allow us to assess the state of the current models for nanoscale friction.

7.4 Results and discussion

As mentioned in chapter 1 of this dissertation, particle size, elastic modulus, and the interfacial surface energy were expected to have an impact on the translation force for the polystyrene microspheres along the substrate. We applied the data reported in chapter 4, 5, and 6 to equations 1.1 and 1.6 to predict the sliding and rolling forces on a 200 nm polystyrene microsphere. We calculated rolling and sliding forces in DI water for 200 nm size polystyrene microsphere of all functionalizations.

Using equation 1.6 from reference [2], we found the predicted rolling force from

$$F_R = 6\pi\gamma\xi \qquad (7.2)$$

where γ is the interfacial surface energy and ξ is the critical displacement required for rolling to be initiated. ξ is given by

$$\xi = \frac{a_{contact}}{12}\left(\frac{G_1 - G_2}{\gamma}\right) \qquad (7.3)$$

where $a_{contact}$ is the JKR radius of the contact area and G_1 and G_2 are the shear moduli of the microsphere and the substrate. True rolling motion,

$$\xi_{critical} = \frac{a_{contact}}{12}\left(\frac{\Delta\gamma}{\gamma}\right) \qquad (7.4)$$

Krijt et al. compared their work with Sitti et al. [4], they used $\frac{\Delta\gamma}{\gamma} = 3$,

Hence equation 7.4 becomes,

$$\xi_{critical} = \frac{a_{contact}}{4} \qquad (7.5)$$

The contact radius is given by JKR model,

$$a_{contact} = \left(\frac{9\,\pi\,\gamma\,R^2}{2\,E^*}\right)^{1/3} \quad (7.6)$$

In equation 7.6, R is the radius of the translating particle and

$$\frac{1}{E^*} = \frac{1-\nu_1^2}{E_1} - \frac{1-\nu_2^2}{E_2} \quad (7.7)$$

Where ν is the Poisson ratio, which we take to be ν = 0.3. Equation 7.7 becomes,

$$E^* = \frac{10\,(E_1 * E_2)}{(E_1 + E_2)} \quad \text{----- (7.8)}$$

E_1 and E_2 are the elastic moduli of the translating particle and the substrate, respectively.

From table 5.2, the elastic modulus E_1 of the 200 nm PS microsphere in DI water was 0.837 GPa. And the elastic modulus E_2 of the Si substrate was 165 GPa [17]. Solving for E^* in equation 7.8, we get E^*, which was 8.32 GPa (dominated by that of the microsphere – the silicon substrate was essentially infinitely stiff in comparison). The contact radii for 'as received' microspheres, amine and carboxylate functionalized microspheres were calculated from equation 7.6, and were found to be 9.59 nm, 6.04 nm, and 14.77 nm. Using the surface energy values from section 6.3 (γ of 200 nm diameter PS 'as received' microspheres = 0.052 J/m^2, γ of 200 nm PS amine functionalized microspheres = 0.013 J/m^2, and γ of 200 nm carboxylate functionalized microspheres = 0.190 J/m^2) we solved for the rolling forces. The rolling forces calculated for the 200 nm diameter microspheres as received, amine functionalized, and carboxylate functionalized were 2.35 nN, 0.37 nN, and 13.21 nN, respectively.

We now use equation 1.1 and the data from chapters 4, 5, and 6 to solve for sliding forces for 200 nm size PS microspheres functionalized differently.

$$F_{slide} = \tau\,A \quad (7.9)$$

where τ is the interfacial shear strength and

$$A = \pi\, a_{contact}^2 \qquad (7.10)$$

Results from the literature using the surface force apparatus (SFA) experiments demonstrated that the shear strength is scale dependent. At some point τ must decrease as the contact size increases from the nano to the micro scale. This equation establishes the frictional stress as a function of contact area, though there is no experimental evidence to date [18].

Sitti et al. proposed a model for a wide range of particle radii. From the results, they defined τ, which is a function of $a_{contact}$, as

$$\tau\,(a_{contact}) = \begin{Bmatrix} G/43, & a_{contact} < 20\ nm \\ G\ 10^N\ (a/b)^M, & 20\ nm\ < a_{contact}\ < 40\ \mu m \\ G/1290, & a_{contact}\ > 40\ \mu m \end{Bmatrix} \qquad (7.11)$$

In equation 7.11, N is $28b$ and b = 0.5 nm, b is known as Burgers vector and $M = \tan^{-1}[(G/43 - G/1290) / (8*10^4 b - 28b)]$. Where $G = 2G_1G_2 / (G_1+G_2)$ is the effective shear modulus given in terms of shear moduli (G_1, G_2). For a particle and a substrate G is defined as $Gi = E_i / [2(1 + v_i)]$, in which E is the Young's modulus and v is the Poisson ratio. In equation 7.10, $a_{contact}$ is the contact radius, which is the same as in equation 7.6. The values for all differently functionalized polystyrene microspheres were the same as reported above, and all of these $a_{contact}$ values were less than 20 nm. Hence, the value used for τ was $G/43$ (from equation 7.11). G_i is calculated for the PS microsphere as mentioned above and G_2 for the substrate is 165 GPa [19]. Combining 7.9, 7.10, and 7.11, we get,

$$F_s = \frac{G}{43}\, \pi\, a_{contact}^2 \qquad (7.12).$$

Inserting the appropriate values into equation 7.12, the sliding forces for 200 nm PS microspheres for as received, amine, and carboxylate functionalized are 11.14 nN, 4.42 nN, and 26.44 nN respectively. The outcomes predicted by the models for our 200 nm microspheres translating in water are summarized in Table 7.1. For this set of 200 nm microspheres under water, rolling is always preferred to sliding. While experiments on these microspheres are not likely to lead us to find the conditions under which the microspheres transition to sliding, they will provide useful information regarding our ability to observe rolling.

In general, both sliding and rolling forces will be higher for higher surface energies. A larger force will be required to translate a particle that has higher surface energy. Considering the models, we expect that, as the particle size decreases, the microspheres eventually will tend to slide rather than roll. Higher values of interfacial energy will tend to cause the microspheres to roll rather than slide. Elastic modulus also will have an impact on the translation forces. Particles with larger elastic moduli will be more likely to roll than slide, and we expect the modified modulus of polystyrene microspheres will be better suited to the search for a transition from rolling to sliding when compared to the microspheres not softened by any solvent.

Table 7.1: Summary of the translation force for rolling and sliding as predicted by the appropriate model.

Surface Functionalization	Surface Energy (J/m^2)	Contact Radius (nm)	Predicted Force (nN)	
			Rolling	Sliding
Amine	0.013	6.0	0.37	4.42
As Received	0.052	9.6	2.35	11.14
Carboxylate	0.190	14.8	13.21	26.44

Figure 7.3 below shows the translation of the 500 nm carboxylate functionalized polystyrene microsphere in air.

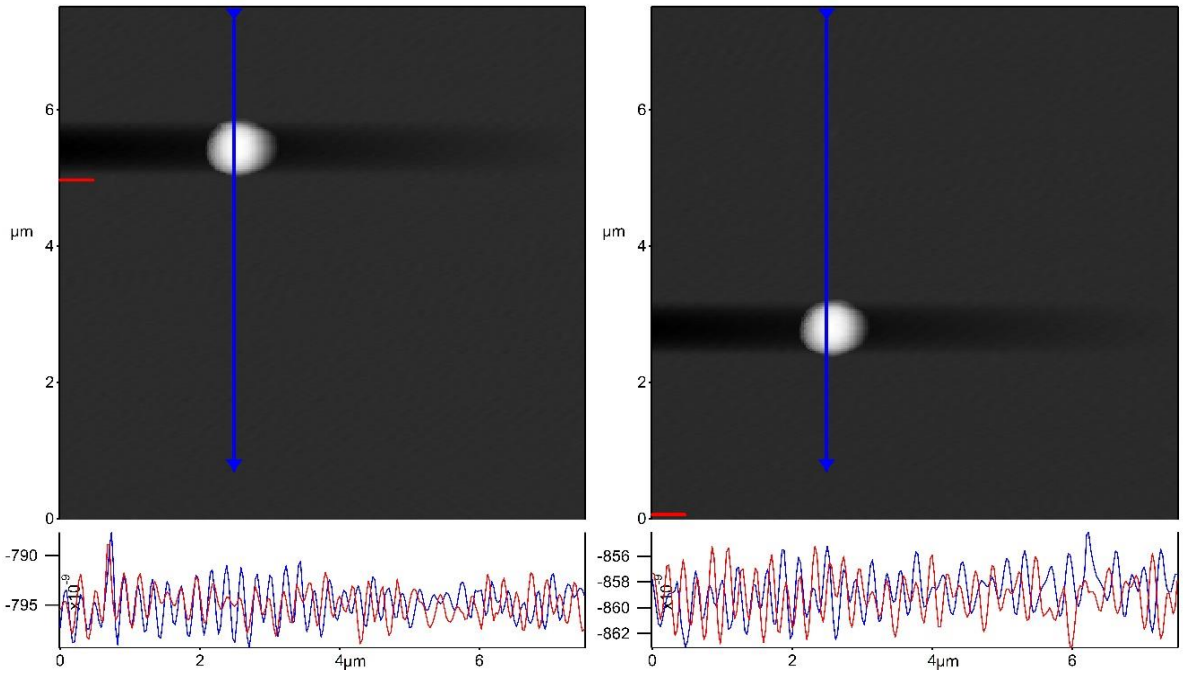

Figure 7.3: AFM images of 500 nm COOH polystyrene beads (before: on the left, and after: on the right, the translation in air using a 4.5 N/m AFM tip in air.

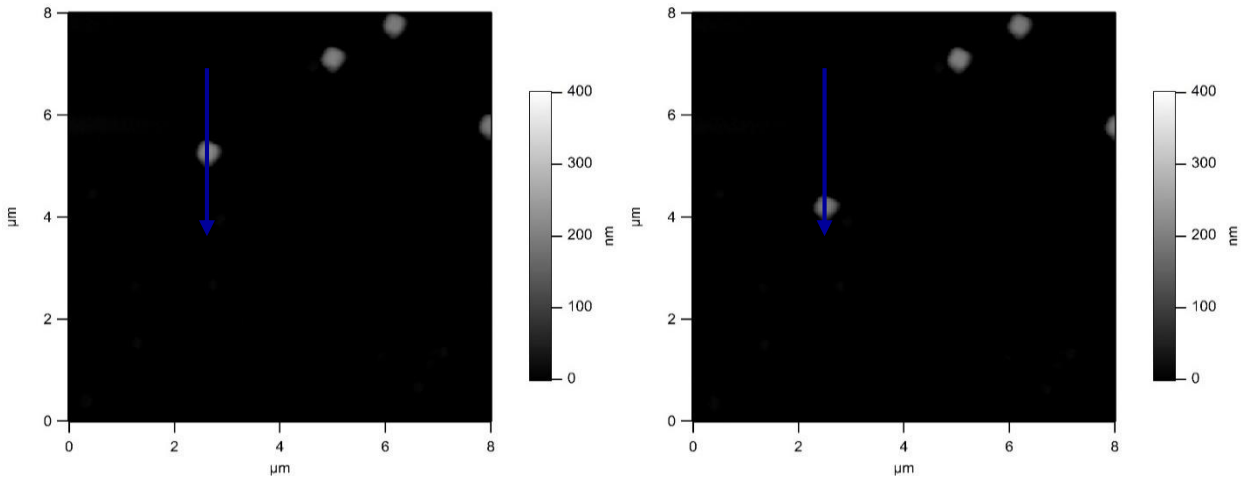

Figure 7.4: AFM images of 200 nm amine polystyrene beads (before: on the left, and after: on the right, the translation in air using a 14 N/m tip in air.

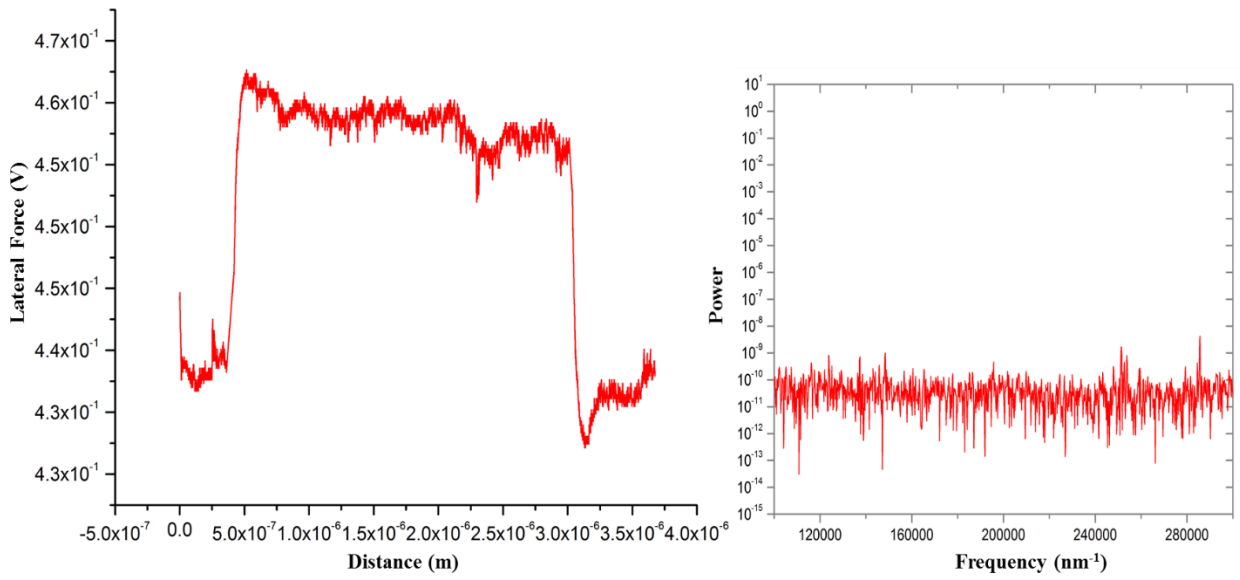

Figure 7.5: Graph on the left shows Lateral Force vs Distance graph of 500 nm COOH PS beads with a 45 N/m AFM tip in DI water. Graph on the right shows Fourier Transform of the lateral force data from the left graph.

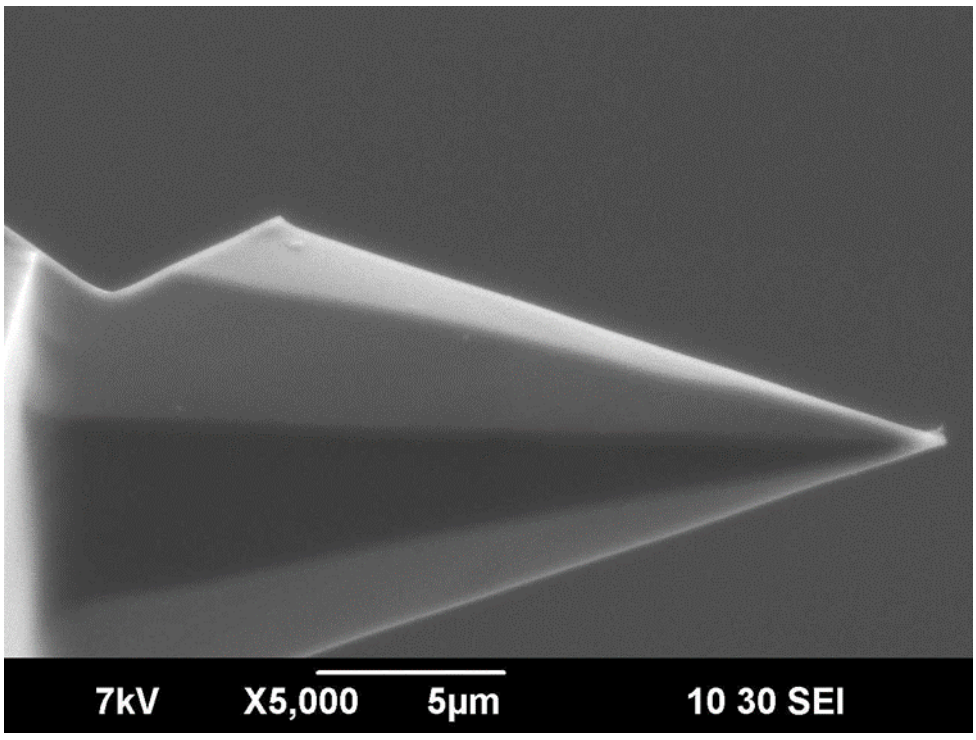

Figure 7.6: Shows the SEM image of an AFM tip. The l_{tip} in equation 7.1 is measured from this figure

Equation 7.1 was used to calculate the torsional spring constant k_{tor}. In equation 7.1, G and E are the shear and elastic moduli for Si. We use G and E for Si as 79.92 GPa and 130.91 GPa respectively [20]. L is the length of the cantilever, and we used the nominal values reported from the manufacturer: 230 μm for the 46.5 N/m normal spring constant cantilever and 90 μm for the 14.75 N/m normal spring constant cantilever. l_{tip} values for the two tips were measured from the SEM images as 19.81 μm for the 46.5 N/m normal spring constant cantilever and 19.37 μm for the 14.75 N/m normal spring constant cantilever. These values gave k_{tor} values for the two AFM tips with different lengths were found to be 5094.63 N/m and 258.55 N/m – substantially more stiff than their normal spring constants.

Figure 7.3 and 7.4 show the translated PS microspheres of 500 nm COOH and 200 nm amine functionalized microspheres in air. From figure 7.3 and 7.4 above, it is evident that these polystyrene microspheres (500 nm COOH, and 200 amine) were translated from one point to another under the lateral force applied by the tip in air. A similar translation was also achieved in liquid. However, when the Fourier transform of the lateral force data was performed as in Figure 7.5, no periodic features were observed. Fourier transforms performed on all the lateral force data were similarly lacking in periodic features. This absence of periodic features, as mentioned in section 7.2.2, implies that these polystyrene microspheres were sliding. This observation held true both under air and liquid environments and for the different spring constant cantilevers used. However, it was more likely that we were unable to permanently deform the microspheres during the hard indentation intended to create a plastic deformation. No such modification of their shape was observed. Thus, there likely was no asymmetry to detect by way of the Fourier transforms.

7.5 Conclusion

Using the data from chapters 4, 5, and 6, and using the rolling and sliding models as detailed in section 1.2.3, rolling and sliding forces were predicted for 200 nm diameter microspheres with three different surface functionalizations: as received, amine, and carboxylate. These calculations assumed that the experiments would be performed under DI water. The sliding and rolling forces predicted were dependent upon both surface energy and elastic moduli, as well as the size of the microspheres.

Lateral force microscopy was performed on 200 nm and 500 nm diameter polystyrene microspheres with amine and carboxylate surface functionalizations. AFM cantilevers of different stiffness ranging from 4.5 N/m to 45 N/m were tested. The lateral force microscopy was performed both in air as well as in DI water. Topographical imaging of pre- and post- lateral force experiments confirmed the translation of these polystyrene microspheres from one given location to another. However, Fourier analysis of the lateral force data did not show any periodic feature for any trial. It is possible all these microspheres are sliding, and no rolling feature occurred during lateral motion. However, due to the sensitivity of lateral force data and dependency on many factors, it was difficult to claim only sliding occurred. This creates room for further optimization of conditions under which the experiments should be performed.

7.6 References

[1] R. Fuchs, T. Weinhart, J. Meyer, H. Zhuang, T. Staedler, X. Jiang, S. Luding, Rolling, sliding and torsion of micron-sized silica particles: experimental, numerical and theoretical analysis, Granular Matter, 16 (2014) 281-297.

[2] S. Krijt, C. Dominik, A. Tielens, Rolling friction of adhesive microspheres, Journal of Physics D: Applied Physics, 47 (2014) 175302.

[3] M.R. Falvo, R.M. Taylor, A. Helser, V. Chi, F.P. Brooks, S. Washburn, R. Superfine, Nanometre-scale rolling and sliding of carbon nanotubes, Nature, 397 (1999) 236-238.

[4] B. Sümer, M. Sitti, Rolling and spinning friction characterization of fine particles using lateral force microscopy based contact pushing, J Adhes Sci Technol, 22 (2008) 481-506.

[5] K. Kendall, Rolling friction and adhesion between smooth solids, Wear, 33 (1975) 351-358.

[6] S.G. Vilt, N. Martin, C. McCabe, G.K. Jennings, Frictional performance of silica microspheres, Tribol Int, 44 (2011) 180-186.

[7] M. Evstigneev, K. Mougin, P. Reimann, Modeling of nanoparticle manipulation by AFM: Rolling vs. sliding regimes, Epl-Europhys Lett, 101 (2013).

[8] M.H. Korayem, H. Badkoobeh Hezaveh, M. Taheri, Dynamic Modeling and Simulation of Rough Cylindrical Micro/Nanoparticle Manipulation with Atomic Force Microscopy, Microscopy and Microanalysis, 20 (2014) 1692-1707.

[9] M. Sitti, H. Hashimoto, Controlled pushing of nanoparticles: Modeling and experiments, Ieee-Asme T Mech, 5 (2000) 199-211.

[10] Y. Kim, C.M. Lieber, Machining Oxide Thin-Films with an Atomic Force Microscope - Pattern and Object Formation on the Nanometer Scale, Science, 257 (1992) 375-377.

[11] T. Junno, K. Deppert, L. Montelius, L. Samuelson, Controlled Manipulation of Nanoparticles with an Atomic-Force Microscope, Appl Phys Lett, 66 (1995) 3627-3629.

[12] O.M. Leung, M.C. Goh, Orientational Ordering of Polymers by Atomic Force Microscope Tip-Surface Interaction, Science, 255 (1992) 64-66.

[13] M. Guthold, M. Falvo, W. Matthews, S. Paulson, J. Mullin, S. Lord, D. Erie, S. Washburn, R. Superfine, F. Brooks Jr, Investigation and modification of molecular structures with the nanoManipulator, Journal of Molecular Graphics and Modelling, 17 (1999) 187-197.

[14] M. Guthold, G. Matthews, A. Negishi, R. Taylor, D. Erie, F. Brooks, R. Superfine, Quantitative manipulation of DNA and viruses with the nanomanipulator scanning force microscope, Surface and interface analysis, 27 (1999) 437-443.

[15] X. Ling, H.-J. Butt, M. Kappl, Quantitative measurement of friction between single microspheres by friction force microscopy, Langmuir, 23 (2007) 8392-8399.

[16] U. Schwarz, P. Köster, R. Wiesendanger, Quantitative analysis of lateral force microscopy experiments, Review of scientific instruments, 67 (1996) 2560-2567.

[17] J. Wortman, R. Evans, Young's modulus, shear modulus, and Poisson's ratio in silicon and germanium, Journal of applied physics, 36 (1965) 153-156.

[18] J.A. Hurtado, K.S. Kim, Scale effects in friction of single–asperity contacts. I. From concurrent slip to single–dislocation–assisted slip, Proceedings of the Royal Society of London. Series A: Mathematical, Physical and Engineering Sciences, 455 (1999) 3363-3384.

[19] J. Dolbow, M. Gosz, Effect of out-of-plane properties of a polyimide film on the stress fields in microelectronic structures, Mechanics of materials, 23 (1996) 311-321.

[20] H.-H. Liao, Y.-J. Yang, A micromirror module using a MEMS digital-to-analog converter and its application for optical surface profiling, Journal of Micromechanics and Microengineering, 20 (2010) 105009.

8.0 Conclusion and future work

8.1 Summary

The scanning probe microscope has become a powerful tool for applications within micro/nano-scopic science because of its straightforward three-dimensional measurements, including precise nano-scale positioning of a mechanical probe, which can be extended to a wide variety of samples under different conditions. Using the atomic force microscope, we applied force spectroscopy, nano-indentation, and lateral force microscopy (LFM) to the study of the mechanical properties, friction, and adhesion of sub-micron diameter polymeric microspheres.

To the best of our knowledge we are the first group to report the elastic modulus of polystyrene microspheres as experimentally measured at the micro/nano-scale, especially under solvent conditions. The work was carried out using an Atomic Force Microscope, performing force spectroscopy on four different sizes of polystyrene microspheres (ranging from 500 nm to 50 nm) deposited on a Si substrate. The obtained data from force spectroscopy was analyzed using the Hertz model, and the measured modulus values ranged between 1.94 – 2.53 GPa under ambient conditions. This result is comparable to the reported bulk modulus of the polystyrene [1]. The elastic moduli were obtained in two different types of data sets: one that was a repeated measure on a single microsphere and one that was comprised of separate measurements on different individual microspheres. These data sets were compared using Student's unpaired t tests. It was found that that elastic moduli obtained were the same, regardless of whether taken from repeated measures on a single microsphere or aggregated measures from multiple microspheres. Moreover,

the modulus had no dependence upon diameter. These results demonstrate both accuracy and precision for the technique. That the measured modulus of the nano-scale materials matched that of the bulk suggests that, at the smallest length scale we tested (50nm), the bulk behavior still holds. It also suggests that the influence of the more rigid substrate does not yet influence the measurements at this scale.

The mechanical properties of the polystyrene microspheres were modified using solvents. We used DI water and ethanol and their mixture as solvents, and the differing miscibility of polystyrene in these solvents differentially swelled the microspheres. The elastic modulus of these polystyrene microspheres was determined to be ~ 0.8 GPa under 100% DI water for both repeated and population averaged measures of all sizes of microspheres. This slight decrease in the modulus was likely caused by the absorption of some small amount of water into these microspheres. There was a much more significant decrease in elastic modulus for these polystyrene microspheres when submerged in pure ethanol. The elastic modulus in pure ethanol ranged from ~ 2.49 – 3.55 MPa: a change of almost three orders of magnitude as compared to the modulus in water. A pattern in the modulus values depending on the swollen size of these microspheres in pure ethanol also was observed, if the ethanol has not fully absorbed into the microspheres. Larger sized microspheres had larger moduli. Because the time submerged approximately was constant, the fraction of the microsphere that had absorbed the solvent would have the same dependence. Flory-Rehner theory predicting the elasticity from the swollen volume of these polystyrene microspheres was tested. The higher slope obtained did not match the prediction value of the Flory-Rehner theory. The higher value of slopes likely were caused by imperfections in the swollen network. Further modification in the Flory-Rehner theory will be needed to precisely predict the elasticity and swelling behavior of polystyrene microspheres in ethanol. Future experiments are needed in which

the dilution of ethanol in water is varied with the goal of producing microspheres with varying but controllable moduli [2, 3].

A technique that uses lateral force microscopy to attach polystyrene microspheres on to the AFM cantilever was developed. Using tip prepared with this technique, force spectroscopy was performed. The adhesion forces between polystyrene microspheres of different surface functionalizations and a silicon substrate was measured. Using JKR theory, the surface energy for these microspheres was extracted. The carboxylate (COOH) functionalized microspheres had the largest interfacial surface energy, whereas the amine functionalized microspheres had the lowest interfacial energy. The regular types (not functionalized with any group) had an interfacial surface energy somewhere between these two functionalized microsphere types. The interfacial surface energy for the unfunctionalized polystyrene microspheres is in complete agreement with the previously published data from bulk measurements (Sumer et al [4]). For the COOH functionalized microspheres, the surface energy is about four times that of amine functionalized beads. For the amine functionalized beads interfacial energy is half that of regular (not functionalized with any group) microspheres.

Data from chapters 4, 5, and 6 were used with the rolling and sliding models described in section 1.2.3. The sliding and rolling forces predicted were higher for higher surface energy PS microspheres. We used Lateral Force Microscopy (LFM) to investigate the translation motion of these micro/nano-micorspheres. LFM was performed on 200 nm and 500 nm diameter polystyrene microspheres which were amine and carboxylate functionalized. AFM cantilevers of different stiffness ranging from 4.5 N/m to 45 N/m were tested. The lateral force microscopy was performed in air as well as in DI water. Pre- and post- lateral force spectroscopy topographical imaging confirmed the translation of these polystyrene microspheres from one given point to another.

However, Fourier analysis of the lateral force data failed to show any periodic feature for any of these polystyrene microspheres. It is possible all these microspheres are sliding, and no rolling feature occurred during lateral motion. However due to the sensitivity of lateral force data and dependency on many factors, it's difficult to claim only sliding is present [5, 6].

The nano-tribological characterization presented in this study likely will be used to understand and control the frictional behavior of micro/nano-size particles for prototypes particle based micro/nano devices and fabrication templates, particle based lubrication, aerosol, and particle removal applications. The study outcomes will help understand the different interaction forces such as electrostatic, van der Waals interactions etc. and how they affect the interfacial energy between a micro/nano-sphere and a flat surface. One suitable application of the findings from this study would be in the cleaning of semiconductor wafers. Unwanted particulates on a semiconductor wafer can cause circuit defects which yields loss in the final product. Chemical mechanical polishing (CMP) is used to planarize the wafer surface, but it leaves residue on the wafer and, again, may cause circuit failure. Post CMP cleaning is expensive and causes critical environmental issues. Using AFM as nano-manipulator and understanding the particle adhesion of these particles on the wafer can help achieve defect free semiconductor wafer post fabrication by removing unwanted particles efficiently and economically.

8.2 Future work

8.2.1 Tuning the modulus between the extremes

We tuned the mechanics of the polystyrene microspheres using DI water and ethanol. Tuning the mechanics using mixtures of DI water and ethanol in different ratios refine our control over the elastic moduli. Performing translation experiments on microspheres as a function of

modulus would provide much needed validation testing of the various models for rolling and sliding friction.

8.2.2 Adhesion and surface energy

Future work will be required to extend the range in works of adhesion to which we have access. Performing adhesion experiments on all sizes (50, 100, 200, and 500 nm) and all types (regular, amine, and carboxylate functionalized) of microspheres would confirm our belief that the surface energy does not vary with size. Surface chemical modification of the silicon substrate through silane chemistry will broaden the range in works of adhesion. These outcomes will provide a larger set of conditions under which we will employ our lateral force experiments. Data from these experiments will again be applied to test the current theories for rolling and sliding friction.

8.2.3 Modify translational motion methods and techniques

A modified lateral force microscopy method and data analysis will be helpful to obtain precise and full-proof data. An alternate method of indenting the translating particles is a potential approach. A more straightforward approach would be to use our technique for the attachment of microspheres to the tip of the AFM force sensor. Lateral force experiments with such a tip would guarantee sliding. The forces measured under these conditions could be compared with that measured when using the tip to apply lateral forces to translate the microspheres across the surface.

8.2.4 Particle size

Using our experimental data with Sumer et al and Krijt et al.'s predictions, we noticed (not reported in this dissertation) a transition in translation mode dependent upon size of the

microsphere [4, 7]. The transition from rolling to sliding was predicted to occur at ~ 25 nm particle size. Polystyrene microspheres of 25 nm in diameter are needed to further verify that result. Currently, the manufacturers of PS microspheres do not supply microspheres at that length scale.

8.2.5 Alternate material

Using silicon as the substrate and polystyrene as the translating material, we were able to vary all the parameters needed to investigate translational motion at the micro/nano-scale. However, it will be of interest to find alternate substrates and particles which may further simplify the outcomes. For example, if a faceted material is used instead of the polystyrene microspheres for the translating particles, the facets would provide the necessary periodic variation in the lateral force for Fourier analysis to confirm rolling.

8.3 References

[1] S. Chizhik, Z. Huang, V. Gorbunov, N. Myshkin, V. Tsukruk, Micromechanical properties of elastic polymeric materials as probed by scanning force microscopy, Langmuir, 14 (1998) 2606-2609.

[2] R.C. Hedden, H. Saxena, C. Cohen, Mechanical properties and swelling behavior of end-linked poly (diethylsiloxane) networks, Macromolecules, 33 (2000) 8676-8684.

[3] S.K. Patel, S. Malone, C. Cohen, J.R. Gillmor, R.H. Colby, Elastic modulus and equilibrium swelling of poly (dimethylsiloxane) networks, Macromolecules, 25 (1992) 5241-5251.

[4] B. Sümer, M. Sitti, Rolling and spinning friction characterization of fine particles using lateral force microscopy based contact pushing, J Adhes Sci Technol, 22 (2008) 481-506.

[5] X. Ling, H.-J. Butt, M. Kappl, Quantitative measurement of friction between single microspheres by friction force microscopy, Langmuir, 23 (2007) 8392-8399.

[6] U. Schwarz, P. Köster, R. Wiesendanger, Quantitative analysis of lateral force microscopy experiments, Review of scientific instruments, 67 (1996) 2560-2567.

[7] S. Krijt, C. Dominik, A. Tielens, Rolling friction of adhesive microspheres, Journal of Physics D: Applied Physics, 47 (2014) 175302.

Appendices

Appendix A: Industrial practicum report

High frequency reciprocating rig (HFRR) lubricity studies of different aviation fuels using a universal materials tester

A.1 Introduction

Lubricity is an important property of diesel fuels. In the last few years the advancement in diesel engine technology, environmental concerns, and the more stringent emission standards have led to increase the lubricity of diesel fuels in order to protect the fuel injection system and various other components of the engine. To comply with the emission standards, the modifications in the engine designs are made to control the fuel injection and fuel injection pressure. The change in hardware requires improved lubricity to avoid excessive wear and failure. Sulfur, nitrogen, and aromatic contents and a higher boiling point of a diesel fuel help to improve the lubricity conditions. Highly polar compounds specially those containing nitrogen and oxygen, form a protective layer on the metal surface. Oxygen containing compounds and its derivatives are a good friction reducing agents. These compounds adsorb or react on the contact surfaces to reduce adhesion between the surfaces and limit the friction, wear and seizure. The modification of the diesel fuel quality to address environmental concerns results in to the loss of polar compounds of nitrogen, sulfur and oxygen and hence the loss of lubricity of the diesel fuels which eventually affects the engine performance and ends up into engine failures and accidents [1].

JP-8 (Jet Propellant – 8) is a widely used aircraft fuel. JP-8 also is a US Department of Defense (DoD) aviation fuel also used by NATO members. However the lower lubricity of JP-8 compared to the distillate fuel has been identified as a major concern for universally adapting this military kerosene for various applications [2]. This could be due to a lower boiling point and

absence of naturally occurring polar compounds that enhance the lubricity. Several issues that arise using a low lubricity fuel are accelerated wear, corrosion, engine speed instability, engine smoke and low engine power [3]. Alternative fuels such as Biodiesel can be used which have better lubricity, although it has drawbacks such as high quality raw materials needed like large amount of alcohol that increase the production cost. The presence of water may also lead to soap formation in the base catalysis [4]. Many alternative fuels are being used in every type of transport but not all of them are suitable for application in air. Kerosene-like drop-in alternative fuels have received a lot of attention recently for use in aircraft engines. Such alternative fuels available can be categorized mainly in three categories, trans-esterification, Fisher-Tropsch (FT), and hydrotreating [5]. Several DoD and DOE (Department of Energy) performance tests on these fuels have determined that these fuels are viable to use by the military. Highly iso-paraffinic kerosene (IPK) FT fuel is an attractive candidate for 'Joint Battlespace Use Fuel of the Future' (JBUFF) [6]. During the low temperature (210-240 ^{o}C) FT synthesis the primary product that come out are long chain n-alkanes (wax). Further processing of n-alkanes into branched alkanes and substitution by mono and di-methyl and separation into the desired distillation range produces iso-paraffinic kerosene (IPK) [7]. Hydrotreated Renewable Jet (HRJ) also known as bio-Synthetic Paraffinic Kerosene (SPK) is another alternative fuel which has attracted a lot of research recently. HRJ uses triglycerides and free fatty acids from plant oils and animal fats as feedstock to process hydrocarbon aviation fuel. The near term application of FT IPK and HRJ are in 50/50 blend with conventional jet fuel JP-8. Various other tests are in progress to establish the application of these fuels as lubricants in jet engines [8].

One approach to enhance fuel lubricity is include additive. A variety of additives can be used which have high affinity to attach onto the metallic surfaces. They form a thin protective

layer between the metal and the metal contact layer. The adsorption of the polar molecules of the additives on the negatively charged metal surface forms the lubricant film [9]. Several studies have investigated the effect of additives on the lubricity of the diesel fuels. Anastopoulos et al. reported the improved lubricity of JP-8 fuel to the satisfactory level when they tested ten types of mono-carboxylic acid esters as an additive. Among the esters tested, those having the ester group in the middle of the molecule showed better lubrication properties [2]. Blending bioethanol with diesel fuel is an alternative to improve the lubricity of diesel fuels but the presence of ethanol causes the loss of lubricity because of the volatility of ethanol. Lapuerta et al. reported better lubricity until the ethanol concentration is 100%. Additionally, increased temperature for lower concentration of ethanol still showed a better lubricity as ethanol evaporated from the lubricating layer at increased temperature [9]. The addition of fatty acids or fatty acid esters have also showed improved lubricity [10]. Many studies agree that adding 1% to 2% biodiesel improves the fuel lubricity [10, 11]. Kulkarni et al. reported that ethyl esters have better lubricity over methyl esters [12].

In this work we have investigated the baseline lubricity of an FT IPK, an R-8 HRJ, and two different JP-8 samples. The difference between JP-8 samples are that A is taken freshly from the drum and B has been in a HDPE bottle for two years. All tests were performed following ASTM D 6079 standard, using a tribometer described below [13]. The wear scars diameters were recorded using an optical microscope. The average wear scar diameters for all four grades of heavy fuel were measured for each test performed. The wear scar diameters came out much larger than the accepted industry adapted standard 460 μm (European EN 590:2009 and US ASTM D 975 regulations) for field performances [14]. Lubricity additives can be added to JP-8 in order to protect aircraft engines from excessive wear, corrosions, and sudden seizure. Further studies are needed

to better understand the role of different additives in order to enhance the lubricity and meet the industry accepted standard.

A.2 CETR UMT-3 (Center for Tribology, Inc. Universal Materials Tester – 3)

The Universal Materials Tester (UMT) is a tribometer, a popular tribological testing system for testing lubricity. It can also be used testing ferrous, non-ferrous metals, plastic, ceramic, paper, composite, thin and thick coatings, oils, greases, solid lubricants, and lubricating fluids. UMT-3 can be used for various tribological testing modes such as; Pin-on-Disc, Ball-on-Disc, Ball-on-one-two-or-three-balls, Pin-on-V-block, Block-on-Ring, Disc-on-Disc, Screw-in-nut etc. The UMT can be used for upper and lower samples of practically any shape. The upper specimen is connected to a vertical linear motion system, which can travel up to 150 mm. Wear measurements with a precision limit of 50 nm can be performed on this instrument. The lower specimen can be rotated with a precision spindle in the range 0.001 rpm to 5000 rpm. Force and load measurements are recorded by ultra-high strain gauges sensors in two to six axes. These forces are measured precisely in the ranges from mg to kg.

A normal load sensor is used to provide feedback to the vertical motion controller which actively adjusts the sample position to maintain a constant load during the testing. The UMT data acquisition and motor control are achieved by a fully automated PC. The test data are displayed, recorded and calculated in real time. The test data can also be stored for future retrieval [15].

A.3 Experimental procedure

A high frequency reciprocating rig of CETR UMT-3 by Bruker Instruments, was used to perform all lubricity tests. The tests were carried out following ASTM D 6079 standard, though European EN ISO 12156-1 standard is also a popular method to perform such tests. The European

standard establishes 60 ^{o}C as the fuel temperature whereas ASTM standard also accepts testing at 25 ^{o}C. The temperature of the engine metallic surface is ideally close to 60 ^{o}C, the ASTM method permits one to separate the effect of loss of fuel due to evaporation. ASTM standard is preferred when there is a high risk of loss of fuel because of its volatility or degradation. The flash point of military aviation fuel at 41 ^{o}C motivated us to follow ASTM standard so that we can compare the wear scar at both temperatures [14, 16].

All the components of the HFRR were subjected to acetone cleaning for 10 minutes prior to each test. The dust particles or an uncleansed specimen can significantly affect the wear scars. A 2 mL JP-8 fuel sample was placed in the test reservoir and temperature was set to 60 ^{o}C. Figure A.1 below shows the schematic of the HFRR system (instrumentation is not included).

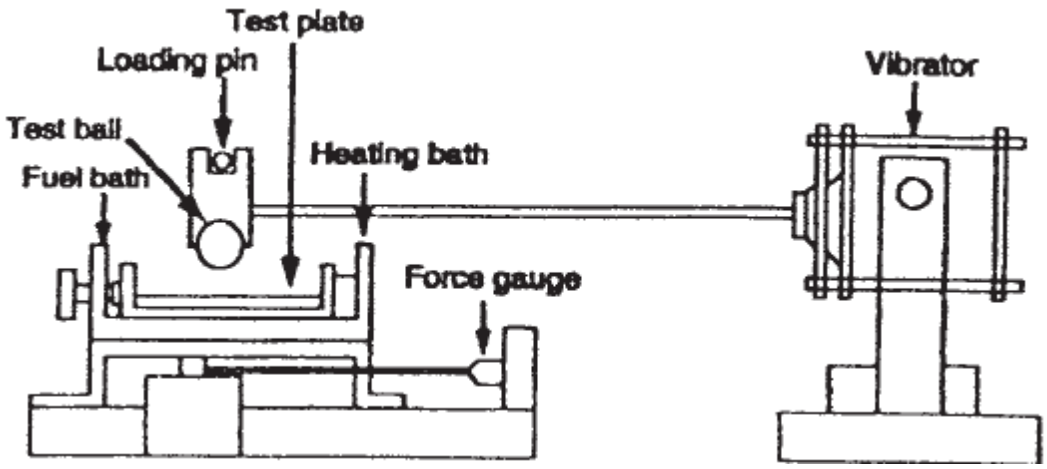

Figure A.1: Schematic of HFRR (taken from ASTM D 6079 manual) [15] (see Appendix B for copyright permission).

It takes about 15 minutes to reach the desired test temperature. A steel ball was placed in the vibrator arm which was loaded with 200 g mass. Using the control panel on the software, the steel ball and the steel disk (both 52100 alloy steel), which were completely submerged in the testing fuel, were brought into contact with each other. The stroke length of the HFRR was set at 1 mm at a frequency of 50 Hz.

Table A.1: Test conditions (chart taken from ASTM D 6079 manual) [14] (see Appendix B for copyright permission)

Fluid volume	2 ± 0.20 mL
Stroke length	1 ± 0.02 mm
Frequency	50 ± 1 Hz
Fluid temperature	25 ± 2°C or 60 ± 2°C
Relative humidity	> 30 %
Applied load	200 ± 1 g
Test duration	75 ± 0.1 min
Bath surface area	6 ± 1 cm^2

The other test conditions for the test were set as per mentioned in table A.1 (taken from ASTM D 6079 manual). The experiment was carried for 75 minutes. The reciprocating motion of the steel ball onto the steel disk resulted into wear scars on both, the carriage ball on the vibrating arm and the specimen plate in the fuel reservoir. After 75 minutes, the test ball and the test disk were removed and cleaned again in acetone for 10 minutes each in ultrasonic bath. After the cleaning procedure the ball and the disk were dried out using a tissue with soft hands carefully, not to make any impact on the wear scars. The wear scars on the ball and the disk were recorded in an Olympus SZ H10 optical microscope at 7*x* magnification. A spherical reference pattern and a ruler reference pattern were also recorded at 7*x* magnification for the precise measurements of the wear scar diameters x and y. The average of both x and y was taken as wear scar diameter (WSD). One out of the five experiments carried was done at 25 ^{o}C to compare the loss of fuel, and the scar severity at higher temperature because of evaporation [14].

A.4 Results and discussion

Four different types of aviation fuels were analyzed in CETR UMT-3. All these fuels were tested following ASTM D 6079 standard. The tests were performed for 75 minutes at 60 ^{o}C. Out

of two JP-8 aviation fuel samples, sample B was tested at two different temperatures, 25 ^{o}C and 60 ^{o}C respectively. Testing at room temperature and at 60 ^{o}C, gives a comparison to estimate the loss of fuel at ideal engine temperature. Reference pattern for the measurement of wear scar diameters, was recorded under the same microscope and at same magnification. The reference patterns are small spheres of which diameters ranging from 10 μm to 200 μm.

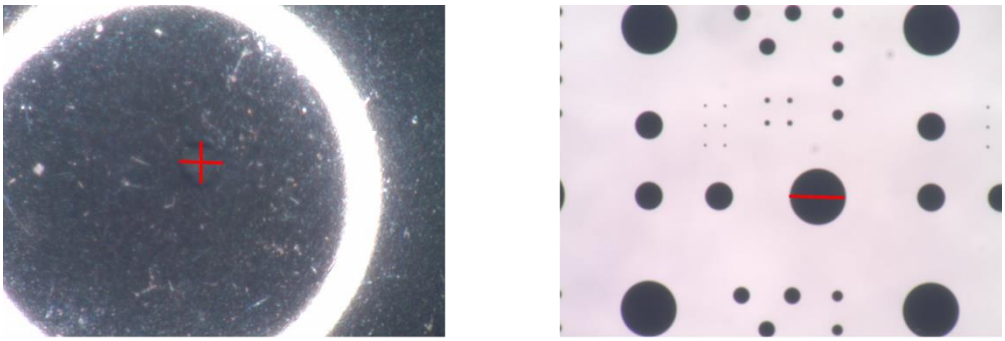

Figure A.2: shows the wear scar, major and minor diameters of JP-8 (left), reference pattern (right).

Figure A.2, above shows the wear scar diameters at the major and minor axes. In the reference pattern the smallest sphere is 10 μm in diameter and the largest is 200 μm. Both images were recorded, at 7*x* magnification of the optical microscope. The mean wear scar diameters of the carriage ball of sample B JP-8 at 25 ^{o}C came out as 156 μm. The MWSD at 25 ^{o}C is much lower than the industry standard i.e. 460 μm. The MWSD from the carriage balls for IPK, R-8 HRJ, and two samples of JP-8 fuels at 60 ^{o}C are shown below in figure A.3. All the images were recorded

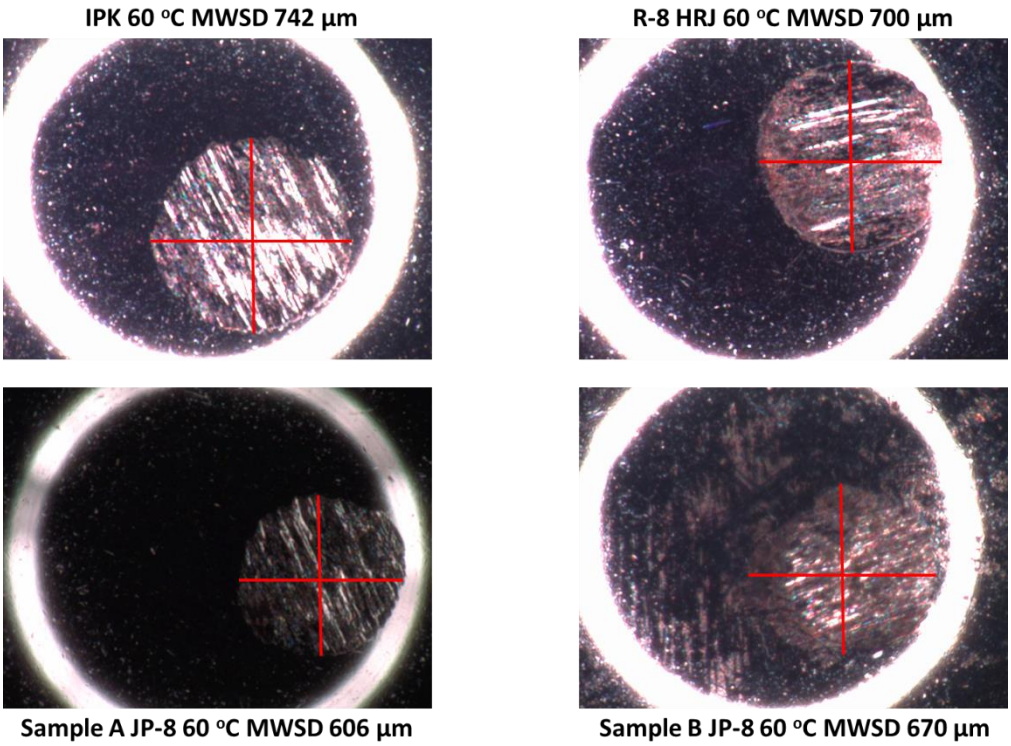

Figure A.3: MWSD of IPK, R-8 HRJ, and two samples of JP-8.

under the optical microscope in 7*x* magnification. The mean wear scar diameters for all types of fuels tested are much severe than the one tested at the room temperature. Temperature affected the wear scars diameters as liquid viscosity of these fuels decreases with the increase in temperature. All MWSD values are way above than the industry standard.

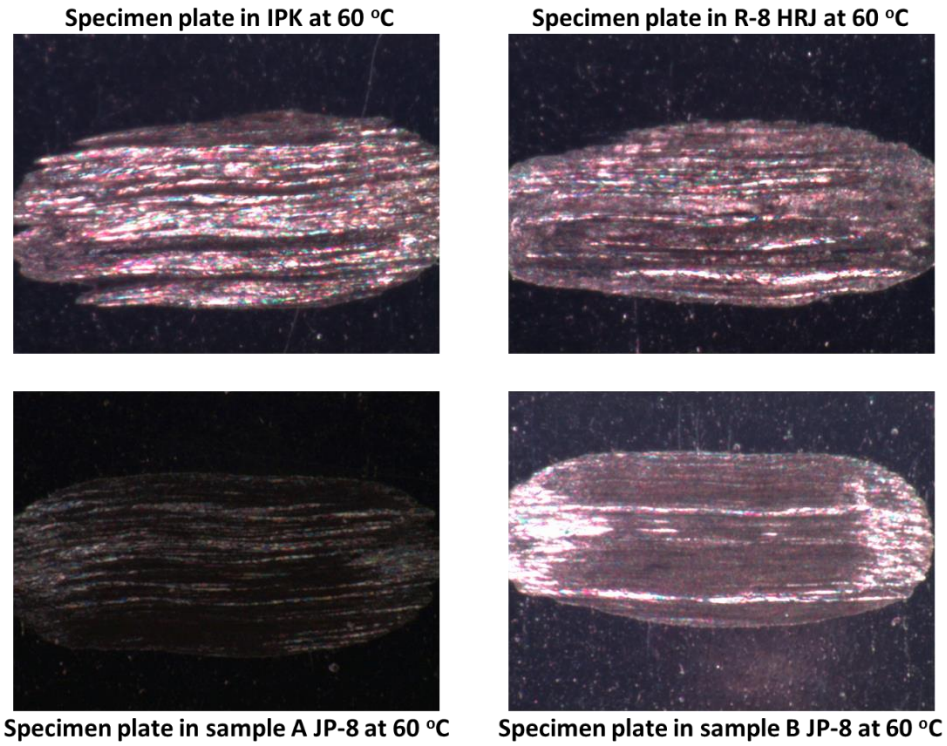

Figure A.4: Optical Microscope images of the wear scars of the plates in different test fuels.

Figure A.4 above shows wear scars on the specimen plates in IPK, R-8 HRJ, and two samples of JP-8. The wear scar from IPK plate seem much worse than all three others. The wear scar on the carriage ball is also worse among all.

The lubricity is measured from the carriage ball average wear scar diameters, in ASTM D 6079 standard. The lubricity of the tested fuel is summarized below in table A.2.

Table A.2: Lubricity from the MWSD of the tested fuels

Test Fuel Type	IPK	R-8 HRJ	JP-8 Sample A	JP-8 Sample B
Lubricity (in μm)	742	700	606	670

Clearly the lubricity for all the fuels measured are way higher than the accepted industry standard value. The lubricity evaluated for all the tested fuels are in agreement with the data reported [17].

A.5 Conclusion

We report here the lubricity of military aviation fuels IPK, R-8 HRJ and two samples of JP-8 (NATO: F-34). Lubricity of four different grades of aviation kerosene were investigated. The tests were also carried out at 25 ^{o}C of sample B JP-8 fuel. The wear scar diameters measured for all four grades are worse than the industry acceptable 460 μm (ASTM D 975). Though JP-8 is economic, less flammable, with the wear scar data, it is not a satisfactory lubrication as a single fuel concept. IPK and HRJ cannot be used as standalone lubricants as well. Further study is needed to find suitable additives and blend of these fuels to improve the lubricity of the military aviation fuel to meet the industry recommended and military approved standard. It will also be interesting to run the test for temperature profile and observe the liquid viscosity of these jet fuels with the change in temperature.

A.6 Acknowledgement

The authors would like to thank Dr. Shashi P. Karna, Senior Technical Executive at US Army Research Laboratory for coordinating this Industrial Practicum opportunity. We would also like to thank US Army Research Laboratory at Aberdeen Proving Ground in Maryland for providing us their research work space for this valuable experience.

A.7 References

[1] A. Bhatnagar, S. Kaul, V. Chhibber, A. Gupta, HFRR studies on methyl esters of nonedible vegetable oils, Energy & Fuels, 20 (2006) 1341-1344.

[2] G. Anastopoulos, E. Lois, F. Zannikos, S. Kalligeros, C. Teas, HFRR lubricity response of an additized aviation kerosene for use in CI engines, Tribol Int, 35 (2002) 599-604.

[3] K. Wadumesthrige, M. Ara, S.O. Salley, K.S. Ng, Investigation of lubricity characteristics of biodiesel in petroleum and synthetic fuel, Energy & Fuels, 23 (2009) 2229-2234.

[4] P.A. Suarez, B.R. Moser, B.K. Sharma, S.Z. Erhan, Comparing the lubricity of biofuels obtained from pyrolysis and alcoholysis of soybean oil and their blends with petroleum diesel, Fuel, 88 (2009) 1143-1147.

[5] S. Blakey, L. Rye, C.W. Wilson, Aviation gas turbine alternative fuels: A review, Proceedings of the combustion institute, 33 (2011) 2863-2885.

[6] C.A. Forest, P.A. Muzzell, Fischer-Tropsch Fuels: Why are they of interest to the United States Military?, in, SAE Technical Paper, 2005.

[7] P.A. Muzzell, E.R. Sattler, A. Terry, B.J. McKay, R.L. Freerks, L.L. Stavinoha, Properties of Fischer-Tropsch (FT) blends for use in military equipment, in, DTIC Document, 2006.

[8] J.T. Edwards, L.M. Shafer, J.K. Klein, US Air Force hydroprocessed renewable jet (HRJ) fuel research, in, DTIC Document, 2012.

[9] M.n. Lapuerta, R. García-Contreras, J.R. Agudelo, Lubricity of ethanol-biodiesel-diesel fuel blends, Energy & Fuels, 24 (2009) 1374-1379.

[10] G. Anastopoulos, E. Lois, A. Serdari, F. Zanikos, S. Stournas, S. Kalligeros, Lubrication properties of low-sulfur diesel fuels in the presence of specific types of fatty acid derivatives, Energy & Fuels, 15 (2001) 106-112.

[11] J.W. Goodrum, D.P. Geller, Influence of fatty acid methyl esters from hydroxylated vegetable oils on diesel fuel lubricity, Bioresource Technology, 96 (2005) 851-855.

[12] M.G. Kulkarni, A. Dalai, N. Bakhshi, Transesterification of canola oil in mixed methanol/ethanol system and use of esters as lubricity additive, Bioresource technology, 98 (2007) 2027-2033.

[13] A. Standard, D6079, 2011,“, Standard Test Method for Evaluating Lubricity of Diesel Fuels by the High-Frequency Reciprocating Rig (HFRR) 1, (2011).

[14] A.S.f. Testing, Materials, ASTM D975, Standard Specification for Diesel Fuel Oils, in, ASTM International West Conshohocken, PA, 2011.

[15] Universal Materials Tester User Manual, in, Center for Tribology, Inc.

[16] E. ISO, Diesel fuel - Assessment of lubricity using the high frequency reciprocating rig, in, 2006.

[17] C.A. Moses, Comparative evaluation of semi-synthetic jet fuels, Contract, 33415 (2008) 2299.

Appendix B: Copyrights permissions

From: hverma@mail.usf.edu [mailto:hverma@mail.usf.edu]
Sent: Monday, June 22, 2015 3:30 PM
To: Hooper, Kathe
Subject: Re: Students & Professors

Dear Cathy,

Thank you for the permission! I actually need to use Figure 1, and Table 1 from ASTM D 6079-04. Could you please provide the permission again?

Title of my dissertation: Nanomechanical and nanotribological characterization of sub-micron polymeric spheres

Thanks and regards,

Himanshu

Sent from Windows Mail

Dear Himanshu,

ASTM International grants a limited, non-exclusive license to reproduce Figure 1 and Table 1 from ASTM D6079-04 in your dissertation, "Nanomechanical and nanotribological characterization of sub-micron polymeric spheres," provided the following credit line is used:

"Reprinted, with permission, from ASTM D6079-04 Standard Test Method for Evaluating Lubricity of Diesel Fuels by the High-Frequency Reciprocating Rig (HFRR), copyright ASTM International, 100 Barr Harbor Drive, West Conshohocken, PA 19428. D6079-04 has been superseded. Contact ASTM for the latest information, www.astm.org."

Kind regards,

Kathe

Kathe Hooper

Manager, Rights and Permissions

ASTM INTERNATIONAL

Helping our world work better

100 Barr Harbor Drive, PO Box C700

West Conshohocken, PA 19428-2959, USA

tel +1.610.832.9634 fax +1.610.834.7018

www.astm.org
